2009-08-18

Template-assisted fabrication of nano-biomaterials

Shelley A. Dougherty
Worcester Polytechnic Institute

Template-assisted fabrication of nano-biomaterials

by

Shelley Dougherty

A Dissertation

Submitted to the Faculty

of the

WORCESTER POLYTECHNIC INSTITUTE

In partial fulfillment of the requirements for the

Degree of Doctor of Philosophy

In

Material Science and Engineering

April 29th 2009

APPROVED:

_____

Jianyu Liang, Ph.D. Advisor
Assistant Professor of Mechanical Engineering

_____

Richard D. Sisson, Jr.
George F. Fuller Professor
Director of Manufacturing and Materials Engineering

ABSTRACT

"One-dimensional" nanostructures like nanotubes and nanorods hold great potential for a wide variety of applications. In particular, one-dimensional nanostructures may be able to provide many significant advantages over traditional spherical particles for drug delivery applications. Recent studies have shown that long, filamentous particles circulate longer within the body than spherical particles, giving them more time to reach the target area and deliver their payload more efficiently. In addition, studies investigating the diffusion of drugs through nanochannels have shown that the drug diffusion profiles can be controlled by varying the nanochannel diameter when the drug diameter and nanochannel diameter are close in size. The combination of increased circulation time and controllable drug release profiles give one-dimensional nanostructure great potential for future drug release applications. To fully realize this potential, a simple, low cost, and versatile fabrication method for one-dimensional nanostructures needs to be developed and exploited.

The objective of this work is to demonstrate the versatility of template-assisted nanofabrication methods by fabricating a variety of unique protein and polymer one-dimensional nanostructures. This demonstration includes the adaptation of two different template-assisted methods, namely layer-by-layer assembly and template wetting, to fabricate glucose oxidase nanocapsules with both ends sealed, segmented polystyrene and poly(methyl methacrylate) nanorods, and poly(L-lactide)-poly(methyl methacrylate) core-shell nanowires with adjustable shell layer thicknesses. The unique nanostructure morphologies that were achieved using our novel fabrication methods will open the arena for future research focused on process control and optimization for specific applications.

ACKNOWLEDGEMENTS

As I reflect on all that I have accomplished during my four years of graduate school at Worcester Polytechnic Institute, many people come to mind who have guided me, encouraged me, given me advice, and ultimately made it possible for me to complete my research and this dissertation.

First and foremost, I want to thank my Ph.D. advisor Professor Liang. I sincerely appreciate all the constructive criticism, feedback, and advice she has given me about my research and writing. She has been a great mentor and friend and I have truly enjoyed working with her. I would also like to thank Professor Shivkumar for all of the random polymer questions he has helped me with over the years. I think he is an exceptional teacher and I have had a lot of fun working with him as a teaching assistant. And I would like to thank Professor Sisson, Professor Camesano, Professor Pins, and Dr. Arthur Coury for being my committee members.

I would like to thank all of my group members in the Nanofabrication and Nanomanufacturing Laboratory at WPI, especially Huanan Duan, who started his Ph.D at the same time and has become a good friend of mine.

Finally, I would like to thank my parents, John and Paula Dougherty, for always supporting me and pushing me to take full advantage of my potential. I love them both very much and can never thank them enough for all the opportunities they have given me. And last, but not least, my fiancé, Edward Fitzgerald, for all his love and support.

TABLE OF CONTENTS

ABSTRACT ..... **I**

ACKNOWLEDGEMENTS ..... **II**

TABLE OF CONTENTS ..... **III**

CHAPTER 1: INTRODUCTION **1**

Research Objective 2

Research Plan 2

Thesis Organization 4

CHAPTER 2: LITERATURE REVIEW **6**

Template-assisted Fabrication 6

Nanostructures for Drug Delivery 12

CHAPTER 3: PUBLICATIONS **20**

Paper 1: Template-assisted Fabrication of Protein Nanocapsules 20

Paper 2: Fabrication of Protein Nanotubes Using Template-assisted Electrostatic Layer-by-Layer Methods 38

Paper 3: Fabrication of Segmented Nanofibers by Template Wetting of Multilayered Alternating Polymer Thin Films 56

Paper 4: Core-Shell Polymer Nanorods by a Two-step Template Wetting Process 64

CHAPTER 4: CONCLUSIONS AND FUTURE WORK **81**

APPENDICES **83**

Appendix 1. Process used to determine average pore size and nanotube wall thickness using ImageJ image analysis software 83

Appendix 2. Fabrication of bovine serum albumin nanotubes through template assisted layer by layer assembly 85

Appendix 3. Towards Biodegradable Segmented Nanorods for Controlled Drug Delivery 96

Appendix 4. Preliminary Data for Drug Release from Nanoporous Alumina Membranes 106

CHAPTER 1: INTRODUCTION

Since the discovery of carbon nanotubes in the early 1990's researchers have put forth a significant amount of effort to fabricate novel nanomaterials and to demonstrate their potential to revolutionize nearly all areas of research. As we approach the end of the second nanotechnology driven and inspired decade, the potential of nanomaterials has not yet been fully exploited and the fabrication of newer, more complex, multifunctional nanostructures continues.

Nanotechnology has and will continue to significantly impact the field of drug delivery. In October 2000 the US National Nanotechnology Initiative (NNI) was initiated and included five research and development targets related to drug development and delivery out of a total of twenty five [1]. These targets included [1],

- no suffering and death from cancer when treated
- advanced materials and manufacturing
- pharmaceutical synthesis and delivery,
- converging technologies from the nanoscale, and
- life-cycle biocompatible/sustainable development.

This thesis focuses on the "advanced materials and manufacturing" target through the development of nanofabrication methods to produce unique nanomaterials for drug delivery that are simple, low cost, and could potentially lead to large scale manufacturing.

Nanotechnology based drug delivery devices are expected to provide a number of advantages over traditional drug delivery. These advantages include enhanced drug bioavailability, improved timed release, precision drug targeting, reduced drug toxicity and more efficient drug distribution [1]. Nanotubular structures, in particular, are expected to offer many advantages over spherical nanoparticles for drug delivery applications. First, the cavity inside nanotubes can have a considerably greater volume than a spherical particle of the same diameter and can therefore hold a larger drug payload [2]. This could be extremely important for targeted drug delivery because significantly fewer nanotubes would need to reach the target area to deliver the necessary drug dosage. The second advantage of nanotubes for drug delivery is the availability of both the internal and external surfaces of the nanotubes for chemical modifications and added functionalities [2]. Lastly, it was recently discovered that nanoparticles with high aspect ratios,

like nanotubes and nanowires, are able to circulate longer within the body than spherical particles of the same diameter [3-8]. This is important for two reasons; first, it gives nanotubes more time to reach targeted areas within the body before they are recognized and removed by the body's immune system and second, it allows nanotubes to release their payload over longer periods of time and would reduce the frequency at which the drug formulation would need to be administered to a patient.

The potential advantages of nanotubular structures for drug delivery are very promising for the future. To explore these potential advantages it is necessary to develop a simple, low cost, and versatile fabrication method that will enable control over important nanostructure features including type of material(s), diameter, length, aspect ratio, nanotube wall thickness, and tube versus rod morphology. A fabrication process that offers precise control of the nanostructure morphology and dimensions will enable researchers to optimize the design of one-dimensional nanostructures for specific applications, including drug delivery.

Research Objective

The objective of this work was to demonstrate the versatility of template-assisted nanofabrication to fabricate one-dimensional nanostructures with unique morphologies and controllable dimensions that may be useful for drug delivery applications.

Research Plan

The research plan for this project focused primarily on exploiting the versatility of template-assisted nanofabrication. It included the fabrication of protein and polymer single and multi-component one-dimensional nanostructures with unique segmented and core-shell morphologies. This work explored the basic principles of two template-assisted methods, namely the layer-by-layer method and template wetting, and investigated how the process variables affected the morphological outcome of the nanostructures.

In addition, this project included the collection of preliminary experimental data for drug release from nanochannels. The purpose of collecting these preliminary data was to begin developing an experimental procedure for loading nanochannels with drugs, estimating the extent of drug loading, and measuring the drug release as a function of nanochannel dimensions.

This experiment revealed many important issues that will be considered to modify our procedure for future drug release experiments.

The research plan is given in more detail in the following outline:

Demonstration of the versatility of template-assisted nanofabrication

1. ***Fabrication of glucose oxidase nanocapsules*** (published in *Journal of Nanoparticle Research*): Layer-by-layer fabrication within porous anodized aluminum oxide (AAO) templates using covalent bonds to demonstrate glucose oxidase nanocapsules. This fabrication process included a cleaving process during template dissolution to produce closed capsules and confirmed that the protein structures retained their biochemical activity after processing.
2. ***Fabrication of avidin nanotubes*** (accepted for publication in *Langmuir*): Layer-by-layer electrostatic assembly method adapted from literature for the fabrication of single component avidin nanotubes within AAO templates. Despite our extensive literature review and experimental trials, the fabrication of avidin nanotubes was not successful. Several hypotheses were drawn regarding our fabrication problems which led to the fabrication of glucose oxidase/avidin nanotubes by using a covalent bonding strategy in conjunction with electrostatic assembly. This study revealed some significant concerns regarding the previously published works from which our initial fabrication method was adapted.
3. ***Fabrication of bovine serum albumin nanotubes*** (submitted to *Nanotechnology* as 2nd author, included in appendix 1): Layer-by-layer electrostatic assembly method adapted from literature for the fabrication of single component bovine serum albumin nanotubes within AAO templates.
4. ***Fabrication of segmented polystyrene-poly(methyl methacrylate) polymer nanofibers*** (published in *Journal of Nanoparticle Research*): Melt wetting of nanoporous AAO templates with multilayered thin polymer films to demonstrate heterogeneous, segmented, polymer nanofiber morphologies.
5. ***Fabrication of core-shell poly(L-lactide)-poly(methyl methacrylate) polymer nanofibers*** (accepted for publication by *Nanotechnology*): Sequential solution wetting and melt wetting of nanoporous AAO templates to demonstrate heterogenous core-shell polymer nanofibers.

This study investigated the relationship between solution concentration, viscosity, and nanotube shell thickness and the effect of melt wetting time on the core-shell morphology.

Preliminary investigation of drug release from one-dimensional nanostructures

5. ***Drug release from polymer thin films*** (Submitted to the *Proceedings of the MRS Fall 2008 meeting*, included in appendix 2): Measured the release of ibuprofen from poly(L-lactide) thin films loaded with different initial concentrations. The purpose of this study was to calculate the diffusion coefficient of ibuprofen from poly(L-lactide) for comparison with future release studies from nanostructures.

6. ***Preliminary measurement of drug release from nanochannels*** (Included in appendix 3 as unpublished work): Measured the release of ibuprofen from AAO templates with 200, 50, and 20 nm diameter pores and lengths of 60, 40, and 20 μm respectively. The preliminary data revealed many important issues with our experimental procedure which will be considered for future drug release studies.

Thesis Organization

This thesis is divided into four chapters. This introductory chapter serves to familiarize the reader with the motivations and goals that have driven this project. The second chapter is a literature review of relevant research which has facilitated the understanding of the basic principles upon which this project is based. The third chapter is a compilation of journal articles that have either been published or accepted for publication by peer-reviewed journals regarding template-assisted fabrication methods. The formatting of the journal articles have been adapted for this thesis. Finally, the fourth chapter reviews the conclusions of this project as a whole and provides suggestions for future work. Included in the appendices are a description and example of the use of ImageJ to analyze pore size and nanostructure length, a journal article submitted to *Nanotechnology* as a second author regarding protein nanostructure fabrication, a conference proceedings paper detailing drug release data from polymer thin films and preliminary data for the release of ibuprofen from AAO templates with 200, 50, and 20 nm diameters and thicknesses of 60, 40, and 20 μm respectively.

REFERENCES

[1] Hughes G A 2005 Nanostructure-mediated drug delivery *Nanomed.: Nanotech. Bio. Med.* **1** 22-30

[2] Son S J, Bai X, and Lee S B 2007 Inorganic hollow nanoparticles and nanotubes in nanomedicine part 1. drug/gene delivery applications *Drug Disc. Today* **12** 650-6

[3] Champion J A and Mitragotri S 2009 Shape induced inhibition of phagocytosis of polymer particles *Pharmaceutical Research*. **26** 244-9

[4] Moghimi S M, Hunter A C and Murray J C 2001 Long-circulating and target-specific nanoparticles: Theory to practice *Pharm. Rev.* **53** 283–318

[5] Champion J A and Mitragotri S 2006 Role of target geometry in phagocytosis *Proc. Natl. Acad. Sci.* **103** 4930-34

[6] Geng Y, Dalhaimer P, Cai S, Tsai R, Tewari M, Minko T and Discher D 2007 Shape effects of filaments versus spherical particles in flow and drug delivery *Nat. Nanotechnology*. **2** 249–55

[7] Nishiyama N 2007 Nanocarriers shape up for long life *Nat. Nanotechnology* **2** 203-4

[8] Cai S, Vijayan K, Cheng D, Lima E M and Discher D 2007 Micelles of different morphologies – advantages of worm-like filomicelles of PEO-PCL in paclitaxel delivery *Pharmaceutical Research*. **24** 2099-109

CHAPTER 2: LITERATURE REVIEW

Template-assisted Fabrication

Template-assisted fabrication is an easy, low cost, and highly versatile method to fabricate nanostructures. When microporous or nanoporous materials are utilized as templates, one-dimensional (1D) nanostructures can be fabricated by depositing a material of choice within the template's nanochannels. After deposition, the template can be selectively removed either partially or completely to produce a nanostructure array or freestanding 1D nanostructures respectively.

Template-assisted fabrication methods can be adapted to accommodate a variety of different materials including metals [1-6], inorganics, semiconductors [1-6], carbon [2-7], polymers and proteins [1-32]. Some methods include electroless deposition[1-2,6] and electrochemical deposition [3,4,6] for metals, sol-gel processes[1-4,6,33,34] for inorganic and semiconductors, chemical vapor deposition [2,3] for carbon, in-situ polymerization [1,2,6,21] and template wetting [3,5-7,15-29,31,32] for polymers, and layer-by-layer deposition [1,3,8-14,30] for proteins and polyelectrolytes. In addition to homogeneous, single component nanostructures, template-assisted methods can be used to fabricate heterogeous, multi-component, composite nanostructures [1,2,4,17,31-33].

Nanoporous media typically used as templates for 1D nanostructure fabrication include track-etch membranes, which are usually made from polymers including poly(carbonate), poly(ethylene terephthatlate), or poly(imide) [1,3], and anodized aluminum oxide (AAO), which can be purchased commercially or fabricated using a well-known anodization process [1,3,4,6,15]. In addition to nanoporous materials, templates can also be fabricated using lithographic techniques.

AAO Template Fabrication

The use of AAO templates is especially attractive because of its simple, low cost, and highly controllable fabrication method. Using the two-step anodization process to fabricate AAO templates allows for control of the nanochannel diameter and nanochannel length by varying the anodizing solution and time respectively.

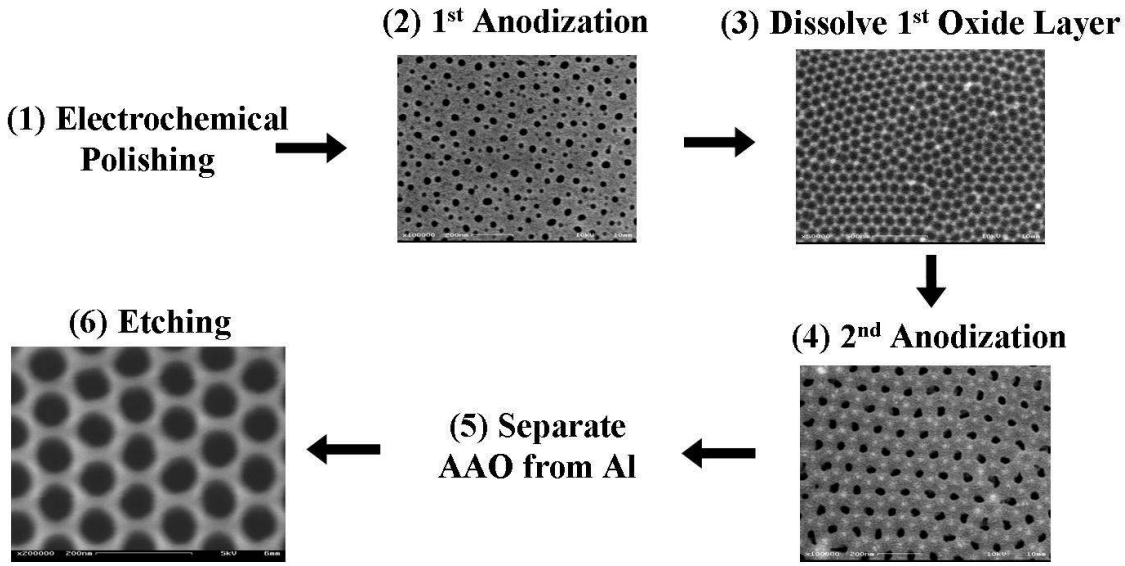

Figure 1: Schematic illustration of the two-step anodization process used to fabricate AAO templates. Scanning electron microscope images of the aluminum/alumina surface are shown for each step of the fabrication process. (**1**) The aluminum foil is electrochemically polished (**2)** then anodized to form a thick oxide layer with a non-uniform pore size distribution. (**3)** The 1st oxide layer is dissolved leaving behind a dimpled aluminum surface. (**4)** The aluminum is anodized a 2nd time to form an oxide layer with a uniform pore size distribution and hexagonal pattern with a thickness which is proportional to the anodization time. (**5)** The oxide layer is separated from the aluminum (**6)** and etched to remove the barrier layer and widen the pores.

In the following sections, template-assisted fabrication methods which are commonly used to fabricate protein and polymer nanostructures are discussed.

One-dimensional Protein Nanostructure Fabrication: Layer-by-Layer Methods

Protein nanostructures can be fabricated using a template-assisted method adapted from layer-by-layer techniques used to electrostatically assemble multilayer thin films [37,38]. Rather than deposit layers onto planar surfaces, layers of material are deposited onto the inner walls of nanopores. This layer-by-layer deposition inside nanopores has been demonstrated using either chemically covalent bonds [1,9,11,30] or electrostatic attractions [3,8,10-14] to bind protein

layers together. Both methods utilize the unique structural properties that are common for most protein molecules so they can be easily adapted to accommodate any protein.

Covalent Crosslinking Method

Proteins are long chains of polyamides formed by joining many amino acids together with peptide bonds. Amino acids, as the name implies, contain an amino group and a carboxylic acid group as well as other side functional groups. Since most proteins have at least some free amino groups, they can be crosslinked with molecules that contain aldehyde functionalities. This enables layers of proteins to be easily bound inside nanopores by covalent bonds. This "alternate immersion strategy" was originally adapted from an approach used by Hou et al to prepare nanotubes within AAO templates using alternating a,w-diorganophosphonate/Zr(IV) chemistry [35]. To make protein nanotubes, Hou et al pretreated AAO templates first with 3-amino propylphosphonic acid (APA) to functionalize the nanopore walls with amino groups, then with glutaraldehyde (GA), a difunctional aldehyde, which binds with the amino groups on the nanopore walls and leaves a free aldehyde group for protein binding [1,9]. Protein solutions were then vacuum filtered through the nanopores and immobilized on the inner walls by alternating protein and GA. This layer-by-layer strategy has been used to demonstrate glucose oxidase [1,9,30] and hemoglobin nanostructures [1,9] and cytochrome c (cyto-c) nanotubes [11].

Although this crosslinking method has proven to be a versatile approach for protein nanotube fabrication, the use of GA and other aldehyde crosslinkers may introduce cytotoxcity problems. GA has been used for the past 25 years for many biomedical applications including bioprostheses, immobilization of enzymes, and crosslinking of proteins and polysaccharides for controlled drug delivery [36]. More specifically, GA has been used to crosslink albumin, bovine casein, gelatin, chitosan, and poly(vinyl alcohol) to fabricate microspheres for drug delivery applications [36]. Despite the widespread use of GA for biomedical applications, there are many studies regarding the toxicity and adverse effects of GA which yield conflicting results and suggest that the toxicity is primarily concentration dependent [36]. Based on the toxicity studies, there is a chance that GA could be used without causing any problems. However, it is desirable to develop an alternative method to bind layers of proteins within nanochannels to avoid the potential controversy and additional precautions associated with the use of GA.

Electrostatic Attractions Method

The bi-functional nature of amino acids makes them amphoteric, which means they can react as either an acid or a base depending upon the conditions. In acid solutions, an amino acid acts as a base and is protonated, making it a cation. In basic solutions, an amino acid acts as an acid and is deprotonated, making it an anion. There is a certain pH value for all amino acids where there is a balance between the cationic and anionic forms. This pH is known as the amino acid's isoelectric point. At this point the amino acid has a neutral charge. Proteins are long chains of polyamides formed by bonding many different amino acids together and they too have an isoelectric point. The isoelectric point for proteins is essentially the pH value at which the charge of all the side functional groups of the amino acids within the protein is balanced, giving the protein a net neutral charge. Therefore, proteins can have a net positive or net negative charge if the solution pH is below or above the protein's isoelectric point respectively. This is the basic principle behind the layer-by-layer build up of electrostatically bound materials.

The use of electrostatic layer-by-layer assembly for multilayer thin films was introduced in 1991 by Decher [37,38]. Since its introduction it has become widely popular because of the simple and inexpensive nature of the process [14]. The pioneering studies that investigated the electrostatic layer-by-layer assembly process focused mostly on full polyelectrolytes, such as polystyrenesulfonic acid (PSS) and polyallylamine hydrochloride (PAH) and determined that the thickness of the films was influenced primary by the ionic strength of the solutions [39]. Although researchers were able to gain control of the thickness to the molecular level using full polyelectrolytes and varying the ionic strength, the process was severely limited by the solubility of the polyelectrolytes, which decreased with increasing ionic strength [39]. To avoid this limitation, researchers began experimenting with weak polyelectrolytes, in which the charge, as described above, is strongly influenced by solution pH [39].

The success of layer-by-layer electrostatic assembly of thin films using full and weak polyelectrolytes has led to the more recent advancements of forming multilayer films on colloidal particles followed by the dissolution of the original colloidal particle to form hollow capsules [14,40] or to encapsulate drug microcrystals [40], and within the pores of nanoporous templates to form nanotubes [3,8,10-14]. Although this method is discussed as being a fabrication technique for protein nanostructures, polyelectrolytes and other charged materials can be used as well. Nanotubes that have been fabricated using the electrostatic layer-by-layer method typically include different materials acting as the cation and the anion. Some examples

include alternating PAH/PSS [8], L-α-dimyristoylphosphatidic acid (DMPA)/human serum albumin (HSA) [10], cyto-c/PSS [11], poly lactic acid (PLA)/HSA [12], PAH/HSA [12], alginate/chitosan [13], and poly(acrylic acid)/PAH with Au nanoparticles [3]. Few researchers have demonstrated the ability to fabricate single component nanotubes with human serum albumim (HAS) using the electrostatic layer-by-layer assembly method [10,12]. The fabrication of single component nanotubes relies on the ability of a protein to act as both a cation or an anion depending upon the solution pH. Although some results have been published to demonstrate the feasibility of this method [10,12], it has not yet been fully explored.

One-dimensional Polymer Nanostructure Fabrication: Template Wetting Methods

Template wetting is a process governed by the basic principles of surface wettibility or capillarity. Wetting occurs when a low-energy liquid, like a polymer melt or solution, spreads partially or completely over the surface of a high-energy solid substrate, like glass, metal, or metal oxide. The wetting of the solid surface can be characterized by the spreading coefficient, S, which is a measure of the interfacial energy differences between solid substrates, gases and liquids. S is given by [15,19],

$$S = \gamma_{SG} - \gamma_{SL} - \gamma \tag{1}$$

where γ_{SG}, γ_{SL}, and γ are the solid-gas, solid-liquid, and liquid-gas interfacial tensions respectively. When the wetting coefficient is greater than or equal to zero, complete wetting occurs. Complete wetting is when a liquid spontaneously forms a thin film over the entire surface of a solid substrate on a very short time scale [19]. When the wetting coefficient is less than zero, partial wetting occurs. Partial wetting is when a liquid partially spreads over the surface of a solid substrate, but eventually reaches an equilibrium shape with a finite contact angle [19].

Wetting of Nanoporous Templates

Nanoporous materials can be wet like planar surfaces. This is of particular interest because, when nanoporous templates are wet with polymers, which can be either polymer melts [6,15,18-23,25-29,31,32] or polymer solutions [6,15-18,21,22,24,26-28,32], polymer nanotubes or nanorods can be formed within the template. When a polymer melt or solution comes into contact with a nanoporous material, the polymer wets the nanochannels either completely or

partially, similar to a planar surface. Complete wetting within a nanochannel yields a nanotube morphology, while partial wetting within a nanochannel yields a nanorod morphology [19]. The driving force for wetting a nanoporous material is heavily dependent on the interfacial tension of the polymer melt or solution and the nanopore radius. The driving force, p, is given by [41]

$$p = \frac{2(\gamma_{SG} - \gamma_{SL})\cos\theta}{R} \tag{2}$$

where R is the hydraulic radius, which can be approximated as half the radius of the nanopores. The interfacial tension of a polymer melt is strongly dependent upon temperature [42], allowing the wetting process to be controlled by varying the wetting temperature. Therefore, by heating a polymer to a temperature far above its glass transition temperature (amorphous polymers) or melting temperature (semi-crystalline polymers), the driving force is high and nanotubes are formed within the nanopores on a short time scale (seconds to minutes). This is the complete wetting regime. By heating a polymer to a temperature only slightly above the glass transition or melting temperature, the driving force is low and nanorods are formed within the nanopores on a much longer time scale (hours to days). This is the partial wetting regime. For each polymer there is a temperature between the glass transition or melting temperature and the decomposition temperature where the wetting regime transitions from partial to complete. This temperature is referred to as the wetting transition temperature, T_W [19]. T_W can be determined for a given polymer by analyzing the nanostructure morphology formed over a range of temperatures.

The length of nanorods formed by wetting a nanoporous template with a polymer melt in the partial wetting regime can be controlled by monitoring the wetting time. The time required to achieve a particular length can be approximated by the rate of flow of polymer melts within nanopores, which has been estimated by [19,43],

$$\frac{dz}{dt} = \frac{R\gamma\cos\theta_c}{4\eta z} \tag{3}$$

where t is the time, z the distance the polymer has traveled through the nanochannel, η the viscosity of the polymer melt or solution, and R the hydraulic radius. For melt wetting the polymer viscosity can controlled by varying the temperature of the melt and for solution wetting the viscosity can controlled by changing the solution concentration.

Although some control over nanostructure morphology can be achieved by simply controlling wetting temperature and time for polymer melts, other variables more specific to the polymer can affect the outcome as well. The molecular weight of the polymer, for example, can have a significant effect on the formation of nanotubes versus nanorods. It has been demonstrated that polymer melts with low molecular weight typically yield nanorods while high molecular weight yield nanotubes [6,16,18]. Researchers expect solution wetting to offer more control over the nanostructure morphology than melt wetting because there are more variables that can be adjusted, which include choice of solvent, concentration of polymer, and molecular weight [16].

Investigations into the controllability of both the melt wetting and solution wetting processes are just beginning and much work is needed to fully understand the relationship between the process and materials properties and the resulting nanostructure morphology.

Nanostructures for Drug Delivery

The Advantages of One-dimensional Nanostructures

One of the most important design considerations for drug delivery vehicles is making sure that the vehicles can circulate in the blood stream for long periods of time. The body's natural immune response is a significant barrier in this respect. When macrophage cells encounter foreign micro-scale particles (1μm and up) they are immediately recognized and internalized by the cells in a process known as phagocytosis [44]. This process prevents the successful delivery of the therapeutic drug to the desired location. Macrophage cells can encounter and internalize foreign particles regardless of delivery method (injection, transdermal, or inhalation) [44].

Many recent studies have focused on developing strategies to prohibit phagocytosis from occurring [44-50]. Before particle modifications were even considered a possible approach to avoid phagocytosis, researchers would essentially "trick" macrophages by administering large doses of placebo particles to overwhelm and impair their phagocytic capacity [45-46]. After the placebo doses, the therapeutic particles were administered and would circulate for longer periods of time. Researchers have since developed more advanced techniques to "trick" macrophages. These include modifications to the actual particles and include three main strategies; modification of surface chemistry, size, and shape. Surface chemistry and size were the most

important considerations until very recently. The surface chemistry of spherical particles was often modified with hydrophilic polymers to prevent or slow the process of opsonization [44-46]. Opsonization is the binding of proteins to the surface of foreign particles to increase the recognition and receptor specific attachment of macrophage cells [44-46]. Previous conclusions regarding size were based solely upon experiments with spherical particles. It was determined that macrophages would internalize particles greater than 1-5 μm [44,47]. Thus, it was thought that nano-scale particles could simply evade phagocytosis and provide long-lasting circulation. Recently researchers realized that size is more than just the particle radius, but also includes surface area, volume, and the ratio of the surface area to volume. These parameters describe more than just particle size, but also particle shape.

It has been shown that long, cylindrical particles circulate much longer than spherical particles [44,47-50]. In particular, researchers at the University of Pennsylvania demonstrated that long polymeric filomicelles that were 22 – 60 nm in diameter and 2 – 8 μm in length circulated 10 times longer than spherical particles [48,48]. Additionally these researchers showed that the optimum length for circulation was 8 μm. Longer particles were rapidly fragmented and did not show any improved circulation beyond what was achieved by particles there were 8 μm long [48]. These results have contributed significantly to the understanding of the phagocytosis of foreign particles. Unfortunately drug delivery studies involving particle shape are limited by existing methods to fabricate non-spherical nanoparticles. Therefore, there is a great need to research and develop simple, low cost, fabrication methods for long, filament-like, one-dimensional nanoparticles, like the template-assisted methods discussed previously.

Hindered Diffusion from Cylinders

In addition to increased circulation time, one-dimensional nanoparticles are also expected to enable researchers to control the drug release of thereputic molecules from the inner cavity of nanotubular structures by varying the particle diameter. This hypothesis is based on the theory of hindered diffusion.

The diffusion coefficient of a spherical solute molecule in bulk solution can be approximated by the Stokes-Einstein equation which is given by,

$$D_\infty = \frac{k_B T}{6\pi\mu r_s} \tag{4}$$

where D_∞ is the bulk diffusion coefficient (cm^2/s), k_B is Boltzmann's constant ($1.38x10^{-23}$ J/K), T is absolute temperature (K), μ is the solvent viscosity, and r_s is the radius of the solute (cm). When a solute molecule is restricted to a cylindrical pore and the pore size is comparable to the solute size, the effective diffusion coefficient is typically less than the bulk diffusion coefficient. This situation is referred to as hindered diffusion [51,52]. The lower diffusivity of a spherical solute in a cylindrical pore is attributed to a thermodynamic phenomenon, where interactions between the solute and pore wall exclude the solute from being in the region near the pore wall, and a transport phenomenon, where the proximity of the pore wall causes the solute to experience a greater hydrodynamic drag [51,52]. Based upon these phenomena and experimental data, researchers have developed empirical equations to approximate the effective diffusion coefficient as a function of the ratio of the solute radius to pore radius ($\lambda = r_s/r_p$) [51,52]. As approximated by Renkin, the effective diffusion coefficient is given by [51,52],

$$D = D_\infty (1-\lambda)^2 \left(1 - 2.104\lambda + 2.089\lambda^3 - 0.948\lambda^5\right) \tag{5}$$

Generally, predictions based on Eq. 5 correspond well with experimental data for rigid and spherical solutes. Using Eq. 5 to estimate the effective diffusion coefficient for a drug in a nanochannel will enable researchers to interpret their data and develop models to describe the drug release from nanochannels. It can also be used to approximate the size of the nanochannel that will be necessary to effectively hinder the diffusion and provide additional control over the release profile.

In summary, template-assisted fabrication methods are just beginning to be explored as simple and low cost fabrication methods for one-dimensional nanoparticles. Many researchers have begun to demonstrate the potential of both covalent and electrostatic layer-by-layer assembly methods to fabricate protein nanostructures and template wetting methods to fabricate polymer nanostructures. There is a need to expand upon these pioneering efforts to exploit the versatility of these methods and demonstrate the fabrication of unique, multifunctional nanostructures that offer potential for specific applications. In particular, drug delivery applications could potentially be improved by utilizing unique one-dimensional nanoparticles to achieve longer circulation times within the body and more controllable drug release profiles.

REFERENCES

[1] Baker L A, Jin P and Martin C R 2005 Biomaterials and biotechnologies based on nanotube membranes *Crit. Rev. Solid State Mater. Sci.* **30** 183-205

[2] Martin C R and Kohli P 2003 The emerging field of nanotube biotechnology *Nature Reviews Drug Discovery* **2** 29–37

[3] Liang Z, Susha AS, Yu A and Caruso F 2003 Nanotubes prepared by layer-by-layer coating of porous membrane templates *Adv. Mater*. **15** 1849–53

[4] Son SJ, Bai X, Nan A, Ghandehari H and Lee SB 2006 Template synthesis of multifunctional nanotubes for controlled release *J. Controlled Release* **114** 143–52

[5] Mark SS, Stolper SI, Baratti C, Park JY and Kricka LJ 2008 Biofunctionalization of aqueous dispersed alumina membrane-templated polymer nanorods for use in enzymatic chemiluminescence assays *Colloids and Surfaces B: Biointerfaces* **65** 230–8

[6] Steinhart M, Wehrspohn RB, Gosele U and Wendorff JH 2004 Nanotubes by template wetting: A modular assembly system *Angew. Chem. Int. Ed.* **43** 1334-44

[7] Chen JT, Shin K, Leiston-Belanger JM, Zhang M and Russell TP 2006 Amorphous carbon nanotubes with tunable properties via template wetting *Adv. Funct. Mater*. **16** 1476-80

[8] Ai S, Lu G, He Q and Li J 2003 Highly flexible polyelectrolyte nanotubes *J. Am. Chem. Soc.* **125** 11140-1

[9] Hou S, Wang J and Martin CR 2005 Template-synthesized protein nanotubes *Nano Lett*. **5** 231–4

[10] Lu G, Ai S and Li J 2005 Layer-by-layer assembly of human serum albumin and phospholipid nanotubes based on a template *Langmuir* **21** 1679-82

[11] Tian Y, He Q, Cui Y and Li J 2006 Fabrication of protein nanotubes based on layer-by-layer assembly *Biomacromolecules* **7** 2539-42

[12] Lu G, Tsuchida E and Komatsu T 2008 Human serum albumin nanotubes comprising layer-by-layer assembly with polycation *Chem. Lett*. **37** 972–3

[13] Yang Y, He Q, Duan L, Cui Y and Li J 2007 Assembled alginate/chitosan nanotubes for biological applications *Biomaterials* **28** 3083-90

[14] Ariga K, Hill JP and Ji Q 2007 Layer-by-layer assembly as a versatile bottom-up nanofabrication technique for exploratory research and realistic application *Phys. Chem. Chem. Phys.* **9** 2319-40

[15] Steinhart M, Wendorff JH and Wehrspohn RB 2003 Nanotubes a la carte: Wetting of porous templates *ChemPhysChem* **4** 1171-6

[16] Schlitt S, Greiner A and Wendorff JH 2008 Cylindrical polymer nanostructures by solution template wetting *Macromolecules* **41** 3228-34

[17] Steinhart M, Murano S, Schaper AK, Ogawa T, Tsuji M, Gosele U, Weder C and Wendorff JH 2005 Morphology of polymer/liquid-crystal nanotubes: Influence of confinement *Adv. Funct. Mater.* **15** 1656-64

[18] Steinhart M, Wendorff JH, Greiner A, Wehrspohn RB, Nielsch K, Schilling J, Choi J and Gosele U 1997 Polymer nanotubes by wetting of ordered porous templates *Science* **296** 1997

[19] Zhang M, Dobriyal P, Chen JT and Russell TP 2006 Wetting transition in cylindrical alumina nanopores with polymer melts *Nano Letters* **6** 1075-9

[20] Moon SI and McCarthy TJ 2003 Template synthesis and self-assembly of nanoscopic polymer 'pencils' *Macromolecules* **36** 4253-55

[21] Cepak VM and Martin CR 1999 Preparation of polymeric micro- and nanostructures using a template-based deposition method *Chem. Mater*. **11** 1363-7

[22] Kriha O, Zhao L, Pippel E, Gosele U, Wehrspohn RB, Wendorff JH, Steinhart M and Greiner A 2007 Organic tube/rod hybrid nanofibers with adjustable segment lengths by bidirectional template wetting *Adv. Funct. Mater.* **17** 1327-32

[23] Lau ST, Zheng RK, Chan HLW and Choy CL 2006 Preparation and characterization of poly(vinylidene fluoride-trifluoroethylene) copolymer nanowires and nanotubes *Mater. Lett*. **60** 2357-61

[24] Chen JT, Zhang M and Russell TP 2007"Instabilities in nanoporous media *Nano Lett*. **7** 183-7

[25] Sun Y, Steinhart M, Zschech D, Adhikari R, Michler GH and Gosele U 2005 Diameter-dependence of the morphology of PS-b-PMMA nanorods confined within ordered porous alumina templates *Macromol. Rapid Commun*. **26** 369-75

[26] Kriha O, Goring P, Milbradt M, Agarwal S, Steinhart M, Wehrspohn R, Wendorff JH and Greiner A 2008 Polymer tubes with longitudinal composition gradient by face-to-face wetting *Chem. Mater*. **20** 1076-81

[27] Dersch R, Steinhart M, Boudriot U, Greiner A and Wendorff JH 2005 Nanoprocessing of polymers: applications in medicine, sensors, catalysis, photonics *Polym. Adv. Technol*. **16** 276-82

[28] Greiner A, Wendorff JH, Yarin AL and Zussman E 2006 Biohybrid nanosystems with polymer nanofibers and nanotubes *Appl. Microbiol. Biotechnol*. **71** 387-93

[29] Shin K, Xiang H, Moon SI, Kim T, McCarthy TJ and Russell TP 2004 Curving and frustrating flatland *Science* **306** 76

[30] Dougherty S, Liang J and Kowalik T F 2009 Template-assisted fabrication of protein nanocapsules *J. Nanopart. Res*. **11** 385-94

[31] Dougherty S and Liang J 2009 Fabrication of segmented nanofibers by template wetting of multilayered alternating polymer thin films *J. Nanopart. Res*. **11** 743-7

[32] Dougherty S and Liang J Core-shell polymer nanorods by a two-step template wetting process *Submitted to Nanotechnology*

[33] Son SJ, Bai X and Lee SB 2007 Inorganic hollow nanoparticles and nanotubes in nanomedicine part 1. Drug/gene delivery applications *Drug Discovery Today* **12** 650-5

[34] Hillebrenner H, Buyukserin F, Kang M, Mota MO, Stewart JD and Martin CR 2006 Corking nano test tubes by chemical self-assembly *J. Am. Chem. Soc*. **128** 4236-7

[35] Hou S, Harrell CC, Trofin L, Kohli P and Martin CR 2004 Layer-by-layer nanotube template synthesis *J. Am. Chem. Soc*. **126** 5674-5

[36] Jayakrishnan A and Jameela SR 1996 Glutaraldehyde as a fixative in bioprostheses and drug delivery matrices *Biomaterials* **17** 471-84

[37] Decher G and Hong JD 1991 Buildup of ultrathin multilayer films by a self-assembly process I. Consecutive adsorption of anionic and cationic biopolar amphiphiles on charged surfaces *Macromol. Chem. Macrom. Symp*. **46** 321-7

[38] Decher G and Hong JD 1991 Buildup of ultrathin multilayer films by a self-assembly process II. Consecutive adsorption of anionic and cationic bipolar amphiphiles and polyelectrolytes on charged surfaces *Ber. Bunsenges. Phys. Chem*. **95** 1430-4

[39] Yoo D, Shirator SS and Rubner MF 1998 Controlling bilayer composition and surface wettability of sequentially adsorbed multilayers of weak polyelectrolytes *Macromolecules* **31** 4309-18

[40] Paragaonkar N, Lvov YM, Li N, Steenekamp JH and de Villiers MM 2005 Controlled release of dexamethasone from microcapsules produced by polyelectrolyte layer-by-layer nanoassembly *Pharmaceutical Research* **22** 826-35

[41] Yung KL, Kong J and Xu Y 2007 Studies on flow behaviors of polymer melts in nanochannels by wetting actions *Polymer* **48** 7645-52

[42] Spearling LH, Introduction to Physical Polymer Science. 3rd ed. New York: J. Wiley & Sons; 2001

[43] Kim E, Xia Y and Whitesides GM 1996 Micromolding in capillaries: Applications in material science *J. Am. Chem. Soc*. **118** 5722-31

[44] Champion JA and Mitragotri S 2009 Shape induced inhibition of phagocytosis of polymer particles *Pharmaceutical Research*. **26** 244-9

[45] Storm G, Belliot SO, Daemen T and Lasic DD 1995 Surface modification of nanoparticles to oppose uptake by the mononuclear phagocyte system *Adv. Drug. Del. Rev*. **17** 31–48

[46] Moghimi SM, Hunter AC and Murray JC 2001 Long-circulating and target-specific nanoparticles: Theory to practice *Pharm. Rev.* **53** 283–318

[47] Champion JA and Mitragotri S 2006 Role of target geometry in phagocytosis *Proc. Natl. Acad. Sci.* **103** 4930-4

[48] Geng Y, Dalhaimer P, Cai S, Tsai R, Tewari M, Minko T and Discher D 2007 Shape effects of filaments versus spherical particles in flow and drug delivery *Nat. Nanotechnology*. **2** 249-55

[49] Nishiyama N 2007 Nanocarriers shape up for long life *Nat. Nanotechnology* **2** 203-4

[50] Cai S, Vijayan K, Cheng D, Lima EM and Discher D 2007 Micelles of different morphologies – advantages of worm-like filomicelles of PEO-PCL in paclitaxel delivery *Pharmaceutical Research*. **24** 2099-109

[51] Shao J and Baltus RE 2000 Hindered diffusion of dextran and polyethylene glycol in porous membranes *AIChE Journal* **46** 1149-56

[52] Ladero M, Santos A and Garcia-Ochoa F 2007 Hindered diffusion of proteins and polymethacrylates in controlled-pore glass: An experimental approach *Chemical Engineering Science* **62** 666-78

CHAPTER 3: PUBLICATIONS

Paper 1: Template-assisted Fabrication of Protein Nanocapsules

Published in Journal of Nanoparticle Research (2009) 11:385 - 394

S. Dougherty, J. Liang, and T. F. Kowalik

ABSTRACT

Bionanomaterials have recently begun to spark a great amount of interest and could potentially revolutionize biomedical research. Nanoparticles, nanocapsules, and nanotubular structures are becoming attractive options in drug and gene delivery. The size of the delivery vehicles greatly impacts cellular uptake and makes it highly desirable to precisely control the diameter and length of nanocarriers to make uniform nanoparticles at low cost. Carbon nanotubes have shown great potential within the field of drug and gene delivery. However, their insolubility and cytotoxicity could severely delay FDA approval. A desirable alternative would be to fabricate nanostructures from biomaterials such as proteins, peptides or liposomes, which are already FDA approved.

In this paper we demonstrate the preparation of protein nanocapsules with both ends sealed using a template-assisted alternate immersion method combined with controlled cleaving. Glucose oxidase nanocapsules with controllable diameter, wall thickness, and length were fabricated and characterized with SEM and TEM. The biochemical activity of glucose oxidase in the form of nanocapsules after processing was confirmed using UV spectrometry. Our future work will explore proteins suitable for drug encapsulation and cellular uptake and will focus on optimizing the cleaving process to gain precise control over the length of the nanocapsules.

INTRODUCTION

Bionanomaterials have recently begun to attract a great amount of interest and could potentially revolutionize biomedical research. In particular, nanoparticles, nanocapsules and nanotubular structures are becoming attractive options in drug delivery and gene therapy research.

Currently viral vectors are the most effective vector in cellular delivery. However, severe side effects and major practical limitations, such as immune response and difficulties in scaling

up production, impair successful application of viral vectors. There is great interest in exploring non-viral technologies to eliminate the inherent immunogenicity concerns and improve the in vivo efficiency. Non-viral carriers, such as organic and inorganic nanomaterials, including calcium phosphate nanoparticles, carbon nanotubes, silicon oxide nanoparticles, iron oxide nanoparticle, lipid and polymer nanostructures, have been shown to enhance the protein uptake and increase the transfer efficiency of proteins or DNA across the cell membrane [1-6].

The mechanism of enhanced cell uptake of nanocarriers has not yet been confirmed and remains a topic for debate. Many virus-like particles as well as common viruses have a size range of 30 – 200 nm [7]. Particles could potentially be taken up by cells by paracellular passage, which requires sizes less than 50 nm, lymphatic uptake, which is typically for larger particles [8], or endocytosis, which facilitates uptake of particles between the two extremes. Most studies regarding CNTs and other nanoparticle systems have suggested an endocytosis mechanism to be responsible for cellular uptake. Mathematical modeling simulations have shown that there is a critical radius for optimum cellular uptake via endocytosis for both cylindrical and spherical particles [9, 10]. Decuzzi and Ferrari gave a critical radius of approximately 14 nm and 28 nm for cylindrical and spherical particles respectively [10]. In addition to a critical value, both maximum and minimum values were calculated [10]. When the radius is below the minimum value, 12 nm and 24 nm for cylindrical and spherical particles respectively, there is not enough ligand-receptor binding at the cell surface to initiate the endocytosis process. Likewise, when the radius is too large, greater than 320 nm and 1,600 nm for cylindrical and spherical particles respectively, the cell surface area is not large enough to wrap around the particle. In addition, when particles are larger than 200 nm diameter they are easily recognized by the reticuloendothelial system which is responsible for eliminating foreign particles from circulation [11]. It was reported that the opsonization process, which involves protein adsorption on particle surfaces and the subsequent recognition and elimination of such coated particles from circulation, decreased when the particle size decreased from 800 nm to 200nm, and further enhancement was observed with a particle size below 200 nm [12]. It was also described, however, that particle size below 100 nm led to a hepatic accumulation instead of long circulation which led to decreased cellular uptake [13]. As a result of the size effect, it is highly desirable to be able to precisely control the diameter and length of nanocarriers and to establish processing conditions for producing uniform nanoparticles efficiently and at low cost.

Recently carbon nanotubes have attracted great interest as vaccine delivery systems, DNA and RNA nanovectors, or protein transporters [14-17]. Studies have shown that carbon nanotubes (CNTs) are able to pass through cell membranes and enter cell nuclei, potentially enabling them to deliver DNA [18-20]. One study showed the successful delivery of the green fluorescence protein gene into cultured human cells through the use of amino-functionalized multi-walled CNTs [19].

For these biomedical applications, CNTs must be functionalized with proteins, enzymes, or other biomaterials to enhance the solubility, biocompatibility, and biochemical functionality. Despite the improvements of functionalized CNTs over un-functionalized CNTs, a major concern of CNT based biomedical technologies is the ongoing controversy surrounding their cytotoxicity. Some studies have shown that CNTs decreased keratinocyte [21], glial [22], and HEK293 cell survival significantly [23] and that single-walled CNTs block potassium channel activities when applied externally to the cell surface [24]. Others have shown CNTs to interact with and affect living systems without any adverse affects [19, 20, 25]. Pantarotto et al. have shown that ammonium functionalized CNTs have low cytotoxicity and the ability to delivery plasmid DNA to cells with a gene expression level 10 times greater than plasmid DNA alone [25]. Despite these discrepancies, CNTs have yielded very promising results for many biomedical applications and have led to an increased interest in fabricating nanotubes from purely biological materials such as proteins, peptides and liposomes.

Protein based nanotubular structures may be very promising since they are biodegradable, provide high drug loading capacity, minimal tissue irritation and toxic effect, and are relatively easy to prepare. There are two preparation approaches, namely self-assembly and template-assisted synthesis for producing nanotubes directly from proteins, polymers or lipids. The self-assembly of biomolecules to form nanotubular structures has been studied for more than a decade. Many different self-assembly mechanisms have been investigated and are typically unique to the chemistry and functionality of certain biomolecules [26-31]. For instance, studies have shown that amphiphilic phospholipids self-assemble by chiral interactions [26] and type IV pilin, a globular protein, self-assembles by a hydrophobe initiated conformational shift [27]. More recently, researchers have utilized a β-sheet forming peptide to form biotinylated peptide nanotubes that can be decorated with proteins to achieve the desired functionality [28]. In

addition to β-sheet forming peptides, ring-shaped cyclic peptides have been designed to interact through extensive hydrogen bonding to form nanotube structures [30]. The functionality of these self-assembled cyclic peptide nanostructures can be varied through surface-initiated atom transfer radical polymerization to functionalize the surface with polymers such as N-Isopropylacrylamide [31]. In all these cases, the morphology and dimensions of the self-assembled nano-tubular structures are restricted by the properties of the original bulk material. This greatly limits the versatility of these fabrication methods. The template-assisted methods, however, are highly versatile, easy processes that rely upon either the chemical crosslinking of proteins, which enables the so-called alternate immersion method [32, 33], or electrostatic charges between protein layers, which enables the so-called layer-by-layer method [34, 35]. These template-assisted synthesis techniques incorporate concepts that can be easily adapted to almost any protein with little to no modifications. This is a huge advantage of template-assisted approaches and makes them viable for a wide range of applications.

Employing template-assisted approaches, a couple of previous studies have fabricated protein nanotubes within commercially available anodized aluminum oxide (AAO) membranes with 200 nm diameter pores [32-34]. Both the diameters and lengths of those protein nanotubes matched that of the original AAO templates. It was also observed that the liberated protein nanotubes were open on both ends. For certain applications, such as drug delivery and gene therapy, it is desirable to have a protein nanostructure capable of encapsulating drug molecules, RNA, or DNA within the protein shell. It is also desirable to be able to control both the diameter and the length of the fabricated protein nanostructures.

In this paper, we demonstrate the preparation of protein nanocapsules with both ends sealed using a template-assisted alternate immersion method combined with controlled cleaving. Glucose oxidase (GOx) nanocapsules were successfully fabricated using AAO templates through alternate immersion in protein and cross-linking solutions. Proteins were immobilized on the inner walls of the nanochannels of the AAO templates. Protein nanocapsules with ends sealed were formed and liberated into solution through a subsequent cleaving process during the dissolution of the AAO template. The overall fabrication procedure is shown schematically in Figure 1.

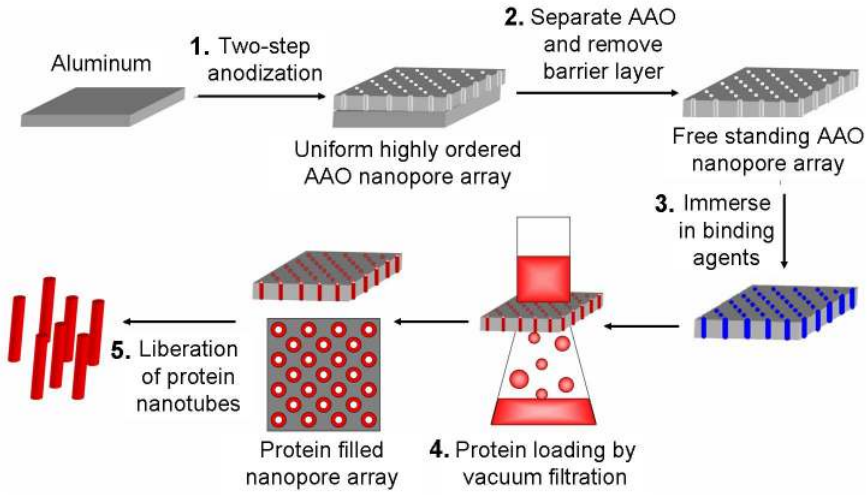

Figure 1: Schematic of the protein nanotube fabrication process: 1. Al is anodized to produce a porous Al oxide layer. 2. The Al oxide layer is separated from the Al and etched to remove the barrier layer. 3. The free standing Al oxide is treated with binding agents. 4. The Al oxide is then loaded with proteins by vacuum filtration. 5. The Al oxide is dissolved to yield liberated protein nanotubes.

MATERIALS AND METHODS

Aluminum oxide template fabrication

AAO templates with nanopore arrays with diameters in the range of 20 to 100 nm were fabricated in our lab using a well established two-step anodization process. Details of the anodization process are published elsewhere [36]. Following anodization, the AAO was separated from the aluminum in a 1% mercury chloride solution. The free-standing AAO templates were then etched with a 0.5 M phosphoric acid solution for 30 minutes to remove the barrier layer and to obtain a nanoporous channel with both ends open in the AAO template. During this wet-etching process the nanopores were widened slightly. For example, for nanopores with 20 and 50 nm diameter immediately after anodization, average pore diameters of 32±2 nm and 67±6 nm were achieved according to scanning electron microscopy (SEM) characterization. In general, the nanopore size can be controlled to a certain extent by varying the anodization conditions, the wet-etching solution concentration, and the wet-etching time. In addition to the AAO templates fabricated in our lab, commercial Anodisc AAO membranes with

200 nm diameter pores and a thickness of approximately 60 μm were purchased from SPI supplies and used as-received.

Protein nanotube fabrication

Protein nanotubes were fabricated within templates with 20 to 200 nm diameter pores using the alternate immersion method adapted from reference [32]. Briefly, both sides of the AAO templates were first coated with thin (~5nm) layers of gold using an e-beam evaporator to prevent protein absorption to the top and bottom surfaces of the templates. The base pressure during the e-beam evaporation was controlled to be between $4 – 5x10^{-7}$ torr. The optimized evaporation rate of 1 Å/s yielded good coating uniformity. The gold coated AAO templates were then immersed in a 5 mM solution of 3-amino propylphosphonic acid (APA) at pH 5.8 for 24 hrs. After rinsing with phosphate buffer solution (PBS) (pH 7.0), the templates were immersed in a solution of 2.5% glutaraldehyde (GA) in PBS for 12 hrs. 10 mL of a 10 mg/mL GOx solution was then vacuum filtered slowly through the template using a Millipore mini-vacuum system. For additional layers, the templates were then immersed again in a 0.025% GA solution for 12 hrs followed by the filtration of GOx solution. This immersion-filtration procedure was repeated until the desired number of protein layers was achieved.

Protein nanotube liberation

The GOx coated AAO templates were immersed in 100 mL of a 0.01 M hydrochloric acid (HCl) solution at room temperature to remove the template and liberate the protein nanostructures. Complete template dissolution took between 24 – 48 hrs depending upon size and thickness of the AAO template.

During the dissolution process, the exposed portion of the protein nanotubes was cleaved periodically from the template and released to the solution by swirling to form protein nanocapsules.

After the AAO template had been completely removed, the HCl solution was filtered with a 0.05 μm polycarbonate nanopore membrane to collect the liberated nanocapsules.

Protein nanostructure characterization and biochemical activity assay

To confirm that the GOx nanotubes retained their biochemical activity in the form of nanocapsules after all the processing, a well-known aminophenazone/peroxidase colorimetric

assay [37] was performed for both template bound proteins and liberated protein nanostructures. For template bound proteins, the templates with various protein layer coatings were immersed in a solution containing 13 mM phenol, 0.7mM 4-aminophenazone, 0.1M glucose, and 10 units of peroxidase in PBS. For the liberated nanocapsules, immediately after they were collected on the polycarbonate nanopore membrane, the whole membrane was immersed in the same amount of the assay solution as described above. In both cases the templates and filters were incubated in the assay solution for 5 min at 37^{o}C. After incubation, 3 mL of solution was transferred to a cuvette and the absorbance was measured at 515 nm using a UV-visible spectrophometric system over a duration of 5 minutes.

SEM and TEM analysis

To confirm that GOx layers were immobilized within the nanopore channels of AAO templates, SEM top views of the AAO template after the immobilization of various protein layers were obtained using a Zeiss 982 SEM. The liberated GOx nanocapsule length, wall thickness, and morphology were characterized using a JEOL 2100 TEM.

RESULTS AND DISCUSSION

AAO template

SEM images of a typical AAO template fabricated using the two-step anodization process in our lab and a commercial Anodisc AAO template are shown in Figure 2.

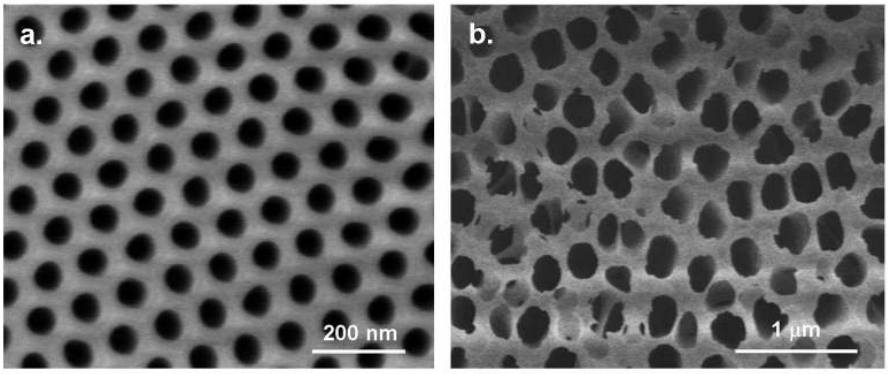

Figure 2: SEM images of a.) highly ordered, uniform, AAO nanopore array fabricated in our lab with 65 nm diameter pores and b.) commercial Anodisc AAO nanopore array with 200 nm diameter pores.

The image of our AAO template was taken on a hexagonal nanopore array with 65 nm diameter. It clearly illustrates the narrow pore size distribution and the uniform shape of the nanopores. These characteristics are particularly beneficial for the fabrication of uniform protein or polymer nanotubes. By adjusting the anodization conditions, the size and spacing of the nanopores can be conveniently adjusted over the range of 20 ~ 300 nm. This property provides the advantage of easily creating nanotubes with controlled size just by controlling the property of the AAO template.

Protein nanotubes in AAO templates

In addition to the control over the outer diameter of the protein nanotubes, another advantage of the template-assisted approach is the easy control over the wall thickness of protein nanotubes. The inner walls of nanopores in AAO templates can be coated with single and multiple protein layers. Figure 3 shows SEM top view images of an AAO template with 100 nm diameter nanopores coated with 1, 3, and 4 protein layers.

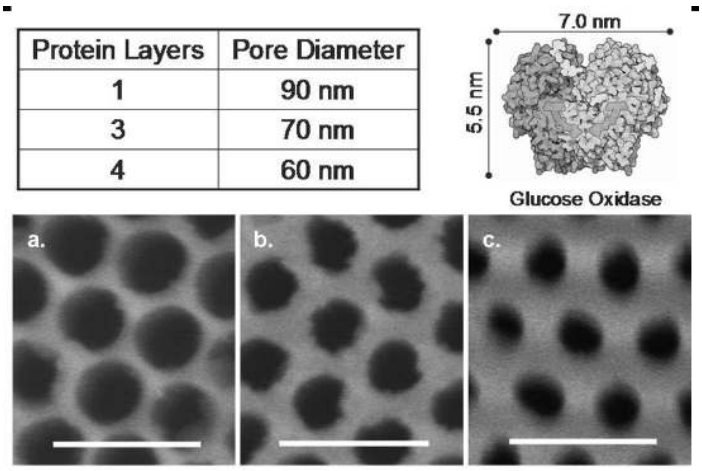

Figure 3: SEM images of glucose oxidase loaded AAO templates with a.) 1 protein layer b.) 3 protein layers and c.) 4 protein layers. A schematic illustration of the glucose oxidase protein dimensions is also given. Scale bars are 200 nm.

It can be seen that the pore openings decrease by approximately 10 nm per protein layer coating. Considering the dimensions of the glucose oxidase molecule, shown schematically in Figure 3, it

is considered that the decrease in pore diameter corresponded well with the size of the protein molecule. This observation strongly indicates that glucose oxidase was successfully immobilized on the inner walls of the nanopores.

Protein nano-capsules

TEM was employed to examine the overall morphology of the protein nanotubes. TEM images revealed that after liberation the nanotubes formed within the nanopore templates became short, sealed nanocapsules. It was observed that the ends of the nanotubes were sealed, as shown in Figure 4, giving them a nanocapsule-like structure.

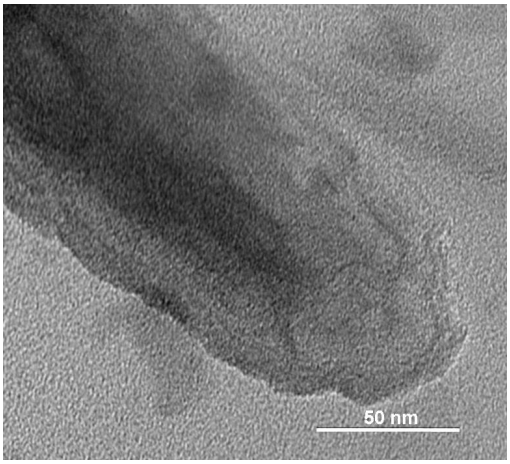

Figure 4: TEM image showing that the nanotubes formed within the nanopore templates became short, sealed nanocapsules after liberation.

In the previous studies, liberated protein nanotubes with length of tens of micrometers, which was the same length as the template thickness, were formed. In our study, through controlled swirling during the dissolution process, the shear forces cleaved the nanotubes to form nanocapsules and also sealed them as a result of the poor mechanical stability of the unsupported tips of the exposed protein nanotubes. As confirmed by the TEM observations we were able to fabricate nanocapsules with lengths that were fractions of the template thickness. Figure 5 shows two different protein nanotubes formed within templates of the same thickness that were cleaved to be approximately 600 nm in one case and 1 μm in another.

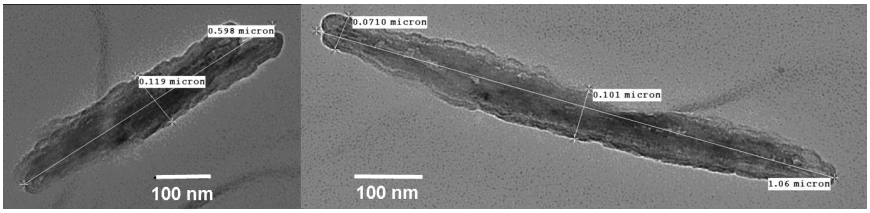

Figure 5: TEM images of protein nanocapsules formed within 80 nm diameter nanopore templates. The lengths of the nanotubes were controlled to be approximately 600 nm on the left and 1 μm on the right.

The process of cleaving provides us with unique control over the length in addition to the control over the diameter and wall thickness of the protein nanostructures. Those short protein nanocapsules could potentially offer great potential for drug delivery and gene therapy applications.

To demonstrate the versatility of this template assisted method, we created Y-shaped protein nanocapsules. Starting with AAO templates with Y-shaped nanochannels, as shown schematically in Figure 6, 1 layer of GOx was immobilized to the inner walls of the nanochannels.

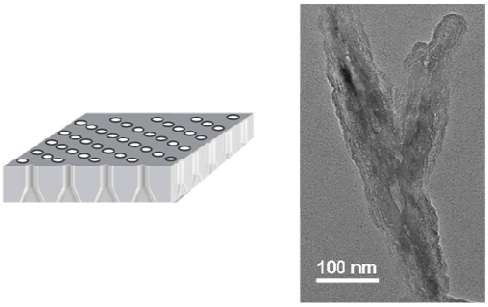

Figure 6: TEM images of branched protein nanocapsules fabricated from Y-shaped nanochannel arrays.

The overall processing is similar to the synthesis of straight protein nanocapsules. The resulting protein nanostructures maintained the shape of the template, yielding Y-shaped or branched protein nanotubes. The formation of Y-shaped protein nanocapsules strongly illustrates the

unique capability of template-assisted fabrication to provide control over the shape and size of protein nanostructures.

Bio-chemical activity of protein nanostructures

To confirm that the enzymatic activity of the GOx molecules had not been sacrificed after the multiple processing steps, the ability of the GOx to catalyze the decomposition of glucose to gluconic acid was measured using UV-vis spectroscopy. The catalytic activity was measured both before and after template dissolution. Figure 7 compares the enzymatic activities of one layer GOx bounded in nanochannels with 32 nm diameters in a 20 μm thick AAO template, and liberated GOx nanocapsules of identical samples after complete AAO template removal in 0.01 M HCl and 0.005 M HCl respectively.

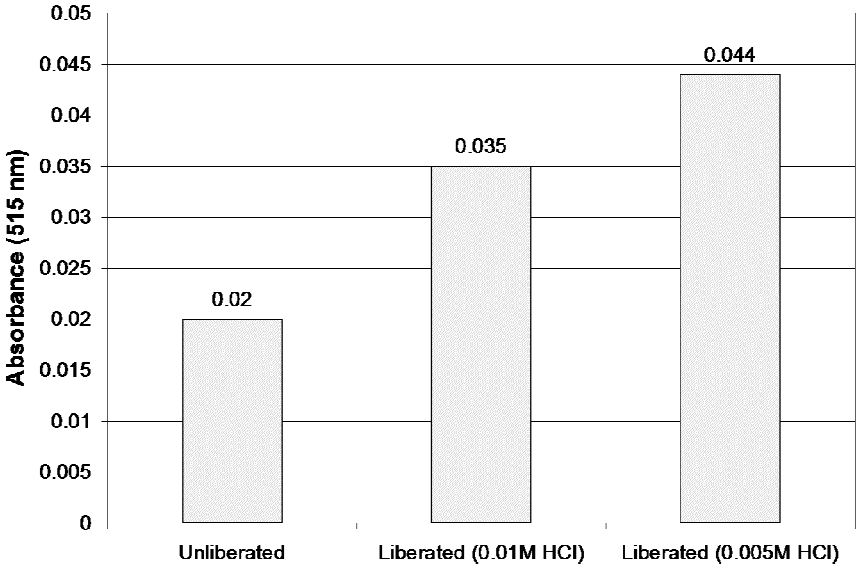

Figure 7: UV spectrometry absorbance data collected after 5 minutes for 32 nm diameter GOx nanocapsules before and after liberation in hydrochloric acid solutions with different concentrations.

The results confirm that the GOx maintained activity after template dissolution and that the activity of the liberated GOx nanotubes was actually greater than the template bound nanotubes. This result can be attributed to the diffusion limited transport of both reactants and products in

confined high-aspect-ratio nanochannels for the template bound nanotubes. While in the case of liberated protein nanocapsules in solutions, there are no significant barriers to mass transport.

Figure 7 also shows that the activity of nanotubes liberated in 0.005 M HCl solution was comparatively higher than the activity of nanotubes when liberated in 0.01 M HCl solution. The results indicate that the concentration of the acid solution used had a considerable affect on the activity of the liberated nanotubes. This observation led us to further study the impact of different acidic solutions on the GOx enzymatic activity. For example, we examined the activity of bulk glucose oxidase in the presence of phosphoric acid solutions with concentrations ranging from 0.001 M to 0.1 M. The experiments revealed that the biochemical activity of bulk GOx could only be maintained using phosphoric acid solutions with concentrations equal to or less than 0.01 M. At such a low concentration the AAO templates could not be fully dissolved within a reasonable length of time. However, by using a low concentration (<0.02 M) solution of hydrochloric (HCl) acid we were able to both retain the protein biochemical activity and dissolve the AAO templates.

We also compared the relative activity of template bound nanotubes with various diameters and wall thicknesses. To compare the effect of nanotube diameter, templates with nanopores of 200 nm, 70 nm, and 32 nm diameter were coated with one layer of GOx. Figure 8, showed that as expected the protein nanotubes in a 200 nm diameter template yielded the highest activity.

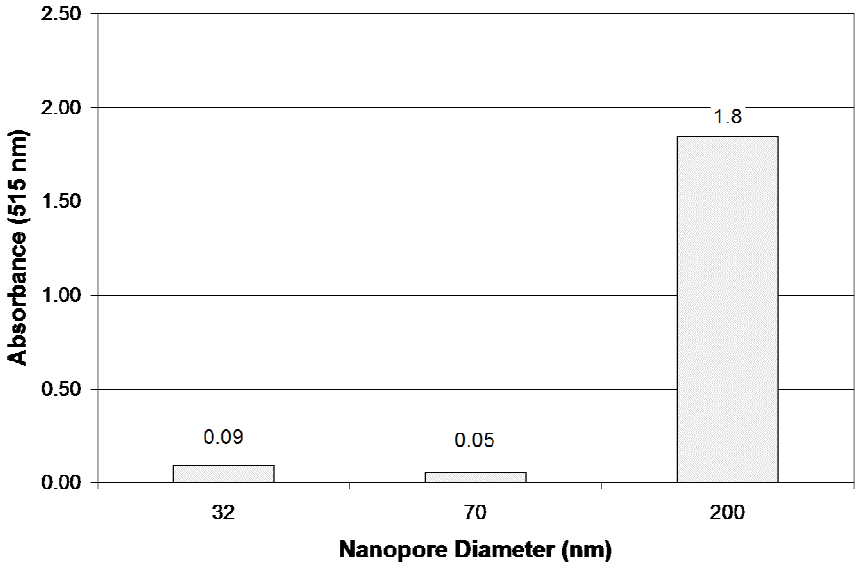

Figure 8: UV spectrometry absorbance data collected after 5 minutes for single layer template bound protein nanotubes within 32 nm, 70 nm, and 200 nm diameter nanopores.

The 70 nm diameter nanotubes, however, had the lowest activity, which was slightly less than the 32 nm diameter. These results can be attributed to the combined effect of diffusion limited transfer of reactants and products within the smaller nanochannels and the amount of adhered protein per unit area. In a previous study, it was noticed that when the GOx nanotube wall thickness increased from 1 layer up to 6 layers, which led to the decrease in the size of nanochannel openings, the measured enzymatic activity of the GOx nanotubes first increased then decreased [32]. The turning point was the 3 layer GOx coating. Combined with our results, it is strongly indicated that depending on the aspect ratio of the nanochannels, the diffusion limited transport kicks in at a certain critical point. Our results on the 70 nm and 32 nm cases suggest that not only diffusion limited transport affects the measured activity, but differences in the relative amount of protein per unit area also contributes. The total surface area available per unit sample size for protein immobilization was analyzed as a function of pore diameter and spacing. It was found that the nanopore array with 32 nm diameter provided the greatest amount of inner pore surface area per unit template size, which very likely leads to the result of larger amount of protein molecules immobilized in the nanopores of 32 nm diameter than that of the 70 nm diameter. Therefore the more protein per unit sample size the higher the measured enzymatic activity. This might outweigh the effect of diffusion limited transport in nanochannels and account for the fact that the activity of the 32 nm diameter nanotubes was slightly greater than the 70 nm diameter nanotubes.

Additionally, activities of template bound GOx nanotubes with various protein wall thicknesses were compared. Figure 9 shows the measured activities of 1-, 2-, and 4- layers of GOx coated on the inner walls of an AAO template with nanopores of 70 nm diameter.

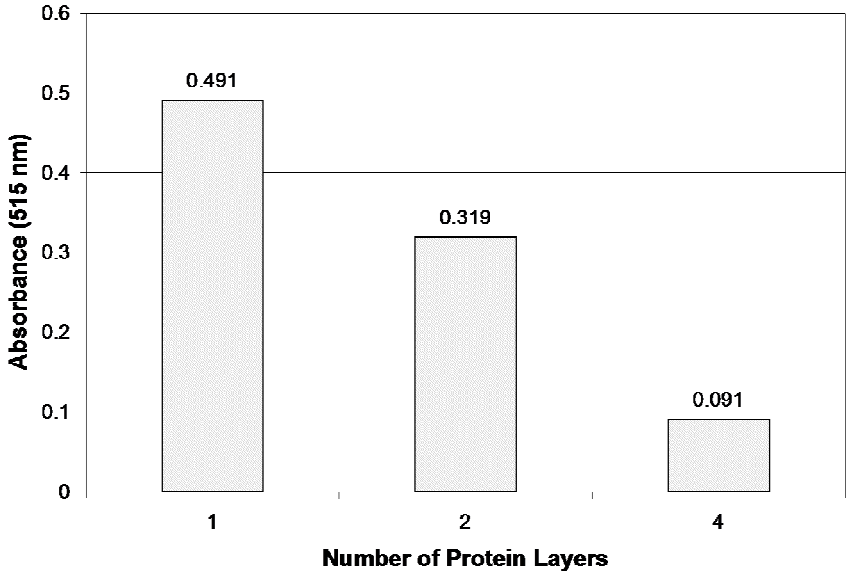

Figure 9: UV spectrometry absorbance data collected after 5 minutes for 70 nm diameter template bound GOx nanotubes with varying wall thickness.

It is clearly shown that the activity decreases consistently with increasing wall thickness. These results further suggest that when the accessible amount of protein per unit sample size is the same, diffusion limitations plays a major role in determining the protein activity.

CONCLUSIONS

A template based nanofabrication method was developed to fabricate nanocapsules from proteins. This method can be easily adapted to a variety of different proteins since the cross linking agent GA immobilizes all different types of proteins. The ability to form nanocapsules of varied lengths and wall thicknesses can be beneficial for potential drug delivery and gene therapy applications. Our future work will explore proteins suitable for drug encapsulation and cellular uptake, and will focus on optimizing the cleaving process to gain precise control over the length of the protein nanocapules.

ACKNOWLEDGEMENTS

The authors would like to thank the National Nanotechnology Infrastructure Network/Center for Nanostructured Systems at Harvard University for use of their nanofabrication and microscopy

facilities. This work is supported in part by the Research Advancement Program of Worcester Polytechnic Institute.

REFERENCES

[1] Kakizawa Y, Furukawa S, Ishii A et al (2006) Organic-inorganic hybrid-nanocarrier of siRNA constructing through the self-assembly of calcium phosphate and PEG based block aniomer. J Controlled Release 111:368–370

[2] Chen JF, Ding HM, Wang JX et al (2004) Preparation and characterization of porous hollow silica nanoparticles for drug delivery application. Biomaterials 25:723–727

[3] Neuberger T, Schopf B, Hofmann H et al (2005) Superparamagnetic nanoparticles for biomedical applications: Possiblities and limitations of a new drug delivery system. J Magnetism and Magnetic Materials 293:483-496

[4] Courvreur P, Gref R, Andrieux K et al (2005) Nanotechnology for drug delivery: Application to cancer and autoimmune diseases. Progress in Solid State Chemistry 1–5

[5] Xu ZP, Zeng QH, Lu GQ et al (2006) Inorganic nanoparticles as carriers for efficient cellular delivery. Chemical Engineering Science 61:1027–1040

[6] Putnam D (2006) Polymers for gene delivery across length scales. Nature Materials 5:439–451

[7] Fifis T, Gamvrellis A, Crimeen-Irwin B et al (2004) Size-dependent immunogenicity: Therapeutic and protective properties of nano-vaccines against Tumors. J Immunology 173:3148–3154

[8] Win KY, Feng SS (2005) Effects of particle size and surface coating on cellular uptake of polymeric nanoparticles for oral delivery of anticancer drugs. Biomaterials 26:2713–2722

[9] Gao H, Shi W, Freund LB (2005) Mechanics of receptor-mediated endocytosis. PNAS 102:9469–9474

[10] Decuzzi P, Ferrari M (2007) The role of specific and non-specific interactions in receptor-mediated endocytosis of nanoparticles. Biomaterials 28:2915–2922

[11] Nishiyama N, Kataoka K (2006) Current state, achievements, and future prospects of polymeric micelles as nanocarriers for drug and gene delivery. Pharmacology & Therapeutics 112:630–648

[12] Harashima H, Sakata K, Funato K et al (1994) Enhanced heptic uptake of liposomes through complement activation depending on the size of liposomes. Pharm Res 11:402–406

[13] Langer K, Balthasar S, Vogel V et al (2003) Optimization of the preparation process for human serum albumin (HSA) nanoparticles. International J of Pharm 257:169–180

[14] Martin CR, Kohli P (2003) The emerging field of nanotube biotechnology. Nat Rev Drug Discovery 2:29–37

[15] Bianco A, Prato M (2003) Can carbon nanotubes be considered useful tools for biological applications? Adv Mater 15:1765–1768

[16] Shi Kam NW, Dai H (2005) Carbon nanotubes as intracellular protein transporters: Generality and biological functionality. J Am Chem Soc 127:6021–5026

[17] Klumpp C, Kostarelos K, Prato M et al (2005) Functionalized carbon nanotubes as emerging nanovectors for the delivery of therapeutics. Biochimica Et Biophysica Acta Article in Press

[18] Bianco A, Kostarelos K, Prato M (2005) Applications of carbon nanotubes in drug delivery. Current Opinion in Chemical Biology 9:674-679

[19] Gao L, Nie L, Wang T et al (2006) Carbon nanotube delivery of the GFP Gene into mammalian cells. ChemBioChem 7:239-242

[20] Pantarotto D, Singh R, McCarthy D (2004) Functionalized carbon nanotubes for plasmid DNA gene delivery. Angew Chem 116:5354-5358

[21] Shvedova A, Castranova V, Kisin E et al (2003) Exposure to carbon nanotube material: Assessment of carbon nanotube cytotixicity using human keratinocyte cells. J Toxicol Environ Health A 66:1909-1926

[22] McKenzie JL, Waid MC, Shi R et al (2003) Decreased functions of astrocytes on carbon nanofiber materials. Biomaterials 25:1309-1317

[23] Cui D, Tian F, Ozkan CS et al (2005) Effect of single walled carbon nanotubes on human HEK293 cells. Toxicol Lett 155:73-85

[24] Park KH, Chhowalla M, Iqbal Z et al (2003) Single-walled carbon nanotubes are a new class of ion channel blockers. J Biol Chem 278:50212-50216

[25] Panarotto D, Briand J, Prato M et al (2004) Translocation of bioactive peptides across cell membranes by carbon nanotubes. Chem Commun 1:16–17

[26] Spector MS, Selinger JV, Singh A et al (1998) Controlling the morphology of chiral lipid tubules. Langmuir 14:3493-3500

[27] Audette GF, van Schaik EJ, Hazes B et al (2004) DNA-binding protein nanotubes: learning from nature's nanotech examples. NanoLetters 4:1897-1902

[28] Matsumura S, Uemura S, Mihara H (2005) Construction of biotinylated peptide nanotubes for arranging proteins. Mol BioSyst 1:146-148

[29] Kol N, Adler-Abramovich L, Barlam D et al (2005) Self-assembled peptide nanotubes are uniquely rigid bioinspired supramolecular structures. NanoLetters 5:1343-1346

[30] Ghadiri MR, Granja JR, Milligan RA et al (1993) Self-assembling organic nanotubes based on a cyclic peptide architecture. Nature 366:324-327

[31] Couet J, Biesalski M (2006) Surface-initiated ATRP of N-isopropylacrylamide from initiator-modified self-assembled peptide nanotubes. Macromolecules 39:7258-7268

[32] Hou S, Wang J, Martin CR (2005) Template-synthesized protein nanotubes. NanoLetters 5:231-234

[33] Baker LA, Jin P, Martin CR (2005) Biomaterials and biotechnologies based on nanotube membranes. Crit Rev Solid State Mater Sci 30:183-205

[34] Tian Y, He Q, Cui Y et al (2006) Fabrication of protein nanotubes based on layer-by-layer assembly. Biomacromolecules 7:2539-2542

[35] Lu G, Ai S, Li J (2005) Layer-by-layer assembly of human serum albumin and phospholipids nanotubes based on a template. Langmuir 21:1679-1682

[36] Liang J, Chik H, Yin A et al (2002) Two-dimensional lateral superlattices of nanostructures: Nonlithographic formation by anodic membrane template. J Appl Phys 91:2544-2546

[37] Syte S, Kumon Y, Ishigaki A (1998) Immobilization of glucose oxidase on poly-(L-lysine)-modified polycarbonate membrane. Biotechnol Appl Biochem 27:245-248

Paper 2: Fabrication of Protein Nanotubes Using Template-assisted Electrostatic Layer-by-Layer Methods

Accepted for publication in Langmuir

S. Dougherty, D. Zhang, and J. Liang

ABSTRACT

One-dimensional protein nanostructures offer many advantages for biomedical applications. Rather than fabricate primary nanostructures with inorganic materials then functionalize with proteins, it is desirable to develop a fabrication method to make nanostructures that are entirely protein. Fabrication of protein and polymer nanostructures is possible by layer-by-layer assembly within nanoporous templates. Typically these structures are composites of two or more materials. Few studies have demonstrated the fabrication of single component protein nanostructures using this method. In this paper, we report our effort towards the fabrication of single-component avidin nanotubes using a layer-by-layer electrostatic assembly method adapted from literature. We investigated the use of two different template pre-treatment methods to strengthen the attraction between the initial protein layer and our template. During our investigation, we revealed a significant flaw with the published works upon which our fabrication method was based which seriously compromised the legitimacy of the approach. As a result, we modified our initial method and we are able to demonstrate the fabrication of glucose oxidase/avidin nanostructures using an electrostatic layer-by-layer assembly in conjunction with one of the template pre-treatment methods we investigated.

INTRODUCTION

Protein nanostructures show great potential for many biomedical applications such as biosensors, enzymatic bioreactors, bioseparations, and drug delivery [1-8]. Functionalizing inorganic nanotubular structures with proteins, enzymes, and antibodies has recently attracted a lot of interest for biomedical applications [1-6]. For example, antibodies have been functionalized on the inside and outside surfaces of silica nanotubes to separate racemic mixtures of drug formulations [6,9], silane chemistry was used to functionalize the inside and outside surfaces of silica nanotubes to give both hydrophilic and hydrophobic surfaces for the removal of lipids from aqueous solutions [3,5] and single walled carbon nanotubes have been functionalized with metelloproteins and enzymes for biosensing applications [4,5]. Using proteins and enzymes

as the main component of the nanostructure alleviates the need for additional functionalization and raises fewer biocompatibility concerns than inorganic materials such as carbon nanotubes.

Recent discoveries suggest that one-dimensional nanostrucures may have great potential for success as drug and gene delivery vehicles. Studies have shown that wormlike, filamentous nanoparticles are able to better avoid the body's natural immune response than spherical particles, allowing them longer circulation [6-8]. It is hypothesized that macrophages, the cells that are responsible for engulfing foreign particles in a process known as phagocytosis, have difficultly stretching and adjusting their shape to engulf filamentous particles. Geng et al have demonstrated that paclitaxel loaded filomicelles can circulate up to ten times longer, and provide the same therapeutic effect as sphereical micelles with an eightfold smaller paclitaxel dosage per injection [7,8]. These results show great potential and demonstrate the need to further investigate the function of size and aspect ratio for delivery applications. Therefore, it is necessary to develop low cost, simple, and versatile nanofabrication techniques to produce cylindrical protein and polymer nanostructures with controllable dimensions such as length, diameter, and aspect ratio.

Recently template-assisted layer-by-layer assembly approaches have become popular methods to fabricate polymer and protein nanotubular structures [10-16]. These methods utilize nanoporous membranes such as anodized aluminum oxide (AAO) or polycarbonate as templates in which the nanopore walls are coated with polymer and protein layers. To avoid the use of glutaralydehyde (GA) as a means to bind multiple protein layers [2,15,17,18], layer-by-layer electrostatic deposition has been adapted to electrostatically immobilize subsequent layers within the nanopores. The electrostatic layer-by-layer method has been traditionally used to fabricate multilayer films on planar surfaces and colloid particles due to its low cost, simplicity, and versatility [10,11]. To date, nanotubes that have been fabricated using this method are primarily composites of at least two different oppositely charged proteins or polymers [11-16, 19]. For example, poly(ethylenimine) (PEI), a cationic polymer, was used to pre-treat alumina templates, followed by the alternate adsorption of poly-(sodium styrenesulfonate) (PSS) and cytocrome c to investigate the use of cytochrome c nanotubes for biosensor and enzymatic bioreactor applications [15]. Similarly, PEI was used to pre-treat polycarbonate templates, followed by the alternate adsorption of poly(acrylic acid) (PAA) or PSS and poly(allylamine hydrochloride) (PAH) [16], and chitosan (CHI) and alginate (ALG) were alternately adsorbed onto alumina

templates to form ALG/CHI nanotubes [12]. Only a few of these studies have demonstrated the ability to fabricate single component nanotubes with human serum albumin (HSA) using the layer-by-layer method [13,14].

In this paper we report our efforts towards the fabrication of single component avidin nanotubes based on the previously published layer-by-layer electrostatic assembly of HSA nanotubes [13,14]. We investigate the use of template pre-treatment methods, i.e. covalent bonding via GA and the use of a cationic polymer PEI, to strengthen the attraction between the initial avidin layer and the AAO template to achieve mechanically stable structures. In addition, we demonstrate the fabrication of glucose oxidase/avidin nanotubes using template pre-treatment with GA in conjunction with electrostatic layer-by-layer assembly.

Avidin was chosen to be the main component of our nanostructures due to its many attractive qualities. Avidin is a highly stable glycoprotein found in egg white and is well known for its strong binding affinity for biotin. Avidin consists of four identical subunits each of which have one biotin binding site [20,21]. Avidin is a positively charged protein at neutral pH and has an isoelectric point of approximately 10 [21]. It is speculated that these properties may be responsible for the ability of avidin to localize rapidly within intraperitoneal tumors [21,22]. This unique ability combined with the biotin binding properties of avidin make it a highly desirable protein for the delivery of drugs or therapeutic genes to tumors.

EXPERIMENTAL

Materials

AAO membranes (13 mm) were purchased from SPI supplies with an average pore diameter of approximately 200 nm and thickness of 60 um. The PEI, glucose oxidase, avidin, 3-amino propylphosphonic acid (APA), and GA were purchased from Sigma. All chemicals were used as received without further purification.

Template Pre-treatment

AAO templates were pre-treated using two different methods aimed to enhance the binding of the initial protein layer to the template by either covalent crosslinking or electrostatic adsorption.

To covalently crosslink the initial protein layer, the AAO templates were sputter coated with Au/Pd and immersed in a 5 mM solution of APA at pH 5.8 for 24 hours. After washing with 0.01 M phosphate buffer solution (PBS), the templates were immersed in a solution of 2.5% GA in PBS for 12 hours. This process functionalizes the inner nanopore walls with aldehyde groups that can easily bind the free amino groups of proteins.

To electrostatically absorb the initial protein layer, the AAO templates were immersed in a 10 mg/mL solution of PEI (pH adjusted to 3 using concentrated HCl) for 1 hour. This process coats the nanopore walls with a thin film of cationic polymer giving them a net positive charge.

Layer-by-Layer Assembly

Avidin nanotubes were fabricated using untreated, PEI pre-treated, and APA and GA pre-treated AAO templates. For both of the pre-treated templates, PBS was first filtered through the template, followed by an avidin solution in a phosphate buffer with basic pH. At a basic pH that is above avidin's isoelectric point the avidin molecules carry a net negative charge. This net negative charge will enable electrostatic binding with the cationic PEI pre-treated template. The net charge of the first avidin solution filtered through the APA and GA pre-treated templates is not important because the binding will be covalent and will utilize free amine groups. Following the alkaline solution, an avidin solution in phosphate buffer with acidic pH was filtered through the template. At an acidic pH that is below avidin's isoelectric point the avidin molecules carry a net positive charge. For the untreated AAO templates, the acidic avidin solution was filtered through before the basic avidin solution, because the AAO templates are negatively charged. The filtration of PBS and the two oppositely charged avidin solutions was repeated to build up the nanotube wall thickness. During this study we evaluated different experimental parameters including the pH of the acidic and basic buffer solutions, the filtration method (vacuum or syringe filtration), avidin concentration, volume of solution, and number of fabrication steps. The experimental matrix we evaluated is given in table 1.

Table 1: Experimental matrix showing the fabrication conditions for avidin nanotubes

Method of Filling	Template Pre-treatment	Acidic pH	Basic pH	Acidic Charge	Basic Charge	Conc.	Vol. per area*	Filtration Steps
vacuum filtration	untreated	5	12	+ 10.3 mV	- 12.3 mV	1 mg/mL	0.002 mL/mm^2	5
vacuum filtration	untreated	5	12	+ 10.3 mV	- 12.3 mV	1 mg/mL	0.004 mL/mm^2	5
vacuum filtration	untreated	3	12	+ 19.8 mV	- 7.1 mV	4 mg/mL	0.015 mL/mm^2	3
syringe filtration	untreated	3	12	+ 19.8 mV	- 7.1 mV	4 mg/mL	0.008 mL/mm^2	4
vacuum filtration	PEI	8	12	+ 7 mV	- 12.3 mV	1 mg/mL	0.002 mL/mm^2	10
vacuum filtration	PEI	3	12	+ 23.1 mV	- 12.3 mV	1 mg/mL	0.002 mL/mm^2	10
soaking	PEI	3	12	+ 23.1 mV	- 12.3 mV	1 mg/mL	0.008 mL/mm^2 for 1hr	-
vacuum filtration	APA + GA	3	12	+ 23.1 mV	- 12.3 mV	1 mg/mL	0.002 mL/mm^2	5

* Volume of solution filtered per surface area of the AAO template

Glucose oxidase/avidin nanotubes were fabricated using untreated and APA and GA pre-treated AAO templates. For both templates, 200 μL of each PBS, glucose oxidase (1 mg/mL in PBS pH 7), and avidin (1 mg/mL in PBS pH 7) were sequentially vacuum filtered through the templates. The filtration of PBS and the two proteins was repeated 15 times to build up the nanotube wall thickness.

The AAO templates were dissolved using NaOH or H_3PO_4 solutions of different concentrations to determine the most suitable solvent to maintain protein structure and bioactivity. After template dissolution the nanotubes were collected by vacuum filtration on a polycarbonate filter with 50 nm diameter pores. The nanotubes were washed several times with PBS and sonicated to disperse them for transmission electron microscopy (TEM) sample preparation.

Characterization

Nanotube morphology was characterized using scanning electron microscopy (SEM) and TEM. The nanotube samples were sonicated to disperse them for TEM sample preparation.

UV-vis spectrometry was used to evaluate avidin stability in the acidic and basic buffer solutions. The UV-vis spectra were obtained using a Genesys 10UV scanning spectrophotometer from Thermo Electron. Zeta potential was used to measure avidin charge in the acidic and basic buffer solutions. Zeta potential was measured using a ZetaSizerNano from Malvern.

RESULTS AND DISCUSSION

Avidin nanotubes

In order to determine the optimum solution conditions for the fabrication of our single component avidin nanotubes, we used UV-vis absorption to verify the stability and secondary structure of avidin in highly acidic and basic solutions [8] and used zeta potential to verify that avidin would be oppositely charged in solutions above and below the isoelectric point and to determine the optimum solution concentration for maximum charge density. The UV-vis spectra obtained for for avidin solutions with pH values of approximately 3, 5, 9 and 12 is shown in Figure 1.

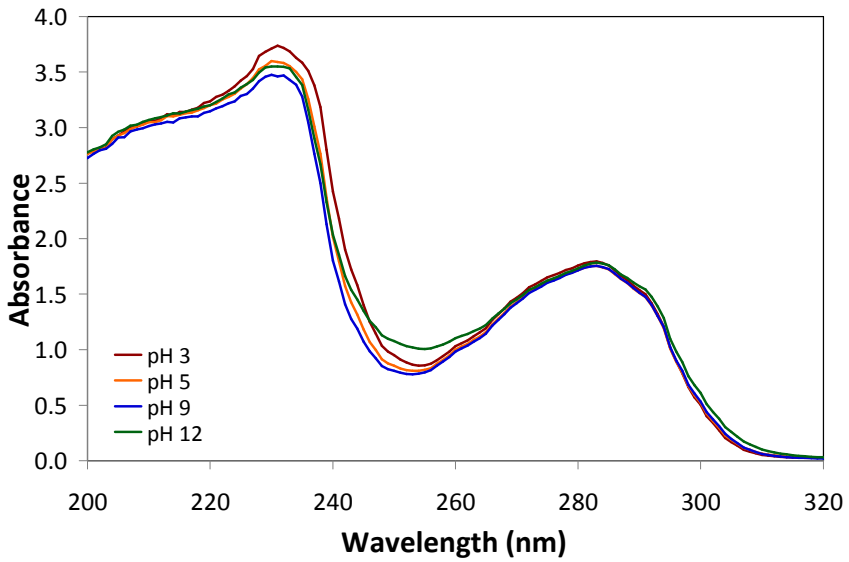

Figure 1. UV spectra of 1 mg/mL avidin solutions at pH 3, 5, 9 and 12.

When avidin is denatured in acidic solutions, the tryptophan residues present in the molecule become exposed and cause an increase in the absorbance at 233 nm [25]. Figure 1 shows that

avidin at pH 3 has the highest absorbance at 233 nm and may be slightly denatured. Despite this observation, it was demonstrated previously by Green [25] that avidin does not completely and irreversibly denature until pH values less than 2. When avidin is denatured in basic solution, the tyrosine residues present in the molecules are ionized and cause an increase in the absorbance at 246 nm [25]. Again, this increase is observed in our UV-vis spectrum, showing that some of the tyrosine was ionized at pH 12 and this result was also demonstrated by Green in alkaline solutions [25]. Through reverse titrations, Green demonstrated that after exposure to a high pH of approximate 13, avidin showed only 5-10% inactivation depending on the duration of the high pH exposure [25]. Green's work confirms that use of buffer solutions up to pH 13 could potentially be used for our proposed electrostatic layer-by-layer assembly process. Both Green's work with avidin under extreme pH conditions [25] and our UV-vis spectrum, shown in figure 1, demonstrate that pH values within the range of 3 to 12 could be used without significant concern for avidin stability.

The zeta potential of avidin was measured as a function of buffer solution pH and avidin concentration in order to determine the optimum solution properties for electrostatic binding. Figure 2 shows the zeta potential as a function of pH for 0.5 and 1 mg/mL avidin solutions. Below pH 5 and above pH 9 it can be seen that the zeta potential changes significantly with small changes in pH.

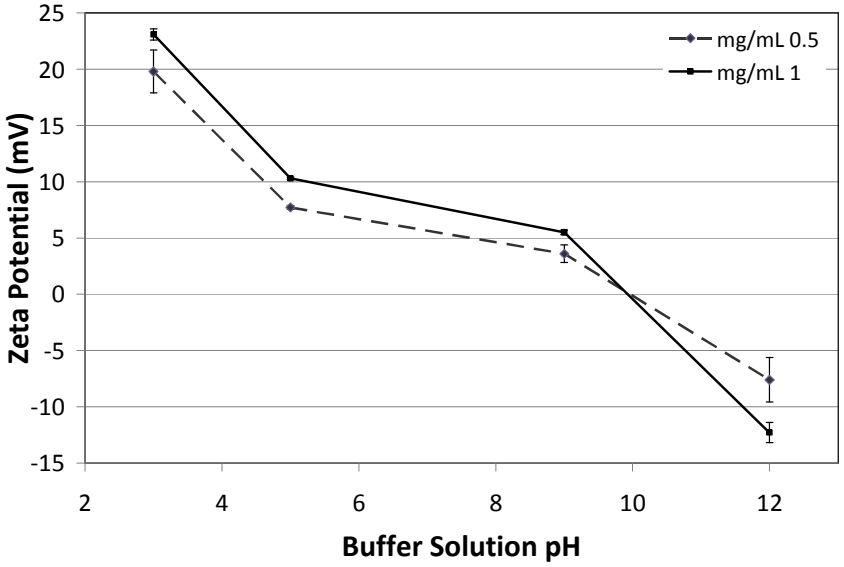

Figure 2: Zeta potential of 0.5 mg/mL and 1 mg/mL avidin solutions as a function of buffer pH. The error bars as given by the standard deviation of 3 measurements.

We chose to use solution pH values of 3, 5 and 8 below the isoelectric point and a solution pH of 12 above the isoelectric point. We chose to use only one basic pH value because of the limited range of pH values above the isoelectric point where avidin is stable. We chose our acidic pH values for the following reasons: pH 8 is two pH values below the isoelectric point and was chosen to correspond to the basic pH of 12, which is two pH values above the isoelectric point, pH 5 has an approximately equal but opposite zeta potential value as the pH 12 solution, and pH 3 was chosen because it is the lowest pH value possible to maintain stability and give the maximum positive charge. The data presented in figure 2 also show that the zeta potential is influenced by the solution concentration. The zeta potential for the lower solution concentration (0.5 mg/mL) showed a smaller positive charge for all pH values below the isoelectric point and a smaller negative charge for all pH values above the isoelectric point in comparison with the higher solution concentration (1 mg/mL). This observation led us to measure the zeta potential at a higher solution concentration to see if the upward trend would continue.

The zeta potential is shown in Figure 3 as a function of solution concentration for avidin in pH 12 and pH 3 phosphate buffer solutions.

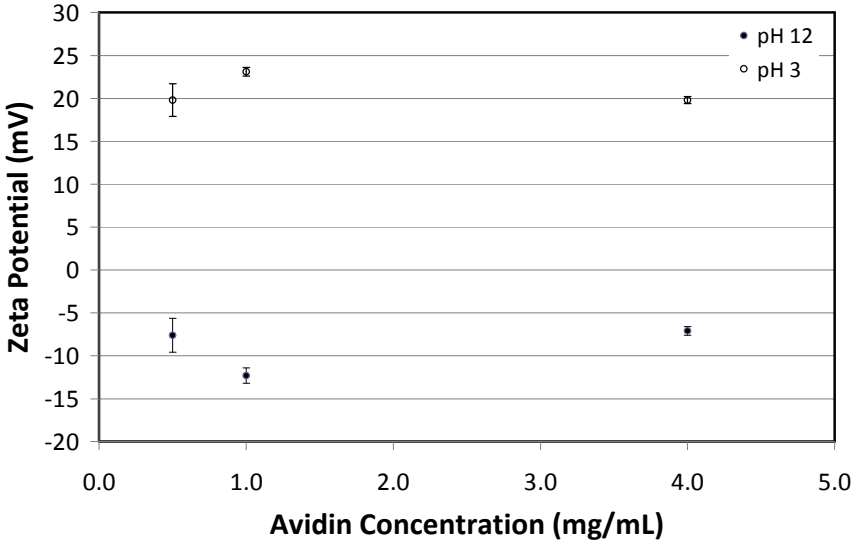

Figure 3: Zeta potential as a function of solution concentration for pH 3 and pH 12 buffer solutions. The error bars are given by the standard deviation of 3 measurements.

We find that increasing the avidin concentration from 1 mg/mL to 4 mg/mL actually decreases the absolute positive and negative charge observed for our two extreme pH 3 and pH 12 solutions respectively. Therefore we chose to use an avidin concentration of 1 mg/mL for the majority of our fabrication efforts for the largest net charge of avidin, but also chose to experiment with a concentration of 4 mg/mL to investigate the effect of an increased number of protein molecules per unit volume.

The layer-by-layer electrostatic assembly of avidin nanotubes was first attempted using untreated AAO templates. This method was adapted based on the results published by Lu et al. [13,14] who demonstrated the fabrication of HSA nanotubes by alternating the filtration of oppositely charged HSA solutions at pH values of 3.8 and 7.0 through AAO templates. Similarly, we alternately filtered oppositely charged avidin solutions through AAO templates according to the condition given in table 1. After several fabrication attempts using a variety of different conditions, the SEM and TEM results we obtained revealed that we were not able to make avidin nanotubes. An SEM image of a partially etched untreated AAO template after 5 avidin filtration steps using pH 3 and pH 12 and etched with 10% H_3PO_4 is shown in figure 4a. The nanopores of the original AAO template are very obviously observed as well as some material on the surface which may be avidin. Although the image shown in figure 4a corresponds to one particular set of experimental conditions, it is representative of the results obtained for all experimental trials using untreated templates detailed in table 1. We did not find any nanostructures during our TEM characterization. We hypothesize that our unsuccessful attempt may be the result of a weakly absorbed initial avidin layer. It may be possible that the electrostatic attraction between the negatively charged untreated AAO template and positively charged avidin in solution is not strong enough to form a continuous, uniform initial layer. Without a strongly bound and continuous initial layer, the subsequent layers will also have weak interactions and will hinder the electrostatic assembly of multiple layers needed form our desired nanotube structures.

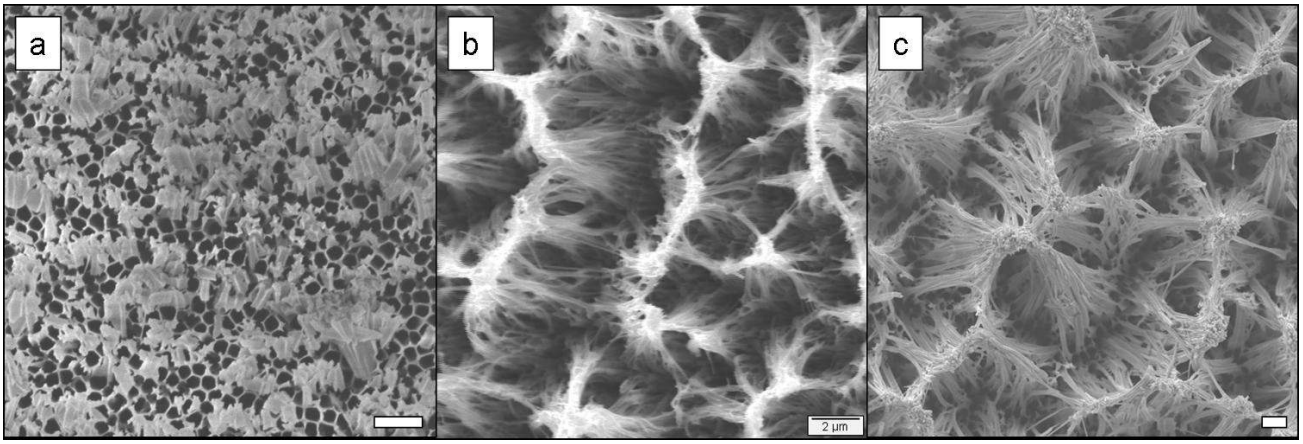

Figure 4: SEM images of AAO templates after partial etching with 10% H_3PO_4 for ~3hrs: a.) untreated AAO templates after 5 avidin filtration steps (scale bar = 1µm), b.) AAO templates pre-treated with APA and GA after 5 avidin filtration steps, c.) AAO templates pre-treated with PEI after 5 avidin filtration steps (scale bar = 1µm).

To investigate whether our problem is partly do the continuity and uniformity of the adsorbed layers, we filtered two avidin solutions (1 mL, 4 mg/mL, pH 3 and 1 mL, 4 mg/mL, pH 12) through the AAO template 4 times and measured the absorbance of the two solutions after each filtration step to see if the concentration of the avidin solutions decreased. Figure 5 shows the absorbance at 295 nm for the two avidin solutions after each of the 4 filtration steps. The same solution was reused after each filtration step.

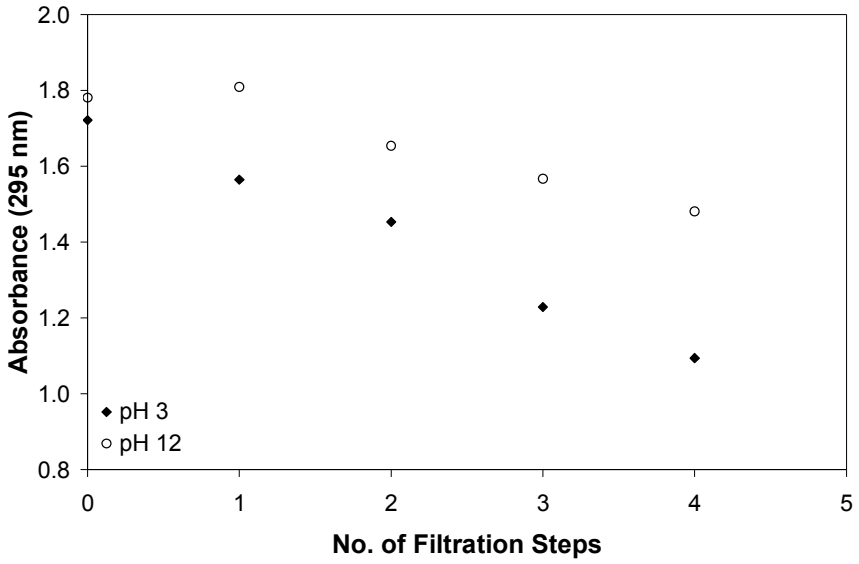

Figure 5: Graph showing the absorbance of avidin solutions (1 mL, 4 mg/mL, pH 3 and 1 mL, 4 mg/mL, pH 12) after a total of 4 consecutive filtration steps.

The absorbance for the pH 3 solution decreased from its initial value at 1.722 which corresponds to a concentration of approximately 4 mg/mL down to 1.094 after the 4th filtration step, which corresponds to a concentration of approximately 1.6 mg/mL. The absorbance for the pH 12 solution initially increased from 1.781 to 1.809 after the first filtration step, which suggests that some of the avidin deposited during the 1st pH 3 filtration step was unattached and washed out with the pH 12 solution. After the second filtration step, the absorbance of the pH 12 solution decreased, and continued to decrease for the remaining filtration steps down to 1.481 after the 4th filtration step and corresponds to a concentration of approximately 2.9 mg/mL. Overall, these results suggest that the initial avidin layer deposited at pH 3 is only weakly attached to the AAO template as we hypothesized. However, our results also suggest that avidin is deposited within the AAO template during the subsequent filtration steps. Our inability to obtain SEM and TEM evidence to demonstrate that the deposited avidin layers form nanostructures within the AAO templates further supports our hypothesis that the deposition and filling of the protein is discontinuous and not uniform.

This led us to explore template pre-treatment methods to strengthen the initial attraction between the AAO template and avidin. We employed two different template pre-treatment

methods; covalent crosslinkers or a cationic polymer. The first pre-treatment method we investigated was to use the covalent crosslinkers APA and GA to initially functionalize the inner walls of the AAO template with aldehyde groups for covalent attachment of the initial protein layer. This pre-treatment method was chosen based on our previous experience using it to demonstrate glucose oxidase nanocapsules [18]. Again, after 5 avidin filtration steps through the APA and GA pre-treated templates we did not find any nanostructures during our TEM characterization. However, our SEM investigation revealed some collapsed and apparently mechanically weak nanostructures protruding from our partially etched AAO templates, which can be seen in figure 4b.

Our second pre-treatment method, using PEI a cationic polymer, to give the AAO template an initially positive charge, was chosen based upon its use in literature as the first layer for the layer-by-layer electrostatic assembly of alginate/chitosan [12] and cytochrome c/PSS [15] nanotubes within nanopores. Both studies showed convincing SEM and TEM images of their protein nanostructures. When we used PEI to pre-treat our templates, however, we observed SEM and TEM results that were similar to our APA and GA pre-treated templates; partially collapsed and mechanically weak nanostructures via SEM, shown in figure 4c, and no nanostructures observed via TEM. The difference between our attempt to fabricate protein nanotubes within PEI pre-treated templates and those presented in literature [12,15] was the use of a single protein at different pH values rather than two different oppositely charged proteins or polyelectrolytes.

The results obtained for both pre-treatment methods led us to the hypothesis that our fabrication approach has not been successful because alternating solutions of different pH may cause some charge reversal of the already adsorbed proteins resulting in the deposition of protein layers that are not uniform or complete. The non-uniformity and discontinuous nature of the protein layers that we deposited may explain why we observed some collapsed and mechanically weak structures via SEM, but then nothing via TEM after the AAO template is completely removed. After complete removal of the AAO template, the avidin layers no longer have any mechanical support and may fall apart. Additionally the sonication that is necessary to disperse the nanotubes for TEM may contribute further to the break down of any weak nanostructures that may have been formed.

After several unsuccessful attempts to demonstrate conclusive SEM and TEM evidence of avidin nanotubes using untreated AAO templates and two different pre-treatment methods in conjunction with our electrostatic layer-by-layer assembly method, we returned to our literature review to re-examine the papers upon which this study was based. Since we adapted our experimental method based on previous established and published methods, we expected to observe mechanically stable, thick walled nanostructures like those presented for single component HSA nanotubes [13,14]. The SEM images presented in figure 4 clearly show that this was not the case. Paying closer attention to the details presented in previously published works, we discovered that we overlooked an important step in the SEM sample preparation described by Lu et al. [14]. Before dissolving their AAO templates, they fixed them on silicon wafers using epoxy resin. Epoxy is a two component polymer system that is initially liquid and hardens after the two components are mixed. Our previous experience with polymer solutions and template wetting [26,27] led us to the hypothesis that Lu et al may have filled their AAO templates with epoxy in addition to protein. To test this hypothesis, we fixed an empty AAO template to a silicon wafer using commercially available superglue (Elmer's Instant Krazy Glue). After partially etching the AAO template, we observed superglue nanotubes, shown in figure 6, which are remarkably similar to those presented in Lu et al's publications [13,14]. Although superglue is a low viscosity cyanoacrylate and epoxy resins, in comparison, are much more viscous we still expect the epoxy to wet the AAO template in a similar fashion. It should also be noted that TEM images of the alleged HSA nanotubes are not shown in either publication, raising serious doubts regarding the fabrication of mechanically stable, purely protein nanotubes. Given the similarity of the SEM images and lack of TEM evidence it would be difficult to claim that the nanotubes presented by Lu et al. are pure protein nanotubes without epoxy. The combination of this new evidence and our unsuccessful fabrication attempts, indicate that we cannot draw any real conclusions regarding the feasibility of this fabrication approach for single component protein nanotubes.

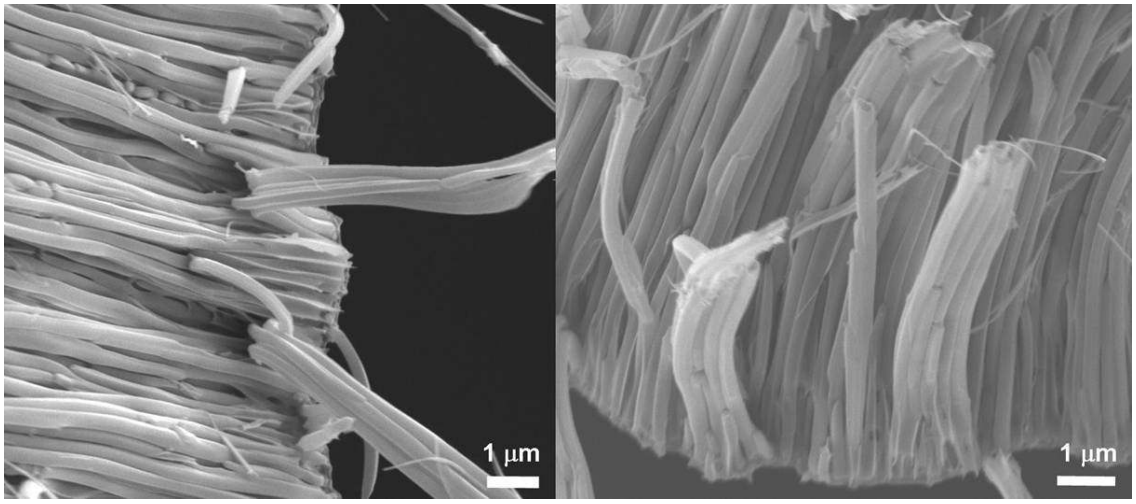

Figure 6: SEM images of superglue nanotubes fabricated by fixing initially empty AAO templates to silicon wafers with superglue (template wetting).

Glucose oxidase/avidin nanotubes

To test our hypothesis regarding the use of two different oppositely charged proteins for electrostatic assembly, we proceeded to fabricate glucose oxidase/avidin nanotubes using layer-by-layer electrostatic assembly in conjunction with APA and GA pre-treated AAO templates. Since glucose oxidase has an acidic isoelectric point (pH 4.2) and avidin has a basic isoelectric point (pH 10), when they are in a neutral buffer solution they possess an opposite net charge which enables electrostatic binding. We again chose to use APA and GA to pre-treat our AAO templates based on our previous work [18]. TEM images of the glucose oxidase/avidin nanotubes are shown in figure 7.

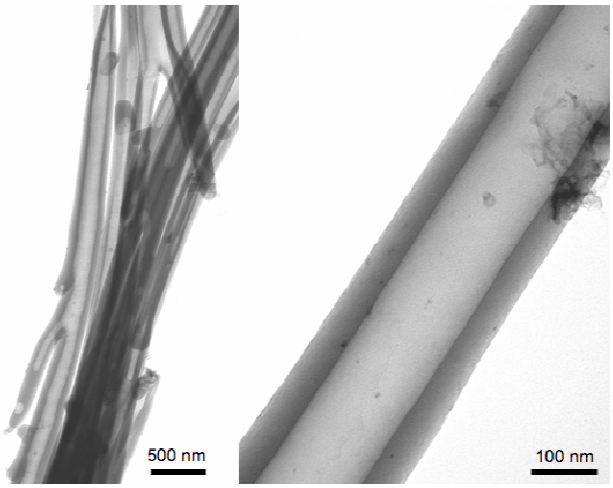

Figure 7: TEM images of glucose oxidase/avidin nanotubes fabricated by electrostatic layer-by-layer assembly using an APA and GA pre-treated AAO template.

This demonstrates that layers of oppositely charged proteins, glucose oxidase and avidin, can be built up electrostatically within the pre-treated nanopores. This result supports the claims made in previously published studies regarding the feasibility of layer-by-layer electrostatic assembly within nanopores [11-16, 19].

Careful examination of the thickness of the protein nanotube walls using the image processing software imageJ [23] reveals that the average wall thickness (measured in 15 different places) is 55.3±9.3 nm. Based on the size of a glucose oxidase molecule (approximately 5.5 x 7 nm) [18] and an avidin molecule (approximately 5.5 x 6 x 4 nm) [24] an average nanotube wall thickness of 55.3 nm could only accommodate approximately 5 layers of each glucose oxidase and avidin. Therefore, we hypothesize that each of the 15 vacuum filtration steps employed to fabricate these nanostructures still did not deposit full protein layers within the AAO template despite the use of different oppositely charged proteins. This might be due to the small volume of the solution we used. The TEM images of our glucose oxidase/avidin nanotubes, shown in figure 7, demonstrate that even with small filtration volumes we were still able to build up relatively thick nanotube walls electrostatically by using two proteins that were oppositely charged at pH 7 to make mechanically stable protein nanostructures.

CONCLUSIONS

In conclusion, we have reported several hypotheses regarding our unsuccessful attempts to fabricate single component avidin nanotubes using a layer-by-layer electrostatic assembly method adapted from literature. Additionally, we have shown there to be a critical problem with the preparation of the SEM samples of the single component HSA nanotubes upon which our method was adapted. This issue prevents meaningful conclusions from being drawn regarding the feasibility of electrostatic layer-by-layer assembly to fabricate single component protein nanotubes. Despite our unsuccessful attempts with single component avidin nanostructures, we were able to successfully demonstrate a method to fabricate glucose oxidase/avidin nanostructures using layer-by-layer electrostatic assembly in conjunction with APA and GA template pre-treatment.

REFERENCES

[1] Martin C R and Kohli P 2003 The emerging field of nanotube biotechnology *Nature Reviews Drug Discovery* **2** 29–37

[2] Baker L A, Jin P and Martin CR 2005 Biomaterials and biotechnologies based on nanotube membranes *Crit. Rev. Solid State Mater. Sci.* **30** 183–205

[3] Mitchell D T, Lee S B, Trofin L, Li N, Nevanen T K, Soderlund H and Martin C R 2002 Smart nanotubes for bioseparations and biocatalysis *J. Am. Chem. Soc*. **124** 11864-5

[4] Azamian B R, Davis J J, Coleman K S, Bagshaw C B and Green M L 2002 Bioelectrochemical single-walled carbon nanotubes *J. Am. Chem. Soc* **124** 12664–5

[5] Son S J, Bai X, Nan A, Ghandehari H and Lee S B 2006 Template synthesis of multifunctional nanotubes for controlled release *J. Am. Chem. Soc.* **114** 143-52

[6] Champion J A and Mitragotri S 2008 Shape induced inhibition of phagocytosis and polymer particles *Pharmaceutical Research* **26** 244-9

[7] N. Nishiyama 2007 Nanocarriers shape up for long life *Nature nanotechnology* **2** 203-4

[8] Geng Y, Dalhaimer P, Cai S, Tsai R, Tewari M, Minko T and Discher D E 2007 Shape effects of filaments versus spherical particles in flow and drug delivery *Nature nanotechnology* **2** 249-55

[9] Lee S B, Mitchell D T, Trofin L, Nevanen T K, Soderlunc H and Martin C R 2002 Antibody-based bio-nanotube membranes for enantiomeric drug separations *Science* **296** 2198-200

[10] Ariga K, Hill J P and Ji Q 2007 Layer-by-layer assembly as a versatile bottom-up nanofabrication technique for exploratory research and realistic application *Phys. Chem. Chem. Phys.* **9** 2319–40

[11] Liang Z, Susha A S, Yu A and Caruso F 2003 Nanotubes prepared by layer-by-layer coating of porous membrane templates *Adv. Mater.* **15** 1849-53

[12] Yang Y, He Q, Duan L, Cui Y and Li J 2007 Assembled alginate/chitosan nanotubes for biological application *Biomaterials* **28** 3083-90

[13] Lu G, Tsuchida E and Komatsu T 2008 Human serum albumin nanotubes comprising layer-by-layer assembly with polycation *Chemistry Letters* **37** 972-3

[14] Lu G, Ai S and Li J 2005 Layer-by-layer assembly of human serum albumin and phospholipid nanotubes based on a template *Langmuir* **21** 1679-82

[15] Tian Y, He Q, Cui Y and Li J 2006 Fabrication of protein nanotubes based on layer-by-layer assembly *Biomacromolecules* **7** 2539-42

[16] Ai S, Lu G, He Q and Li J 2003 Highly flexible polyelectrolyte nanotubes *J. Am. Chem. Soc.* **125** 11140-1

[17] Hou S, Wang J and Martin C R 2005 Template-synthesized protein nanotubes *Nano Lett.* **5** 231-4

[18] Dougherty S, Liang J, and Kowalik T 2009 Template-assisted fabrication of protein nanocapsules *J. Nanopart. Res.* **11** 385-94

[19] Qu X, Lu G, Tsuchida E and Komatsu T 2008 Protein nanotubes comprised of an alternate layer-by-layer assembly using a polycation as an electrostatic glue *Chem. Eur. J.* **14** 10303-8

[20] Diamandis E and Christopoulos T 1991 The biotin-(strept)avidin system: Principles and applications in biotechnology *Clin. Chem.* **37** 625-36

[21] Sakahara H and Saga T 1999 Avidin-biotin system for delivery of diagnostic agents *Adv. Drug Del. Rev.* **37** 89–101

[22] Yao Z, Zhang M, Sakahara H and Saga T 1998 Avidin targeting of intraperitoneal tumor xenografts *J. National Cancer Inst.* **90** 25–29

[23] imageJ software: http://rsb.info.nih.gov/ij/

[24] Caruso F, Furlong D N, Niikura K, and Okahata Y 1998 In-situ measurement of DNA immobilization and hybridization using 27 MHz quartz crystal microbalance. *Colloids and Surfaces B:* Biointerfaces **10** 199-204

[25] Green N M 1963 Avidin: Stability at extremes of pH and dissociation into sub units by guanidine hydrochloride *J. Biochem*. **89** 609-20

[26] Dougherty S and Liang J 2009 Fabrication of segmented nanofibers by template wetting of multilayered alternating polymer thin films *J. Nanopart. Res.* **11** 743-7

[27] Dougherty S and Liang J Core-shell polymer nanorods by a two-step template wetting process *Submitted to Nanotechnology*

Paper 3: Fabrication of Segmented Nanofibers by Template Wetting of Multilayered Alternating Polymer Thin Films

Published in Journal of Nanoparticle Research (2009) 11:743-747

S. Dougherty and J. Liang

ABSTRACT

Segmented polystyrene (PS) and poly(methyl methacrylate) (PMMA) nanofibers were fabricated by wetting nanoporous alumina templates with multilayered polymer thin films. The order and thickness of the polymers within the thin films affected the resulting nanofiber morphology, PS and PMMA segment properties, and created unique core-shell structure in the PMMA segments. The core-shell structure suggests a complex wetting phenomenon. Fabrication of polymer nanostructures by wetting of layered thin films opens the arena of multifunctional, one-dimensional, polymer nanostructures with segments having individual and specific functionalities.

INTRODUCTION

One-dimensional nanostructures offer a wide range of opportunities for a number of scientific fields. The resemblance of nanofibers and nanotubes to pipes, cavities, capsules and wires and the ability to fabricate them from metals, semiconductors, ceramics, and polymers lend them to an endless number of potential applications [1]. The ability to fabricate polymer nanofibers and nanotubes is of particular interest because of the vast array of natural and synthetic polymers available. The utility of polymer nanostructures could be further exemplified with a technique to fabricate heterogeneous nanostructures with discrete and/or alternating segments that provide individual and specific functionalities. This concept has not yet been fully explored for one-dimensional polymer nanostructures. In this communication a variation of the well known template wetting approach is introduced to fabricate alternating, segmented nanofibers of polystyrene (PS) and poly-methylmethacrylate (PMMA) and opens the idea of polymer nanofibers with multiple, discrete, segmented functionalities to the scientific community.

Template wetting is a well established template-assisted nanofabrication approach for producing one-dimensional nanostructures [1,2]. It is easy, cost effective, and accommodates

almost all types of polymeric materials. High energy porous materials such as anodized aluminum oxide (AAO) or silicon are generally utilized for the wetting of low energy polymer melts [1,2]. Two wetting regimes can be achieved, complete wetting or partial wetting, to produce either nanotubes or nanofibers respectively. Complete wetting occurs when the interfacial driving force is high, causing a thin film of polymer to spontaneously form over the entire nanopore surface area in a very short span of time. Partial wetting, on the other hand, occurs when the interfacial driving force is low. With a low driving force, the polymer melt slowly travels up the nanopore channel is a plug via capillary force to form nanofibers. The formation of nanotubes versus nanofibers can be controlled by varying the melt temperature, which affects the polymer interfacial tension [3]. At temperatures only slightly above the polymer glass transition temperature (T_g), the polymer interfacial tension is high and nanofiber morphology is favored [3], as illustrated in Figure 1 (a) and (b), which show both a transmission electron microscope (TEM) and scanning electron microscope (SEM) image of PS nanofibers obtained by wetting an AAO template with a thin film of PS at 150^{o}C for 48 hours.

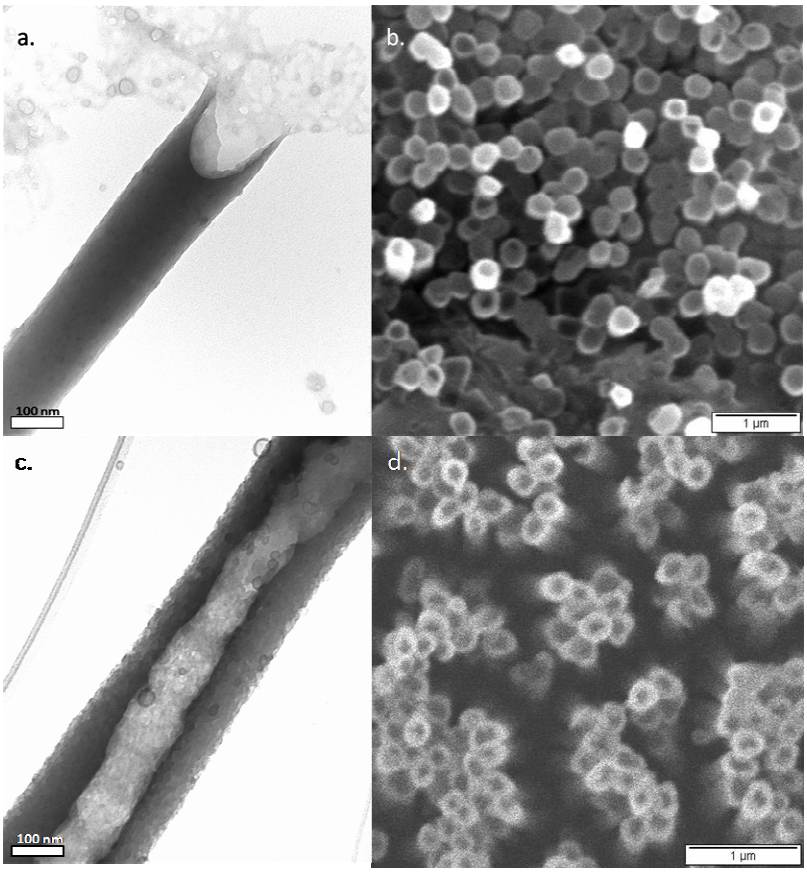

Figure 1: PS nanofibers fabricated by template wetting at 150^{o}C for 48 hrs. a.) TEM image showing completely filled nanofiber structure with meniscus. b.) SEM image showing the dimpled tips of nanofibers in a partially dissolved AAO template resulting from the formation of a meniscus in the nanopore. PS nanotubes fabricated by template wetting at 200^{o}C for 10 minutes. c.) TEM image showing the hollow center and wall of the nanotube. d.) SEM image showing the opened tips of nanotubes in a partially dissolved AAO template.

At temperatures much greater than the polymer T_g, the polymer interfacial tension is low and nanotube morphology is favored [3], as illustrated in Figure 1 (c) and (d), which show a TEM and SEM image of PS nanotubes obtained by wetting an AAO template with a thin film of PS at 210^{o}C for 10 minutes. These results indicate that there exists a certain wetting transition temperature for all polymers at which the wetting regime changes from partial to complete wetting [3]. In addition to melt temperature, the polymer interfacial tension is also a function of the polymer molecular weight and the interfacial driving force can be further affected by varying the pore diameter of the template [3].

Within the past 15 years a great amount of progress has been made by researchers to better understand the wetting of porous materials and utilize this phenomenon to create a wide array of functional nanomaterials. Steinhart et al. first demonstrated PS, poly-tetrafluoroethylene (PTFE), and PMMA nanotubes by template wetting and introduced the concept of adding functionality by preparing palladium/polymer composites through wetting with a solution of poly-L-actide (PLLA) and palladium(II) acetate [4]. Since the introduction of template wetting researchers have explored many different variations of this process to produce unique structures. One group fabricated PS nanofibers with partially exposed tips and hydrophilically functionalized them to create hydrophilic-tipped hydrophobic PS nanofibers [5], while others have experimented with co-polymer template wetting using PS-b-PMMA [6] and poly(vinylidene fluoride-trifluoroethylene) for energy transduction and information recording [7]. This process can even accommodate biodegradable polymers such as poly(ε-caprolactone) (PCL). PCL nanofibers were fabricated for biomedical applications in which controlled release is desired [8]. More recently a bidirectional template wetting [9], also referred to as face-to-face wetting [10], was introduced where both surfaces of the porous template are simultaneously

wetted. This variation was used to create one dimensional nanosturctures with two different materials to produce either a discrete interface or polymer gradient between the two polymers.

In this communication we introduce the idea of using multilayered polymer films to fabricate heterogeneous, segmented nanofibers via nanoporous template wetting. PS and PMMA were chosen as a model system. The thin film properties and interfacial energies associated with PS and PMMA have been extensively studied [11-13]. This knowledge helps to understand the unique morphology of our heterogeneous nanofibers. By wetting AAO templates with multilayered, alternating PS and PMMA films of different layer thicknesses we were able to fabricate nanofibers with distinct segments of PS and PMMA and achieve very unique core-shell morphology in the PMMA segments.

EXPERIMENTAL

Spincoating polymer thin films

PS (Mw =230,000) and PMMA (MW =120,000) were purchased from Sigma Aldrich. Polymer solutions were made by dissolving PS in toluene and PMMA in 2-Butanone. Polymer solutions were spin coated using a Laurell Technologies model WS-65OS-6NPP/LITE spin coater with speeds from 500 – 8000 RPM, total spin times of 60s and acceleration of 10,000 RPM. Films were coated onto 18 mm^2 glass coverslides. The thickness of the thin films was measured via UV-vis spectroscopy [14] using a Genesys 10UV scanning spectrometer.

Template wetting

Nanoporous AAO templates were purchased from SPI supplies. The AAO templates were 60 μm thick and had an average pore size of 200 nm. The AAO templates were placed on top of polymer thin films and the whole stack was heated to 150^{o}C by hotplate for 48 hrs. This temperature is 50^{o}C above the T_g of both PS and PMMA, which have T_gs of approximately 100^{o}C. After annealing and cooling to room temperature the polymer thin film was removed from the glass coverslip by soaking in DI water. Next the alumina was dissolved in 1M NaOH, leaving only the polymer nanomaterials. The nanofibers were collected by centrifuge, washed with DI water, and dispersed in ethanol by sonication.

Characterization with TEM

Nanofiber morphology was analyzed using transmission electron microscopy (TEM). Prior to imaging, the nanofiber coated TEM grids were stained using RuO_4, a well known gas phase stain which exclusively darkens PS [6, 15]. Briefly, $RuCl_3 \cdot 3H_2O$ (0.2 g) was added to a solution of NaOCl (10 mL) to form RuO_4. A small amount of this mixture was placed inside one chamber of a dual chamber glass container. The nanofiber TEM grid was place in the other chamber and exposed to the volatile RuO_4 for approximately 1 minute.

RESULTS AND DISCUSSION

A multilayered polymer thin film with 1 μm PMMA, 4 μm PS, 1 μm PMMA, 4 μm PS, and 1 μm PMMA layers was used to wet an AAO template with nanopores of 200 nm diameter. The polymer nanofibers were released from the AAO template by dissolution of the AAO in 1 M NaOH solution and collected by centrifugation. The PS segments of the nanofibers were darkened by staining with RuO_4. Characterization via TEM revealed distinct, dark PS segments ranging in length from 200 nm to 1 μm, shown in Figure 3a.

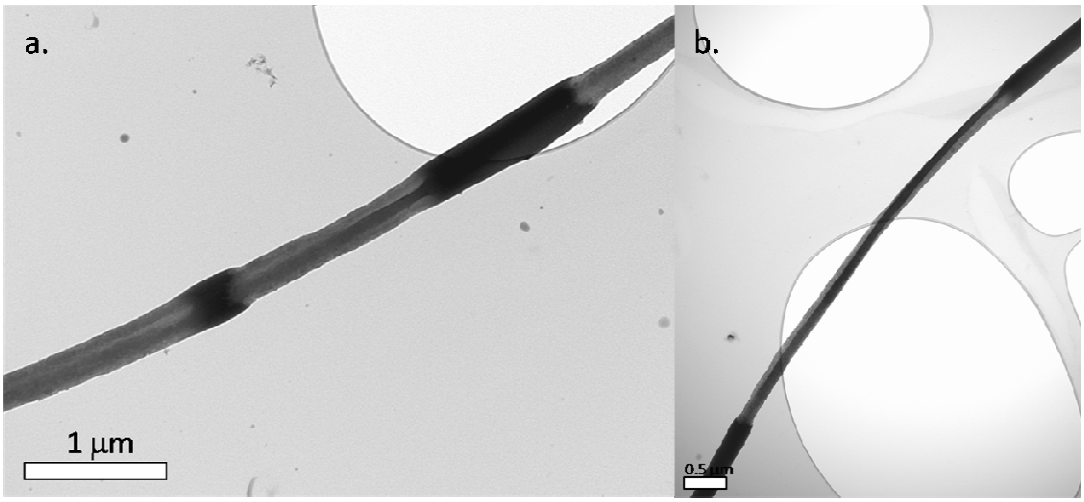

Figure 3: TEM images of segmented PS and PMMA nanofibers. a.) Shows the short and varied length of the PS segments. b.) Shows the length of the PMMA segments to be up to 5 μm. Darkened polymer segments are PS.

The PS segments appear to be slightly larger in diameter than the PMMA segments due to a combination of the volume expansion of PS during staining and the electron irradiation-induced thinning of PMMA during imaging [6, 11]. The PMMA segments were typically longer than the

PS segments with PMMA segment lengths up to 5 μm, shown in Figure 3b. This result was unexpected since the PS layers were 4 times thicker than PMMA layers. Conservation of material demands that the PS must be accounted for somewhere in or along the nanofiber. A closer look at the junction of the PS and PMMA segments reveals a unique core-shell morphology, shown in Figure 4.

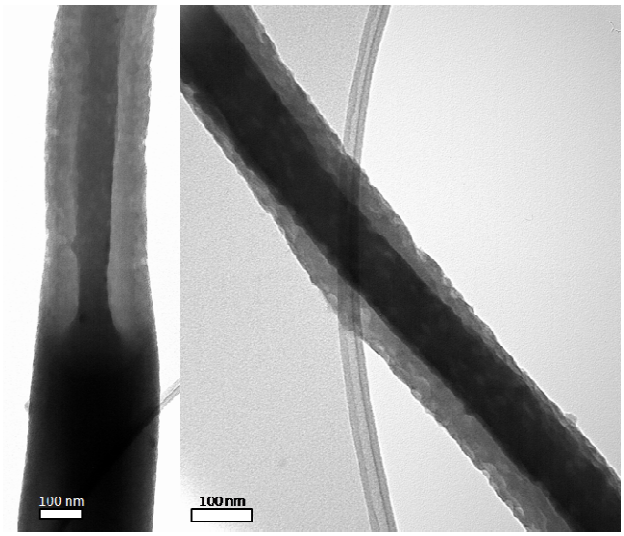

Figure 4: TEM images of segmented PS and PMMA nanofibers showing the core-shell morphology of the PMMA segments. Darkened polymer segments are PS.

It is shown that the PMMA segments have a PS core. This is understood based upon the behavior of PS and PMMA co-polymers and blends. PMMA is more polar than PS and has been shown to preferentially wet the hydrophilic metal oxides surfaces before PS [11, 12]. This results in the formation of the PMMA shell and PS core. The formation of core-shell morphology rather than a homogeneous segmented structure is due to a combination of the difference in PMMA and PS film thickness and the competitive interfacial driving forces present at the AAO template/polymer interface.

CONCLUSIONS

Heterogeneous, segmented PS and PMMA nanofibers with novel core-shell morphology have been fabricated via template wetting by multilayered, alternating PS and PMMA thin films. These unique structures offer great future opportunities including multifunctional nanofibers that

could theoretically be composed of any number of polymers with the desired functionalities and single polymer nanofibers with segments of different diameter by selectively dissolving the polymer shell in the core-shell segments. Our future work will explore the formation and controllability of core-shell segments and will experiment with the formation of segmented polymer nanofibers with both tube and fiber morphology by template wetting of multilayered, alternating polymer films for potential drug delivery and biosensor applications.

REFERENCES

[1] Steinhart M, Wehrspohn RB, Gosele U et al (2004) Nanotubes by template wetting: a modular assembly system. Angew Chem Int Ed 43:1334-1344

[2] Greiner A, Wendorff JH, Yarin AL et al (2006) Biohybrid nanosystems with polymer nanofibers and nanotubes. Appl Microbiol Biotechnol 71:387-393

[3] Zhang M, Dobriyal P, Chen J et al (2006) Wetting transition in cylindrical alumina nanopores with polymer melts. Nano Lett 6:1075-1079

[4] Steinhart M, Wendorff JH, Greiner A, et al (2002) Polymer nanotubes by wetting of ordered porous templates. Science 296:1997

[5] Moon SI, McCarthy TJ (2003) Template synthesis and self-assembly of nanoscopic polymer "pencils". Macromolecules 36:4253-4255

[6] Sun Y, Steinhart M, Zschech D et al (2005) Diameter-dependence of the morphology of PS-b-PMMA nanorods confined within ordered porous alumina templates. Macromol Rapid Commun 26:369-375

[7] Lau ST, Zheng RK, Chan HL et al (2006) Preparation and characterization of poly(vinylidene fluoride-trifluoroethylene) copolymer nanowires and nanotubes. Mater Lett 60:2357-2361

[8] Tao SL, Desai TA (2007) Aligned arrays of biodegradable poly(□-caprolactone) nanowires and nanofibers by template synthesis. Nano Lett 7:1463-1468

[9] Kriha O, Zhao L, Pippel E et al (2007) Organic tube/rod hybrid nanofibers with adjustable segment lengths by bidirectional template wetting. Adv Funct Mater 17:1327-1332

[10] Kriha O, Goring P, Milbradt M et al (2008) Polymer tubes with longitudinal composition gradient by face-to-face wetting. Chem Mater 20:1076-1081

[11] Sohn BH, Yun SH (2002) Perpendicular lamellae induced at the interface of neutral self-assembled monolayers in thin diblock copolymer films. Polymer 43:2507-2512

[12] Harris M, Appel G, Ade H (2003) Surface morphology of annealed polystyrene and poly(methyl methacrylate) thin film blends and bilayers. Macromolecules 36:3307-3314

[13] Walheim S, Boltau M, Mlynek J et al (1997) Structure formation via polymer demixing in spin-cast films. Macromolecules 30:4995-5003

[14] Huibers PD, Shah DO (1997) Multispectral determination of soap film thickness. Langmuir 13:5995-5998

[15] Trent JS, Scheinbeim JI, Couchman PR (1983) Ruthenium tetraoxide staining of polymers for electron microscopy. Macromolecules 16:589-598

Paper 4: Core-Shell Polymer Nanorods by a Two-step Template Wetting Process

Publication in Nanotechnology (2009) 20

S Dougherty and J Liang

Abstract

One-dimensional core-shell polymer nanowires offer many advantages and great potential for many different applications. In this paper we introduce a highly versatile two-step template wetting process to fabricate two-component core-shell polymer nanowires with controllable shell thickness. PLLA and PMMA were chosen as model polymers to demonstrate the feasibility of this process. Solution wetting with different concentrations of polymer solutions was used to fabricate the shell layer and melt wetting was used to fill the shell with the core polymer. The shell thickness was analyzed as a function of the polymer solution concentration and viscosity and the core-shell morphology was observed with TEM. This paper demonstrates the feasibility of fabricating polymer core-shell nanostructures using our two-step template wetting process and opens the arena for optimization and future experiments with polymers that are desirable for specific applications.

Introduction

One-dimensional (1D) nanostructures such as nanotubes and nanowires are receiving a great amount of attention for a variety of different applications including fluidics[1], purification[1], separation[1], gas storage[1], sensors[1-4], optoelectronic devices[2], catalysis[1,5], drug delivery[1,3,4,6], and tissue engineering[3,5-7]. Recently, the realization of core-shell nanowires [1-12], has further expanded the potential of 1D nanostructures because of the ability to incorporate separate functionalities within the core and the shell material to achieve novel properties [3]. The realization of nanocables that have conductive metallic cores, such as silver, and insulating shells, such as silica, has shown great potential for nanoelectronic devices [2]. Other examples include polymer core-shell nanofibers with cores loaded with metal nanoparticles for catalysis[4], core-shell polymer nanofibers with the incorporation of enzymes into the core for controlled catalytic processes[7], and the fabrication of water-soluble polyaniline (PANI) nanofibers wrapped in a schizophyllan coating for biological sensor

applications[3,9]. In addition, core-shell polythiophene/fullerene nanofibers have been fabricated to demonstrate that different charge transport behavior can be achieved for the core and shell materials and charge transport has been explored for polymer solar cell applications [10]**;** gold-PANI core-shell nano fibers have been fabricated for incorporation into solar-cell and OLED devices [11], and Si-CdSSe core-shell nanowires have been fabricated with continuously tunable band gap for light emission in the visible region [12].

To date, core-shell polymer nanowires have been fabricated using a co-electrospinning method [1,3-6]. In addition to co-electrospinning, traditional electrospinning has been employed to fabricate the nanofiber core material in conjunction with coating processes such as chemical or physical vapor deposition, spin coating, or spraying to coat the core nanofiber with a layered shell [4].

In this paper we describe the use of a template-assisted sequential solution wetting and melt wetting process to demonstrate the fabrication of heterogeneous core-shell polymer nanowires with adjustable shell thicknesses. Template wetting is a simple, low cost, and versatile nanofabrication method, which relies on capillary forces to draw polymer solutions or polymer melts into the nanochannels of nanoporous materials to form either nanotubes or nanowires [13-18]. The template wetting process has been exploited to fabricate a wide variety of heterogeneous nanostructures including segmented nanowires [19,20], copolymer nanowires and nanotubes [21,22], and nanotubes with longitudinal composition gradients [23]. In our exploration, anodized aluminum oxide (AAO) templates with hexagonally ordered nanopore arrays were used as the basic template to demonstrate the fabrication of poly(L-lactic acid) (PLLA)-poly(methyl methacrylate) (PMMA) core-shell nanowires using our novel two-step wetting process. PMMA was chosen as a model polymer for the nanowire shell because of its low cost and availability and PLLA was chosen in part for its low glass transition temperature in comparison with PMMA and based on our previous experiences with fabricating homogenous PLLA nanowires by melt wetting [24]. The importance of choosing a polymer for the core with a lower T_g than the shell polymer is discussed later. The sequential solution wetting and melt wetting approach that is proposed in this paper to fabricate core-shell polymer nanowires is not limited to the use of AAO as a template material or to the particular polymers used in this study. Our fabrication process is easily adapted to almost any type of nanoporous or microporous material, like AAO and silica, or lithographically fabricated nanochannel arrays and any

combination of polymers. In addition to versatility, our fabrication process also offers unprecedented control of the nanofiber morphology. The shell thickness can be controlled by the polymer solution properties used for the initial wetting step, the diameter can be controlled by the diameter of the nanochannels of the template, and the maximum length of the nanowires can be controlled by the thickness of the template material. For example, the diameter of the nanochannels of AAO templates is adjustable over a range of 20 nm – 300 nm and is controlled by the solution conditions used for electrochemical anodization and the thickness of AAO templates can range from tens of nanometers up to a few hundred microns and is controlled by the anodization time [25,26]. Figures 1a and 1b show SEM images of some of the pore sizes that can be achieved in our laboratory by varying the anodization conditions.

For the purposes of this proof-of-concept study, commercially available AAO membranes were used for our template material. Commercial AAO templates typically have less uniform pore diameters than the templates that can be fabricated in our laboratory. For this reason, we have included a graph, shown in figure 1e, illustrating the pore size distribution of the commercially available templates used for this pioneering work and examples of the templates that can be fabricated in our laboratory. The average pore size distribution was analyzed using the image processing software imageJ [27].

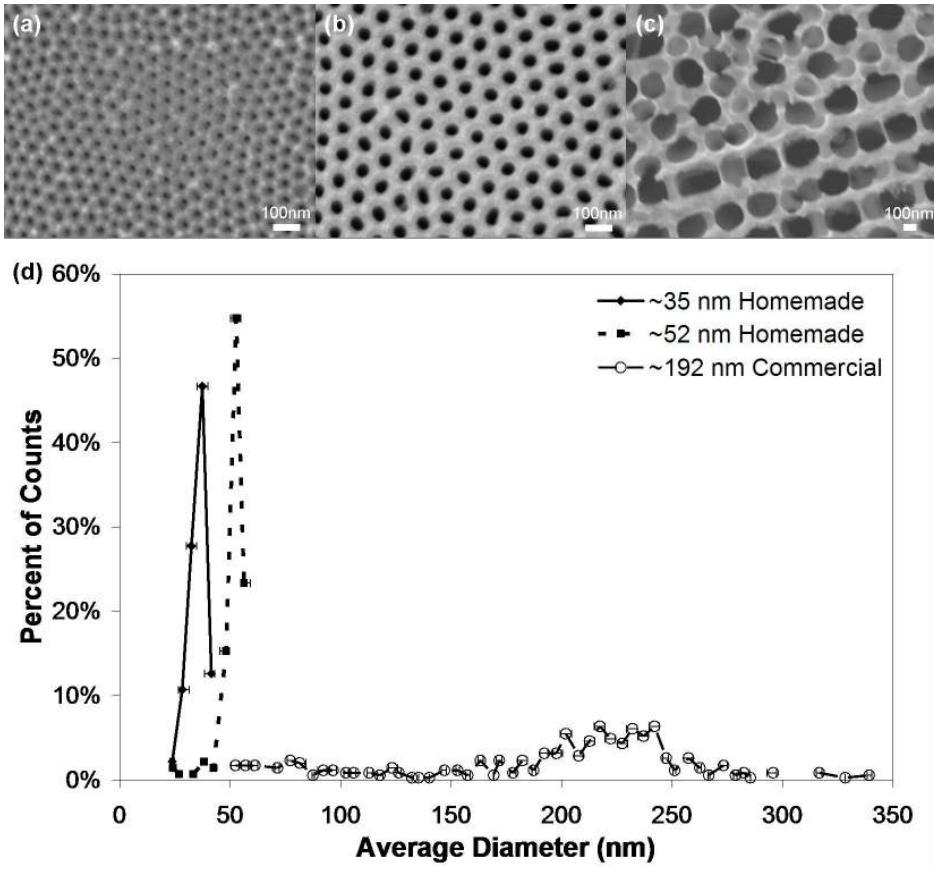

Figure 1: SEM images of AAO templates (a) homemade with average pore diameter of 35 nm (b) homemade with average pore diameter of 52 nm (c) commercial with average pore diameter of 192 nm and (d) graph showing the distribution of pore diameters for the homemade versus commercial templates.

Figure 1 shows that the pore diameter distribution is very large for the commercially available templates in comparison to the homemade templates. The templates in figures 1a, 1b, and 1c, were found to have average pore diameters of 35.3±4.4, 51.7±5.7, and 192±65 nm respectively. Although this wide distribution of pore diameters may affect the morphology of our nanostructures, we chose to use the commercial templates for convenience since this is a proof-of-concept study. Future process control and optimization experiments will utilize our homemade AAO templates.

Experimental

Materials

PLLA (Mw: 100,000 – 150,000 g/mol, T_g: 48.6^{o}C), PMMA (Mw: 996,000 g/mol, T_g: 105^{o}C) and methyl ethyl ketone (MEK) were purchased from Sigma Aldrich and used as received. Anodisc 13 commercial AAO templates with average pore diameter of ~190 nm were purchased from Whatman and used as received.

Template Wetting

AAO templates were wetted with 5%, 8%, 10%, or 15% PMMA solutions in MEK. The wetted templates were left overnight under ambient conditions to allow the solvent to evaporate. Following solution wetting, a thin film of PLLA was placed on top of the template and was heated on a hot plate at 100^{o}C for 2 hrs or 24 hrs. After the wetting steps, both sides of the AAO template were sanded to remove excess polymer from the surfaces and the AAO template was completely etched in 2M NaOH. The nanostructures were washed several times with DI water, and collected by centrifugation.

Analysis of Nanofiber Morphology

Nanofiber morphology was characterized with transmission electron microscopy (TEM). Our TEM samples were prepared using carbon coated copper grids. It was not necessary to stain the polymer nanowires before imaging because the PLLA core showed enough contrast without staining to differentiate the shell and core layers. Aspects of the core-shell nanofiber morphology, such as shell thickness, diameter, and length, were analyzed using the image processing software imageJ [27]. Shell thickness, in particular, was measured 10 times from multiple TEM images for each PMMA solution concentration and the average and standard deviations were reported.

Results and Discussion

Polymer core-shell nanowires were fabricated by a sequential solution wetting and melt wetting process. Solution wetting was used to deposit a thin film of polymer within the nanochannels of AAO templates to form the shell layer. Solution wetting was chosen to fabricate the shell layer because melt wetting does not offer as many process variables to control the morphology and is generally limited to high molecular weight polymers [18]. The thickness of the thin film formed by solution wetting depends upon solution properties such as solvent

quality, polymer molecular weight, and solution concentration [18] as well as template attributes such as nanopore diameter, surface energy of the nanochannels, and the aspect ratio of the nanochannels. For the purposes of this initial investigation, the shell thickness was varied by using different PMMA concentrations. All other variables that affect shell thickness were held constant and will be investigated in the future. Figure 2a shows a graph relating both the thickness of the PMMA shell and the natural log of the solution viscosity to the solution concentration. The PMMA shell thickness is reported as the average and standard deviation of 10 different measurements, as described in the experimental section.

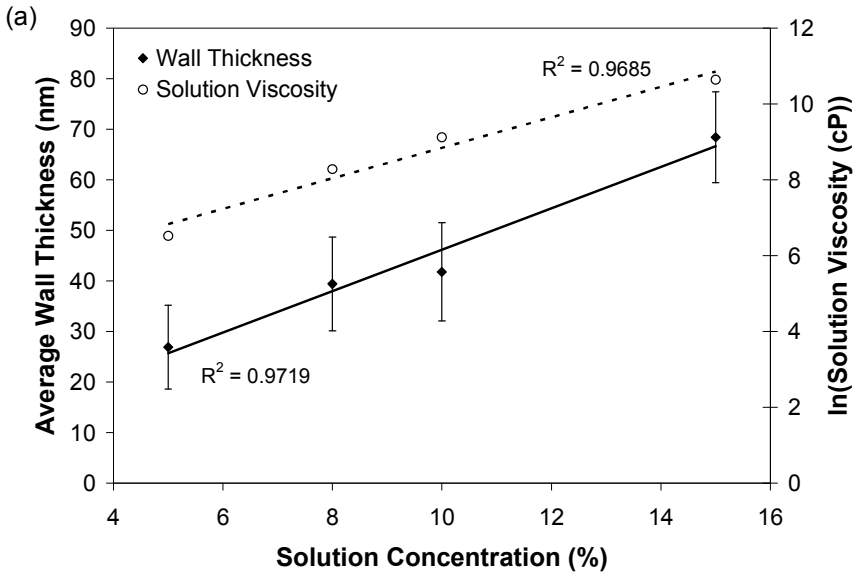

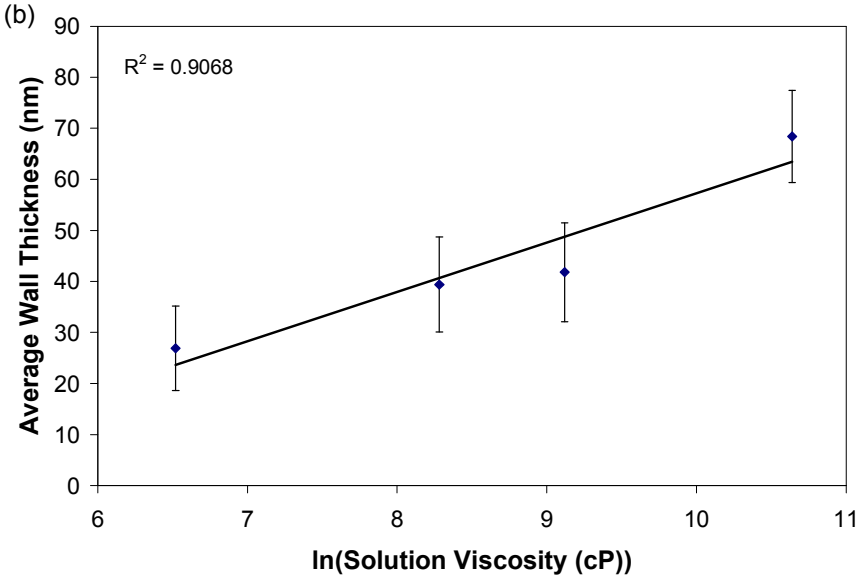

Figure 2: (a) Graph showing the average wall thickness of the PMMA shell and the natural log of the solution viscosity as a function of the PMMA solution concentration in MEK. (b) Graph showing the average wall thickness of the PMMA shell as a function of the natural log of the PMMA solution viscosity.

The calculated average wall thicknesses were found to have very large standard deviations. Based on other studies which have shown there to be a linear relationship between wall thickness and pore diameter [18], we expect that the wide range of pore diameters of the commercial AAO templates used for this study leads to the correspondingly wide range of wall thicknesses that we observed. Therefore, we attribute our large standard deviations to the wide pore diameter distribution that is observed for commercial AAO templates (figure 1). Future studies that will aim to optimize this process to achieve more control over the wall thickness will utilize homemade AAO templates which have a much narrower pore diameter distribution than the commercial templates (figure 1).

The increase in shell thickness that results from increasing the PMMA solution concentration appears to be a logarithmic relationship and therefore is likely a function of the solution viscosity. Typically polymer solution viscosity increases exponentially with polymer concentration for a given molecular weight when the concentration is above some critical concentration. The critical concentration, C*, is the concentration at which polymer chains begin to become entangled and is approximated by the dimensionless product of the intrinsic viscosity and the concentration, $[\eta]C$, which is referred to as the Berry number, B_e [32]. The concentration at which the Berry number is approximately equal to 1 is the critical concentration [32]. To determine the critical concentration for our PMMA-MEK polymer-solution system, the intrinsic viscosity was first calculated according to the Mark-Houwink-Sakurada equation, which is given by [29,30]

$$[\eta] = KM^{a} \qquad (1)$$

where K and a are both constants which have been reported in literature to be 6.8×10^{-3} mL/g and 0.72 respectively for PMMA solutions in MEK [30]. Using equation (1), the intrinsic viscosity for PMMA with a molecular weight of 996,000 g/mol was calculated to be 141.7 mL/g. From this value, C* was calculated to be 0.007 g/mL by assuming a value of 1 for the Berry number.

Since all of our PMMA solutions have a concentration greater than 0.007 g/mL we can conclude that we are within the semi-dilute solution regime.

The critical concentration can be used to predict the solution viscosity for semi-dilute polymer solutions where the concentration is greater than C* and is given by [32],

$$\eta = \eta_0 \left(\frac{C}{C^*} \right)^{3/(3\upsilon-1)} \quad (2)$$

where η is the viscosity of the solution, η_o is the viscosity of the solvent, which is 0.426 cP for MEK, C is the polymer concentration (g/mL), and ν is the Flory exponent which is 0.5 for theta solvents and 0.6 for good solvents. Using equation (2) we determined the viscosity of our 5, 8, 10, and 15% PMMA solutions in MEK and plotted them as a logarithmic function of solution concentration, which is shown in figure 2a. In addition, the average wall thickness was also plotted as a logarithmic function of the calculated solution viscosity, in figure 2b to illustrate this relationship. The relationship between solution viscosity and nanotube wall thickness has not yet been fully explored and to our knowledge our data are the first of this kind. A systematic study that investigates the viscosity, molecular weight, nanopore diameter, polymer type and surface energy will enable us to better understand the physical mechanism contributing to the wall thickness, and which property the thickness is more dependent upon. A better understanding of these variables will help researchers gain more control of the core-shell fabrication process described in this paper.

TEM images of PLLA-PMMA core-shell nanostructures formed using 5, 8, and 10% PMMA solutions are given in figure 3. It can be seen that the light PMMA shell thickness directly correlates to the solution concentration, as reported in figure 2.

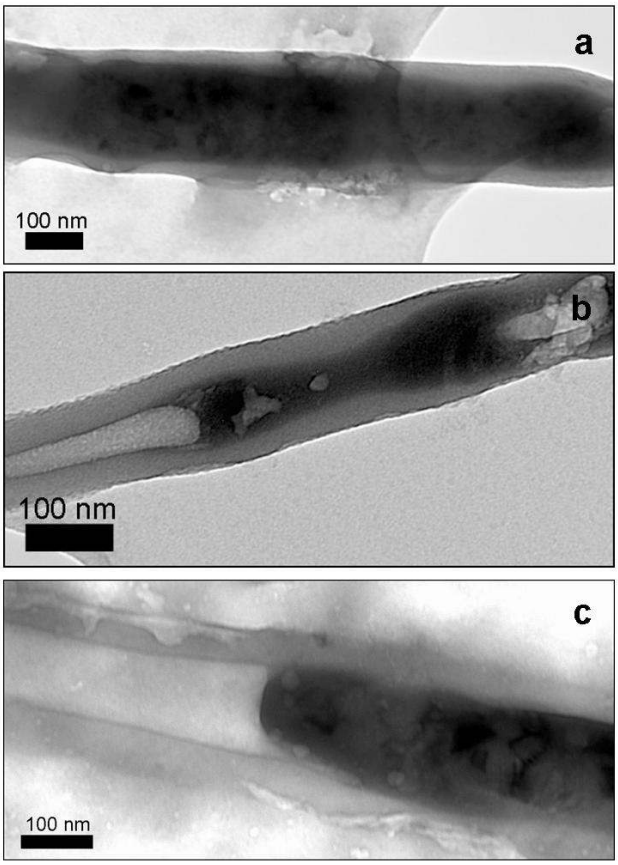

Figure 3: TEM images of PLLA-PMMA core-shell nanowires using a) 5% PMMA solution, b) 8% PMMA solution, and c) 10% PMMA solution to form the shell layer and melt wetting at 100^{o}C for 2 hours to form the core layer.

Melt wetting was used for filling our PMMA polymer shell with a PLLA core. The wetting approach chosen for the core polymer could be either solution or melt wetting depending upon the properties of the core polymer. The choice of solution wetting versus melt wetting is dependent upon the melting or glass transition (T_g) temperatures of the shell and core polymers and whether they are mutually soluble in the solvent of choice. To fill the core via melt wetting, it is important that the T_g of the core polymer be lower than the shell polymer to enable an intermediate temperature to be chosen for the second wetting step. Likewise, to fill the core via solution wetting, the core polymer should be dissolved in a non-solvent for the shell polymer to prevent mixing at the interface during wetting. For our PMMA and PLLA system, we chose to use melt wetting because of our previous work with fabricating homogeneous PLLA nanorods

via melt wetting [24] and because the T_g of PLLA is about 48^{o}C, which is lower than PMMA, which is about 105^{o}C.

Our previous work with PLLA nanorods demonstrated that by melt wetting with a commercial AAO template at 100^{o}C for 24 hours we were able to achieve homogenous PLLA nanowires. We chose to use the same melt wetting temperature to fill our PMMA shells with PLLA because we wanted to utilize conditions that were known and had already proven to be successful for our previous work with homogeneous PLLA nanorods. At a temperature within the range of the T_g for PMMA, we expected that there may be some mixing at the interface of the two polymers, especially for longer melt wetting times. Although mixing is not desirable, it was more important for us to use known conditions so we could compare our heterogeneous core-shell structures with the homogenous PLLA structures fabricated using the same conditions. In addition, we chose to use two melt wetting times, 2 and 24 hrs, to observe how it would affect the extent to which the core was filled and the extent of mixing between the core and shell layers. Our TEM results for homogenous PLLA nanorods revealed relatively short nanorods, in comparison to the thickness of the template, with a large distribution of lengths ranging anywhere from 1 – 10 μm. Theoretically the length of the nanorods should be approximately 60 μm, which is the thickness of the template. The short length and large length distribution that we observed is a result of the sonication step used during template dissolution. In addition the strong base may also be truncating the nanorods by hydrolyzing PLLA. Based on our TEM study of the homogenous PLLA nanorods, we expected to see core-shell nanostructures after 24 hr melt wetting. We also expected to observe more mixing between the core and shell layers after 24 hr melt wetting in comparison with the 2 hr melt wetting.

A mixture of two different core-shell morphologies was observed for both 2 hr and 24 hr melt wetting times. TEM images of PLLA-PMMA core-shell nanostructures fabricated using 5% PMMA solutions for solution wetting and 100^{o}C for melt wetting are shown in figure 4. The two morphologies that were observed for each wetting time can be described generally as a "random" morphology and a "periodic" morphology, and the random morphology was observed to be most prominent for both wetting times.

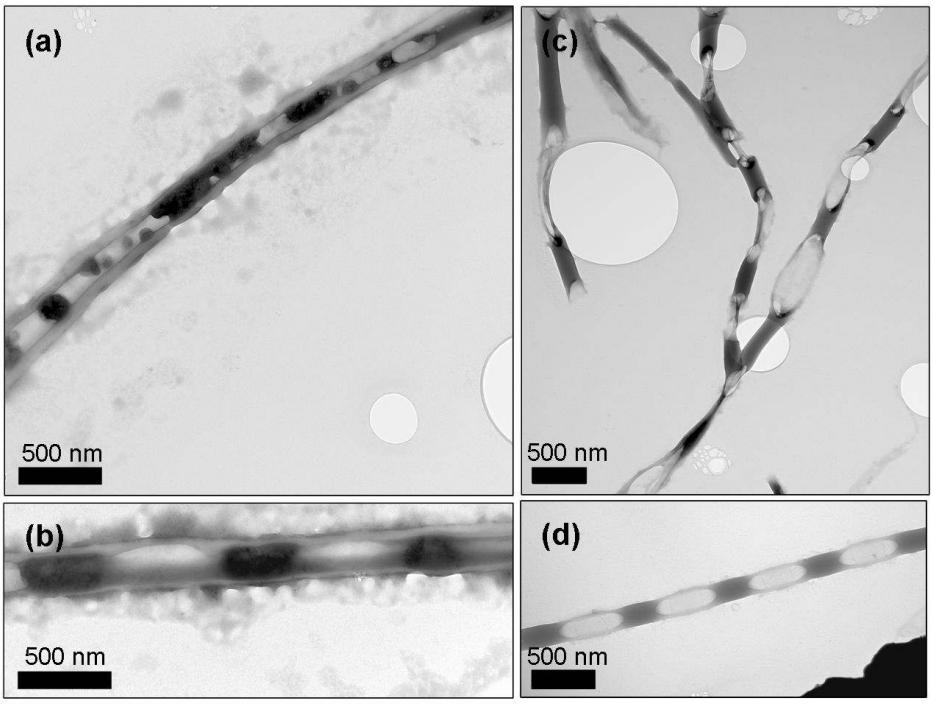

Figure 4: PLLA-PMMA core-shell nanostructure fabricated by melt wetting for 2 hrs (a) showing a random, segmented core morphology, (b) showing a periodic, segmented core morphology. PLLA-PMMA core-shell nanostructure fabricated by melt wetting for 24 hrs (c) showing a segmented structure with mixing between the core and shell layers, and (d) showing a periodic structure with mixing between the core and shell layers.

The random core-shell nanostructures observed for the 2 hr wetting time contained several short, discontinuous segments of PLLA at locations throughout the entire length of the PMMA shells (figure 4a). The dark PLLA segments inside the PMMA shell are only a few hundred nanometers in length, which is very short in comparison to the homogeneous PLLA nanowires. This result can be explained by the shorter melt wetting time. The presence of multiple, discontinuous segments, may be a consequence of the difference in the interfacial driving force, which would be weaker between two low surface energy polymers (heterogeous core-shell nanostructures) than between a low surface energy polymer and a high surface energy ceramic, like AAO (homogenous polymer nanostructures).

We did not anticipate the surface energy of the polymers to be a problem based on our previously published work where we melt wetted multilayered polymer thin films of poly(styrene) (PS) and PMMA to achieve core-shell structures (figure 5) [19]. By melt wetting

PS and PMMA simultaneously in a layered thin film we demonstrated core-shell structures with complete core filling. Unfortunately the controllability of the shell thickness was not as easy to achieve using this melt wetting approach, which was the reason for developing the two-step wetting approach described in this paper. Future work will focus on identifying the process variables that enabled the complete and continuous filling demonstrated in our previous work [19] and applying them to this new method which offer much better control of the shell thickness.

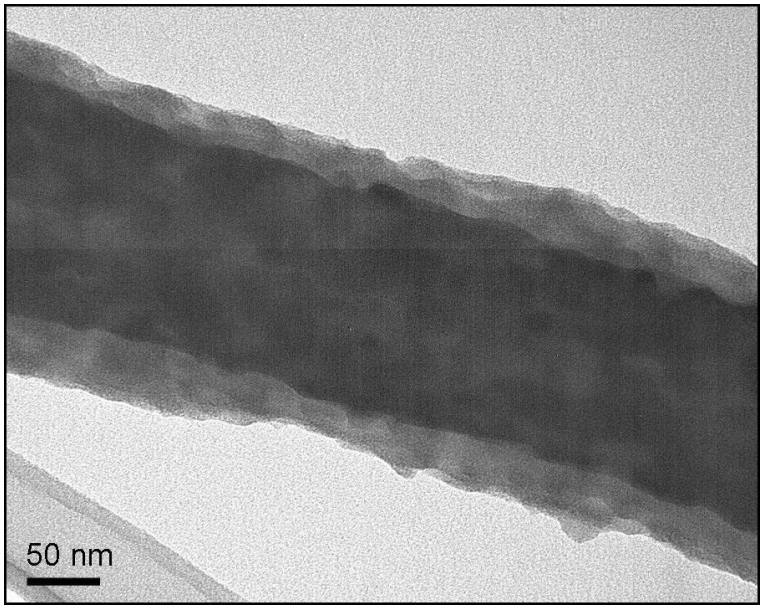

Figure 5: TEM image of PMMA/PS core-shell nanowires fabricated by melt wetting a multilayered PMMA and PS thin polymer film at 150^{o}C for 48 hrs. PS was stained dark using RuO_4.

Nanostructures with a much different "random" morphology were observed for the longer melt wetting time. Figure 4c shows TEM images of nanorod segments of various lengths that are only weakly connected. The nanorod segments appear to be within the same size range as the discontinous PLLA core segments observed for the shorter melt wetting time, however, the contrast between the core and shell layers is much less discernable. These fragmented structures are very similar to structures reported by T. P. Russel et al, who studied structures resulting from Rayleigh instabilities [31]. Russel's research demonstrated that PMMA films formed on the walls of nanochannels by solution wetting produced nanorods with encapsulated

holes when annealed at temperatures between 150°C and 200°C [31]. The encapsulated holes were formed as a result of the PMMA films undulating to reduce the surface area and the undulations eventually growing enough in amplitude to merge and leave behind holes [31]. We hypothesize that Rayleigh instabilities could have contributed to the fragmented structures that we obtained by lengthening the melt wetting time for the PLLA core filling. Similar to Russel's work with PMMA, we annealed PLLA at a temperature of 100°C, which is approximately 50°C higher than the T_g. At this temperature we were also within the range of the T_g of the PMMA film that was originally solution wetted within the pores, and it is likely that the PMMA molecules were also somewhat mobile, though not as much as the PLLA. Under these conditions, it is possible that the PLLA could have started to undulate within the PMMA shell to reduce its surface area and, as a result of this motion, the two polymers could have mixed within the nanochannels. This mixing combined with the Rayleigh instabilities could lead to the more homogeneous appearance at the interface of two polymers of the fragmented nanostructures observed in figure 4c. Furthermore, when the template is completely removed, the nanostructures are no longer mechanically supported by the AAO nanochannels, and it is likely that the removal of the AAO template caused the collapse of the thin walls surrounding the nanopores formed by the Rayleigh instabilities resulting in the fragmented structures that we observed.

In addition to the random morphologies that were observed for both melt wetting times, a small percentage of the nanostructures exhibited a very unique periodic morphology which is shown in figure 4b and 4d. It was observed that the periodic morphology of the PLLA segments within the PMMA shell for the 2 hr melt wetting time appeared to have the same periodicity as the nanosegments that were observed for the 24 hr melt wetting time. An important difference, which was also observed for the random morphologies, is that it the longer melt wetting time caused the PMMA and PLLA to mix within the nanochannel making the core and shell layers less discernable while the shorter melt wetting time resulted in a distinct contrast between the PMMA shell and PLLA core. The formation of the periodic morphology is not completely understood at this time, and does not represent a significant portion of the core-shell nanostructures that were fabricated for either melt wetting time. However, it may be beneficial to investigate what process parameters contribute to the formation of periodic structures in order to intentionally fabricate core-shell nanostructures with this periodicity.

Conclusions

In summary, we demonstrate the feasibility of fabricating polymer core-shell nanowires using our two-step wetting process. We were able control the thickness of the polymer shell by varying the polymer solution concentration and relate the thickness to the solution viscosity. We investigated the effect of wetting time on the extent of core filling and mixing of the core and shell layers. We observed that the shorter melt wetting times created many differently sized PLLA plugs within the PMMA shell and very discrete core and shell polymer layers. For longer melt wetting times we observed many weakly connected nanorod segments and significant mixing between the core and shell polymer layers, both of which were likely caused by Rayleigh instabilities within the nanopores. Future work will focus on investigating different polymers, melt wetting temperatures, and melt wetting times to achieve more uniform and complete core filling and reduce the amount of mixing between the core and shell. This pioneering work opens the arena for future studies to better understand and control the formation and properties of core-shell polymer nanostructures using our two-step wetting process.

References

[1] Li D and Xia Y 2004 Direct fabrication of composite and ceramic hollow nanofibers by electrospinning *Nano Letters*. **4** 933-38

[2] Yin Y, Lu Y, Sun Y and Xia Y 2002 Silver nanowires can be directly coated with amorphous silica to generate well-controlled coaxial nanocables of silver/silica *Nano Letters*. **2** 427-30

[3] Wei M, Lee J, Kang B and Mead J 2005 Preparation of core-sheath nanofibers from conducting polymer blends *Macromol. Rapid Commun*. **26** 1127-32

[4] Greiner A, Wendorff J H, Yarin A L and Zussman E 2006 Biohybrid nanosystems with polymer nanofibers and nanotubes *Appl. Microbiol. Biotechnol*. **71** 387-93

[5] Dersch R, Steinhart M, Boudriot U, Greiner A and Wendorff J H 2005 Nanoprocessing of polymers: applications in medicine, sensors, catalysts, photonics *Polym. Adv. Technol*. **16** 276-82

[6] Sun Z, Zussman E, Yarin A L, Wendorff J H and Greiner A 2003 Compound core-shell polymer nanofibers by co-electrospinning *Adv. Mater*. **15** 1929-32

[7] Jun Z, Aigner A, Czubayko F, Kissel T, Wendorff J H and Greiner A 2005 Poly(vinyl alcohol) nanofibers by electrospinning as a protein delivery system and the retardation of enzyme release by additional polymer coatings *Biomacromolecules*. **6** 1484-8

[8] Huang J, Liu S, Wang Y and Ye Z 2008 Fabrication of ZnO/Al_2O_3 core-shell nanostructures and crystalline Al_2O_3 nanotubes *App. Surface. Sci*. **254** 5917-20

[9] Numata M, Hasegawa T, Fujisawa T, Sakurai K and Shinkai S 2004 □-1,3-glucan (schizophyllan) can act as a one-dimensional host for creation of novel poly(aniline) nanofiber structures *Organic Letters*. **6** 4447-50

[10] Wang H S, Lin L H, Chen S Y, Wang Y L and Wei K H 2009 Ordered polythiophene/fullerene composite core-shell nanorod arrays for solar cell applications *Nanotechnology*. **20** 1-5

[11] Lahav M, Weiss E A, Xu Q and Whitesides G M 2006 Core-shell and segmented polymer-metal composite nanostructures *Nano Letters* **6** 2166-71

[12] Pan A L, Yao L, Qin Y, Yang Y, Kim D S, Yu R, Zou B, Werner P, Zacharias M and Gosele U 2008 Si-CdSSe core/shell nanowires with continuously tunable light emission *Nano Letters*. **8** 3413-7

[13] Steinhart M 2008 "Supramolecular organization of polymeric materials in nanoporous hard templates *Adv. Polym. Sci*. **220** 123-87

[14] Steinhart M, Wehrspohn R B, Gosele U and Wendorff J H 2004 "Nanotubes by template wetting: a modular assembly system *Angew. Chem. Int. Ed*. **43** 1334-44

[15] Zhang M, Dobriyal P, Chen J T and Russell T P 2006 Wetting transition in cylindrical alumina nanopores with polymer melts *Nano Letters*. **6** 1075-9

[16] Steinhart M, Wendorff J H and Wehrspohn R B 2003 Nanotubes a la carte: wetting of porous templates *Chem. Phys. Chem.* **4** 1171-6

[17] Steinhart M, Wendorff J H, Greiner A, Wehrspohn R B, Nielsch K, Schilling J, Choi J and Gosele U 2002 Polymer nanotubes by wetting of ordered porous templates *Science*. **296** 1997

[18] Schlitt S, Greiner A and Wendorff J H 2008 Cylindrical polymer nanostructures by solution template wetting *Macromolecules*. **41** 3228-34

[19] Dougherty S and Liang J 2009 Fabrication of segmented nanofibers by template wetting of multilayered alternating polymer thin films *J. Nanopart. Res*. **11** 743-7

[20] Kriha O, Zhao L, Pippel E, Gosele U, Wehrspohn R B, Wendorff J H, Steinhart M and Greiner A 2007 Organic tube/rod hybrid nanofibers with adjustable segment lengths by bidirectional template wetting *Adv. Funct. Mater*. **17** 1327-32

[21] Lau S T, Zheng R K, Chang H L W and Choy C L 2006 Preparation and characterization of poly(vinylidene fluoride-trifluoroethylene) copolymer nanowires and nanotubes *Mater. Letter*. **60** 2357-61

[22] Sun Y, Steinhart M, Zschech D, Adhikari R, Michler G H and Gosele U 2005 Diameter-dependence of the morphology of PS-b-PMMA nanorods confined within ordered porous alumina templates *Macromolecular Rapid Communications*. **26** 369-75

[23] Kriha O, Goring P, Milbradt M, Agarwal S, Steinhart M, Wehrspohn R, Wendorff J H and Greiner A 2008 Polymer tubes with longitudinal composition gradient by face-to-face wetting *Chem. Mater.* **20** 1076-81

[24] Dougherty S and Liang J, Towards heterogeneous biodegradable nanorods for controlled drug delivery Submitted to the proceedings of the MRS Fall 2008 Meeting in Boston, MA

[25] Liang J, Chik H, Yin Y and Xu J 2002 Two-dimensional lateral superlattices of nanostructures: nonlithographic formation by anodic membrane template *J. Appl. Phys*. **91** 2544-6

[26] Dougherty S, Liang J and Kowalik T F 2009 Template-assisted fabrication of protein nanocapsules *J. Nanopart. Res*. **11** 385-94

[27] imageJ software: http://rsb.info.nih.gov/ij/

[28] Shimura Y 1967 Solution properties of methyl methacrylate-acrylonitrile copolymer *Bulletin of Chemical Society of Japan* **40** 273-9

[29**]** Spearling L H. Introduction to Physical Polymer Science. 3rd ed. New York: J. Wiley & Sons; 2001

[30] Wagner HL 1987 The Mark-Houwink-Sakurada relation for poly(methyl methacrylate) *J. Phys. Chem. Ref. Data*. **16** 165-73

[31] Chen J T, Zhang M and Russell T P 2007 Instabilities in nanoporous media Nano Letters. 7 183-7

[32] Gupta P, Elkins C, Long T E and Wilkes G L 2005 Electrospinning of linear homopolymers of poly(methyl methacrylate): exploring relationships between fiber formation, viscosity, molecular weight and concentration in a good solvent Polymer. **46** 4799-810

CHAPTER 4: CONCLUSIONS AND FUTURE WORK

This thesis presents a series of papers that demonstrate the versatility of template-assisted nanofabrication methods and exploit the fundamental principles to realize unique, multifunctional nanostructure morphologies with great potential for drug delivery applications. This work began by exploring two potential template-assisted fabrication approaches, namely the layer-by-layer method to fabricate protein nanostructures and template wetting to fabricate polymer nanostructures. Through literature review and our experimental trials we determined that template wetting was a versatile and controllable template-assisted fabrication approach.

Using the layer-by-layer method we were able to demonstrate the fabrication of glucose oxidase nanocapsules by covalently bonding multiple protein layers within the nanochannels of AAO templates [Paper 1]. The major drawback of this method was the use of a crosslinker, glutaraldehyde, to bind the protein layers together. Glutaraldehyde is a known carcinogen and draws an immediate red flag for biomedical applications like drug delivery. As an alternative to covalently binding protein layers to form protein nanostructures, we attempted to use electrostatic attractions to build up protein layers within AAO templates [Paper 2 and Appendix 2]. Unfortunately, despite our extensive literature review and persistent experimental trials, we were only able to fabricate mechanically weak single protein, bovine serum albumin, nanostructures using electrostatic attractions alone and this was done with very minimal success. During this study, however, we revealed some questionable results published by other researchers regarding this fabrication method. This evidence raises significant doubts about the feasibility of the layer-by-layer method to fabricate stable single protein nanostructures via electrostatic assembly. By incorporating an additional protein we were able to demonstrate glucose oxidase/avidin protein nanotubes by electrostatic layer-by-layer assembly in conjunction with glutaraldehyde to bind the initial protein layer to the template. As a result of our limited success fabricating protein nanostructures without the use of glutaraldehyde, we shifted the focus of our fabrication to polymeric materials.

Using template wetting methods, which are based on capillary action, we were able to fabricate a much larger array of unique nanostructures. Building upon the pioneering work done by other researchers, we were able to fabricate heterogeneous segmented nanowires by melt wetting with multilayered polymer films [Paper 3], and heterogeneous core-shell nanowires by

sequential solution wetting and melt wetting [Paper 4]. These novel fabrication techniques provide simple, low cost, and versatile approaches to fabricate multifunctional nanostructures. The demonstration of these novel template-assisted fabrication techniques opens the arena for future studies focused on process control, optimization, and applicability towards specific applications.

The use of layer-by-layer techniques to fabricate protein nanostructures and template wetting to fabricate unique polymer nanostructures illustrates the versatility of template-assisted nanofabrication. The demonstrated versatility, ease of fabrication, and low cost of template-assisted nanofabrication make it a viable option for the future manufacturing of one-dimensional nanomaterials and optimization for a wide variety of applications including drug delivery.

Future work should focus on utilizing and optimizing the fabrication methods that were demonstrated in this dissertation to design and fabricate nanostructures specifically for drug delivery. The core-shell nanostructures presented in Paper 4 are expected to be the most useful and promising nanostructure we fabricated for use as a drug delivery device. The first step that must be done before incorporating therapeutic molecules within the core of these nanostructures is to improve the filling of the core material to achieve more continuous core filling. As discussed in Paper 4, it is likely that the filling is not continuous because of the low interfacial driving force between two low energy polymers. To overcome this interfacial energy problem, the following potential approaches should be investigated:

1. Chemically oxidize the inner surface of the shell polymer through mild acidic treatment to increase the surface energy of the shell material, and subsequently increase the driving force for wetting.
2. Use a material with a higher surface energy for the shell, such as a metal or ceramic. Metals could be depositing within AAO templates via methods such as electrodeposition and ceramics could be deposited via methods such as sol gel.

Once complete and continuous core-shell filling has been achieved, this project can move forward with application based experimentation which focuses on drug delivery. This work should include the incorporation of therapeutic molecules within the core material, evaluation of the drug loading, and measurement of the drug release profiles for nanostructures with different diameters, lengths, and aspect ratios. Preliminary experiments and thoughts regarding the future work for this project are presented in Appendix 4.

APPENDICES

Appendix 1. Process used to determine average pore size and nanotube wall thickness using ImageJ image analysis software

After opening the imageJ software, an SEM or TEM image can be dragged onto the ImageJ tool bar for analysis. The first step for any type of quantitative analysis using ImageJ is to set the scale in according to the scale bar for the image. This is done by drawing a line that is equal in length to the length of the scale bar on the image and selecting "Set Scale" from the Analyze menu.

Using ImageJ to Analyze Pore Size

An example of an SEM image that may be used to determine the average pore size of AAO templates is shown in Figure 1a. To analyze the pore size, the image must be adjusted to include only black circles where the pores are. This is done by adjusting the image's threshold. The resulting threshold image is shown in Figure 1b. Next the size of all the pores is measured by selecting "Analyze Particles" from the Analyze menu. The minimum and maximum size of the particles can be set to avoid measuring partial pores along the edges of the SEM images. After analyzing the particles, ImageJ creates a drawing, shown in Figure 1c, with outlines of all the pores that were measured and displays a table with the number of the pores and the area of the pores. Using excel, the area can be used to calculate the diameter of all the pores. Then the average diameter of all the pores can be calculated with the error given by the standard deviation. The number of pores measured is strongly dependant upon the magnification of the SEM image. Higher magnification will contain fewer pores, whereas lower magnification will include more.

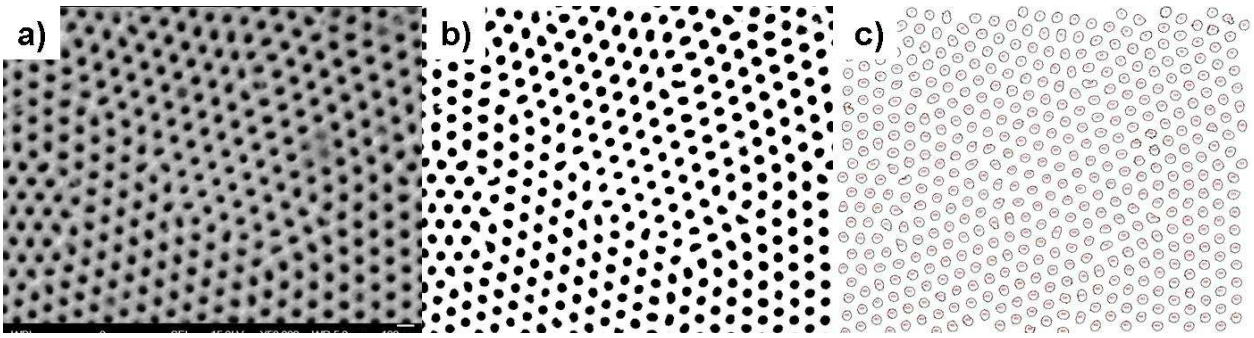

Figure 1: a) SEM image of an AAO template with uniform nanopores b) Threshold image of the SEM image showing black circles in place of the nanopores c) Particle analysis image showing outlines of all the nanopores analyzed.

Using ImageJ to Analyze Nanotube Wall Thickness

An example of a TEM image that may be used to determine the average wall thickness of a set of nanotubular structures is shown in Figure 2a. After setting the scale, lines can be drawn across the nanotube walls, as shown in Figure 2b, to determine the thickness of the walls. To calculate the average wall thickness for a given sample of nanotubes, at least 2 different images of nanotubes were analyzed, and the wall thickness was measured in at least 5 different areas for each nanotube giving an $n \geq 10$. This analysis method was used primarily to determine the effect of polymer solution viscosity on the average wall thickness of our polymer nanotubes.

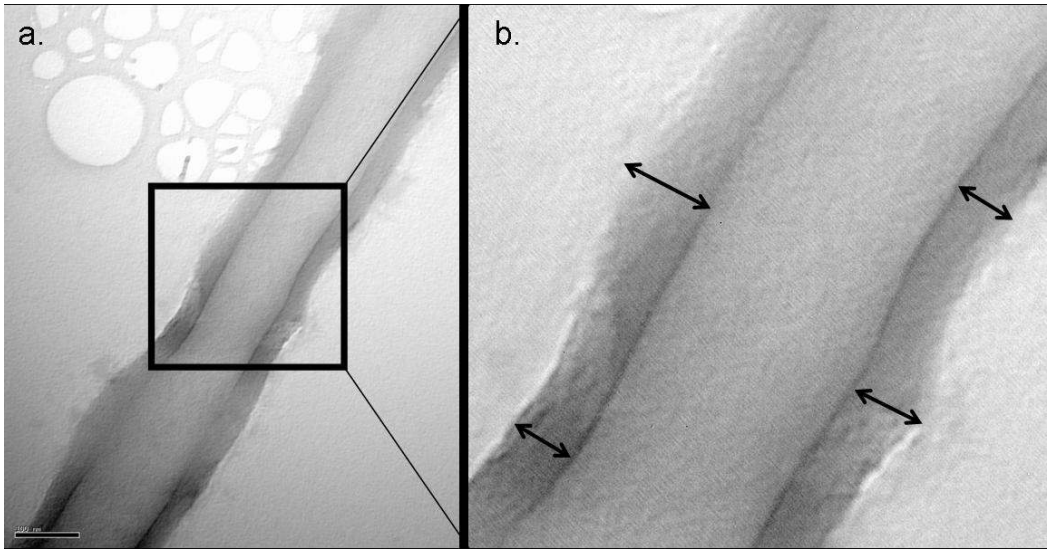

Figure 2: a.) TEM image of a polymer nanotube structure b) Magnified version of the TEM image that illustrates the lines drawn using ImageJ to measure the wall thickness.

Appendix 2. Fabrication of bovine serum albumin nanotubes through template assisted layer by layer assembly

Dawei Zhang, Shelley A. Dougherty and Jianyu Liang

Abstract

Protein nanotubes have been successfully fabricated via sequential filtration of bovine serum albumin (BSA) solution at pH 3.8 and pH 7.0 through the nanochannels of anodic aluminum oxide (AAO) templates. The morphology of the nanostructures has been examined using SEM and TEM. Also, a simple analysis from UV/Vis spectroscopy has shown that the pH values of the solutions in our experiment did not significantly damage the bioactivity of BSA. Our future work will focus on strengthening the mechanical stability of the protein nanotubes and more precisely controlling their morphology.

Introduction

Since Iijima first discovered carbon nanotubes,[1] researchers worldwide have been enthusiastically exploring the characteristics and applications of one-dimensional nanostructures composed of carbon,[2] ceramics,[3] metals[4] and polymeric materials.[5] Out of all the synthetic and natural materials, protein based nanotubes are particularly desirable for biomedical applications due to their ease of functionalization and intrinsic biocompatibility. Two preparation approaches, namely self-assembly and template-assisted synthesis have been investigated for producing protein nanotubes directly. Self assembly methods have been successfully employed to fabricate protein nanotubes based on flagella,[6,7] viral capsids,[8,9] tubulin[10] and Hcp1.[11] However, self assembly methods are typically limited to the unique chemistry and functionality of the biomolecules. In addition, the morphologies and dimensions of the self-assembled nano-tubular structures are restricted by the properties of the original bulk materials. The template-assisted method provides a highly versatile alternative. The template-assisted processes for the fabrication of protein nanotubes rely upon either the chemical crosslinking of proteins, the so-called alternate immersion method,[12,13] or electrostatic charges between protein layers, the so-called layer by layer (LbL) method.[14,15] These mechanisms can be easily adapted to many different proteins with little to no modifications. This advantage renders template-assisted methods viable for a wide range of applications.

The LbL assembly method has long been used in the electrostatic deposition of thin films on flat substrates and surfaces of particles.[16-18] Multilayers composed of different charged species can be built up following a conventional procedure: A negatively charged solid substrate is alternately immersed in solutions of cationic polyelectrolyte and anionic polyelectrolyte[16] to build up a film consisting of alternating layers of polyelectrolytes by the electrostatic interaction between them. It is also well established that by tuning the ionic strength and pH environment of the solution, the layer thickness, surface roughness and permeability of the multilayer can be precisely controlled.[19-21]

Recently, the LbL assembly approach has been applied in anodic aluminum oxide (AAO) templates to demonstrate the successful fabrication of protein based nanotubes. For example, nanotubes of cytochrome C have been fabricated inside polyethylenimine (PEI)-pretreated AAO templates by the alternate adsorption of positively charged cytochrome C with negatively charged poly-(sodium styrenesulfonate) (PSS).[14] Similarly, human serum albumin (HSA)-based nanotubes have been synthesized by alternating HSA with poly-L-arginine (PLA) or PEI.[15] To date, the published works have been primarily focused on composite nanotubes of protein molecules and charged polymers. Only a few of these studies have attempted the fabrication of single component nanotubes with HSA.[22,23] In this paper we have demonstrated the fabrication of bovine serum albumin (BSA) nanotubes using LbL deposition of protein molecules inside a nanoporous AAO template.

Albumin, the most abundant plasma protein in the bloodstream, is an acidic protein with high solubility in water. It is very robust in extreme pH environments and organic solutions. It can be heated to 60 ˚C for up to 10 hours without catastrophic damage to its chemistry.[24] BSA consists of 583 amino acids and has a molecular weight of 66 kDa.[25] BSA has been successfully used in biological applications like HSA, but is much lower in cost since it can be readily purified from bovine blood. The isoelectric point (pI) of BSA is 4.7. Under pH 4.7, BSA molecules carry a positive charge. And above pH 4.7, BSA molecules carry a negative charge. In the present work, oppositely charged BSA molecules have been assembled into nanotubes inside the nanochannels of AAO templates in an LbL fashion. The obtained protein nanostructures have been characterized using scanning electron microscopy (SEM) and transmission electron microscopy (TEM). The effect of solution pH on BSA bioactivity has been investigated by UV/vis spectroscopy.

Experimental Part

Materials. AAO templates (13mm) were purchased from Whatman Co., with an inner pore diameter of ca. 200 nm and thickness of 60 μm. The BSA was obtained from Sigma and was stored at 2 ˚C before use. All the chemicals were used as received without further purification.

Layer-by-layer Assembly. The AAO template was sandwiched between two cellulose membranes (MF-Millipore) and was fixed into a stainless steel microsyringe filter (Whatman Co.). 9 mL of BSA in a citric-phosphate buffer solution (2 mg/mL, 10 mM) at pH 3.8 and pH 7 were sequentially injected into the filter at a speed of 0.5 mL/min. Between each filtration step, 9 mL of DI water was filtered through the template at a speed of 1 mL/min, followed by drying the template in air for 10 min. After three sequential filtration steps, the AAO template was washed thoroughly with DI water. The BSA aggregated on the surface of the template was carefully removed using Kimwipes before the template was dried overnight in the air.

Characterization. Nanotube morphology was characterized using SEM (JSM-7000, JEOL) and TEM (Philips CM 12). UV/vis spectrometer (Genesys 10UV scanning spectrophometer, Thermo Electron) was used to evaluate the absorbance of BSA molecules in a wide range of pH environments (pH 1.15~12). Zeta potential was used to measure BSA charge in the acidic and basic buffer solutions. Zeta potential was measured using a ZetasizerNano (Malvern Zen3 600).

Results and discussions

BSA is a heart-shaped molecule comprised of three domains at its pI.[26] However, it undergoes several well-recognized conformational changes under different pH conditions. Associated with the variation of the BSA conformation, the ionic properties of albumins are also dependent on pH environment. Figure 1 shows the pH dependent zeta-potentials of BSA solutions at a concentration of 2 mg/mL, which represents the net charge that BSA molecules carry. The curve agrees well with the model from the early work by Fogh-Anderson *et al*.[27] The albumin's zeta potential decreases from 25.1 mV to zero at around pH 4.7 and becomes negative with increasing pH. BSA solutions at pH 3.8 and 7 were chosen for the alternate filtrations based on literature reviews.[22] Additionally, we demonstrated that the zeta potential is positive (12.3 mV) at pH 3.8 and negative (-17.9 mV) at pH 7 which allows the electrostatic assembly of the adsorbed BSA layers.

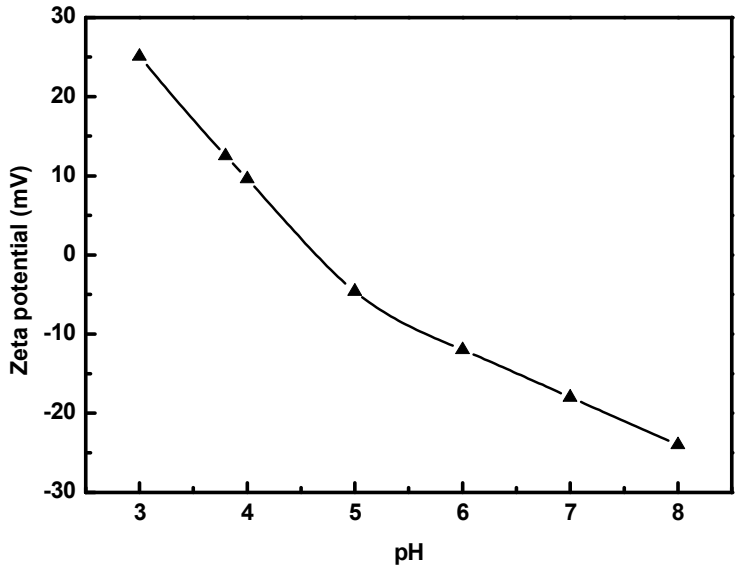

Figure 1. pH-dependent zeta potential of BSA molecules

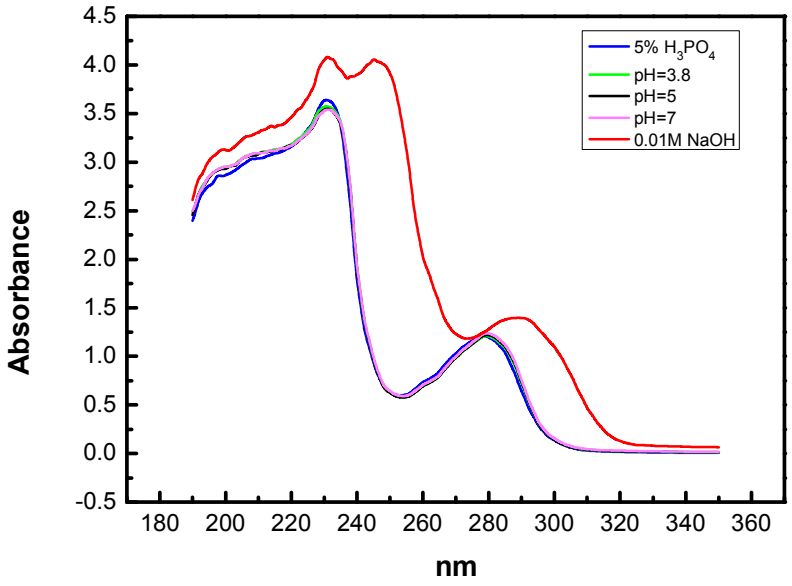

Figure 2. UV/Vis spectroscopy of BSA solution at different pH

To examine the bioactivity of BSA molecules at pH 3.8 and 7, UV/Vis spectroscopy was performed on the same solutions that we used for LbL filtrations. As shown in Figure 2, the absorption curves of positively charged BSA at pH 3.8 and negatively charged BSA at pH 7 are overlapped with the curve obtained at its nature state (pH 4.7). It is known that without being irreversibly denatured, the BSA molecule is significantly adaptive to a wide range of pH values

by frequent expansion and contraction. The pH-dependent conformations of BSA are classified as N, the native form (pH 4.3-8); F, the fast-migrating form (pH 2.7-4.3) and E, the expanded form (pH<2.7). In a basic environment, BSA will adapt to B, the basic form (pH 8-10) and A, the aged form (pH>10).[26,28] Albumin can recover from structural changes caused by almost any condition except long periods of treatment with heat and alkalinity.[24] Our observation complies with the fact that at pH 3.8 (F form) and 7.0 (N form), BSA still maintains a relatively natural state, in which the molecules are not yet expanded enough to lose their original 3D structures.[28,29]

In addition, based on our previous experience of making SEM and TEM samples, AAO templates can only be dissolved by strong acids or strong bases. To explore the effect of the pH values of different solutions used to remove the AAO on the bioactivity of BSA molecules, UV/Vis spectroscopy was also used on the bulk solutions (2 mg/mL) of BSA in 5% H_3PO_4 and 0.01 M NaOH. For BSA in 5% H_3PO_4 solution, there is a slight difference in the region of 200 nm-230 nm, but no significant deviation of the UV/Vis curve has been found. However, for BSA in 0.01 M NaOH solution, the typical absorbance peak at 280 nm from tryptophan and tyrosine residues exhibits a red shift, indicating the change in the secondary structure. Also, the far-ultraviolet region below 240 nm splits into two peaks which is further evidence of the degradation of the albumin molecule caused by alkaline.[30] Consequently, 5% H_3PO_4 was preferred for the etching of AAO templates in our experiment.

In this work, positively charged BSA molecules were first adsorbed onto the anionic sites on the pore wall of the AAO templates at pH 3.8, followed by a quick washing of the loosely bound molecules and drying of the protein surface. Negatively charged BSA solution at pH 7.0 was then filtered through the membrane. Like weak polyelectrolyte multilayers obtained on flat substrates, long incubation times of at least 10 min are required to ensure a sufficient charge interaction.[31-34] This is especially important for the first layer of protein adsorbed on the alumina surface, which plays an important role in the successful build-up of the consecutive layers.[35] In comparison, we have also tested filtrations of the same amount of BSA solution at a speed of 1 mL/min and 3 mL/min, i. e. for 9min and 3min respectively. It is not evident from SEM and TEM characterizations that stable protein multilayers have been deposited at those fast speeds.

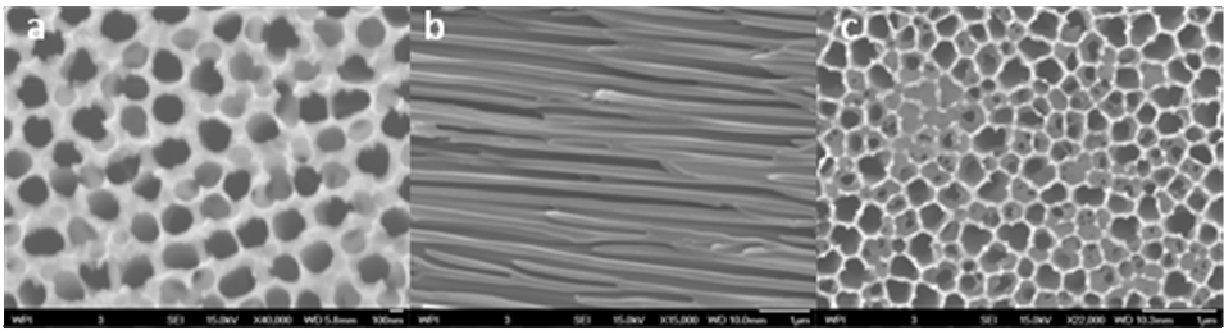

Figure 3. a) Top view of an empty AAO template; b) Cross-sectional view of an empty AAO template; c) Top view of BSA multilayers deposited inside AAO template. (The scale bars are a) 1 um; b) 100 nm; c) 1 um)

Figure 3-a, b show the top view and the cross section of the AAO template we used to fabricated BSA nanotubes. Figure 3-c is the top view of an AAO template after deposition of BSA multilayers inside the nanopores. It is seen that after six filtrations, the pores in the AAO template (Figure 3-c) are filled with protein. However, the thicknesses of the BSA multilayers are not uniform. This may be attributed to complex morphology of the substrates provided by AAO for LbL deposition. It is known from studies on LbL assemblies on planar surfaces, that the amount of deposited polyelectrolytes significantly depends on the surface roughness[36-38] and the curvature[39,40] of the substrate. The nanochannels in the AAO template, however, are not perfectly cylindrical pores with uniform diameter and are full of uneven surfaces, branches and discontinuities, as seen in Figure 3-a, b. These irregularities may have directly contributed to the inhomogeneous adsorption of BSA multilayers.

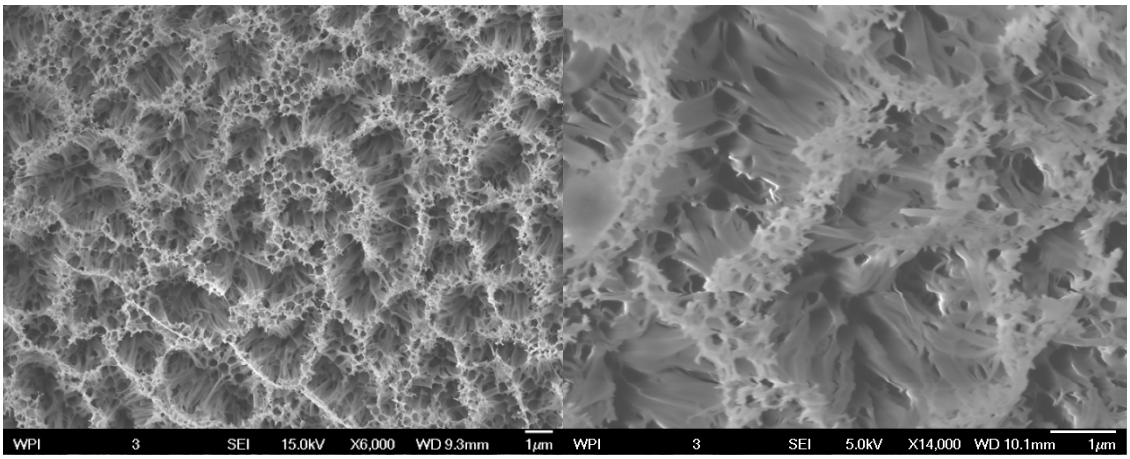

Figure 4. SEM images of AAO template after etching with 5% H_3PO_4 for 16 hours

(The scale bars are both 1μm)

Figure 4 shows an AAO template after protein deposition that was partially etched away in a 5% phosphoric acid for 16 hours at 0 ˚C, in order to liberate the top portion of the protein nanotubes from the template. However, collapsed nanostructures were observed and individual protein nanotubes could not be differentiated. We hypothesize that this is because of the intrinsic weakness in the mechanical stability of protein nanotubes. In the early work in which LbL assemblies were performed on flat substrates, it has been demonstrated that the chain length of polyelectrolytes plays a critical part in the stability of protein multilayer. Unlike flexible polyions, the globular molecules of BSA are less capable of penetrating into each other to form a network that provides a sustainable support to the whole structure.[41-44] Consequently, the BSA nanotubes fabricated within the AAO template, which are multilayers composed of weakly attracted globular protein molecules, may have an inherent disadvantage in maintaining its structural integrity. Additionally, at both pH 3.8 and pH 7.0, electrolytic groups on BSA molecules are only partially ionized. Therefore the charge provided by the coiled molecules of protein is limited for the electrostatic interaction between protein layers. As the aluminum oxide is being etched away, mechanical support gradually disappears and the soft and thin walls of the protein nanotubes cannot stand on their own, resulting in a structure of collapsed bundles. On the other hand, the acidic post-treatment of the protein multilayer in H_3PO_4 during the preparation of SEM samples may protonate many of the carboxylate groups within the protein layers. It may interfere with the electrostatic crosslink and mobilizes the protein chains to a certain extent, therefore further weakens the structural stability of the protein nanotubes.[45]

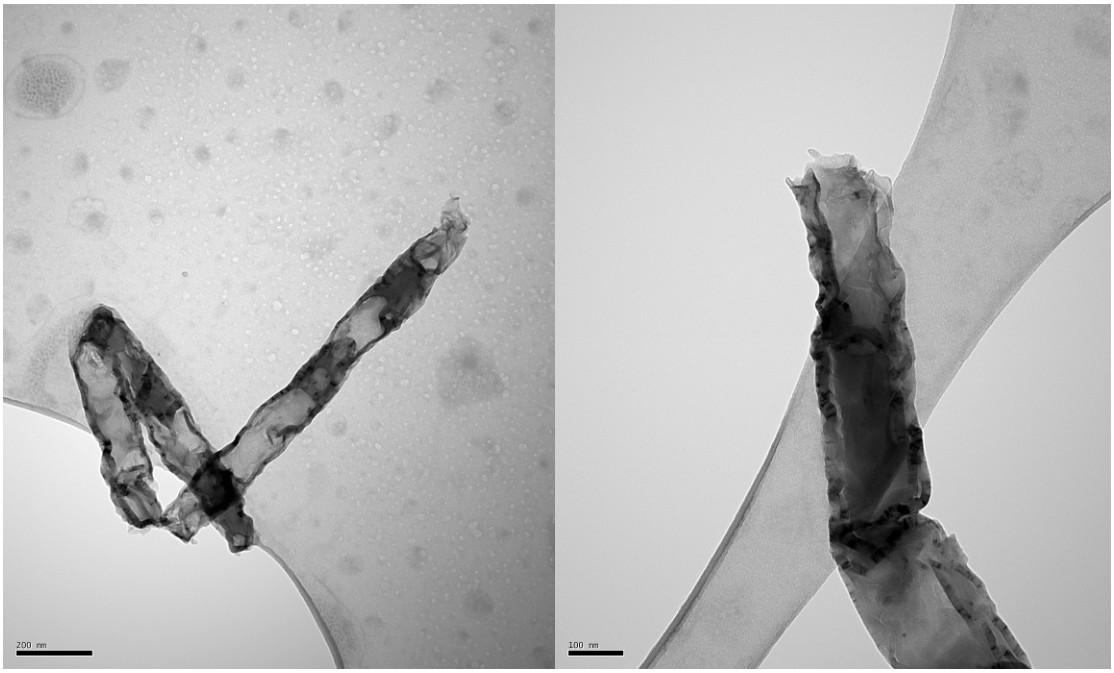

Figure 5. TEM images of BSA nanotube. The scale bars are 200 nm (left) and 100 nm (right).

To study the morphology of individual BSA nanotubes, TEM samples were prepared by completely dissolving the AAO template containing protein multilayers in a 5% phosphoric acid solution at 0 ˚C for 24 hours. It is seen that although the harsh environment that is necessary to etch away the alumina can compromise the stability of the protein multilayers, it is still possible to observe the tubular protein structure even after acidic treatment for as long as 24 hours. The walls of the obtained nanotubes are wavy due to the intrinsic softness of protein multilayers. Careful examination of the thickness of the protein nanotube walls using the image processing software imageJ reveals that the average wall thickness (measured in 15 different places) is 19 nm±1.5 nm, i.e. an average of 3 nm for the deposition of each single BSA layer. This is in agreement with the size of BSA molecules (140 A×40 A) in its unfolded form.[46] Some Y-shaped protein nanostructures are also seen from TEM characterization (See Figure 6), which replicates the branched channels in AAO templates well. This demonstrates the versatility of template-assisted method using AAO templates as scaffold.

Figure 6. TEM image of a Y-shaped BSA nanotube. The scale bar is 200nm.

Conclusion

In conclusion, we have deposited single component BSA multilayers onto the nano-channels within AAO templates via the electrostatic interaction between oppositely charged protein molecules. A simple analysis from UV/Vis spectroscopy in both near and far ultraviolet region has demonstrated that the pH of the solutions we used will not cause irreversible denaturation to the BSA molecules. The obtained protein nanotubes were shown by SEM to have collapsed into bundles due to the intrinsic mechanical weakness of protein multilayers and the acidic post-treatment. After the AAO template has been completely etched away, the morphology of the liberated protein nanotubes was characterized using TEM. Our future work will focus on reinforcing the mechanical stability of our BSA nanotubes. We will also investigate various filtration conditions and AAO template dimensions, to enable us to precisely control the nanotube morphology.

References

[1] Iijima, S. *Nature* **1991,** 354, 56.

[2] Baughman, R. H.; Zakhidov, A. A.; de Heer, W. A. *Science* **2002,** 297, 787.

[3] Kasuga, T.; Hiramatsu, M.; Hoson, A. *Langmuir* **1998,** 14, 3160.

[4] Wang, J.; Li, Y. *Adv.Mater.* **2003,** 15, 445.

[5] Steinhart, M.; Wendorff, J. H. *Science* **2002,** 296, 1997.

[6] Kumara, M. T.; Srividya, N.; Muralidharan, S. *Nano Lett.* **2006,** 6, 2121

[7] Ngweniform, P.; Li, D.; Mao, C. *Soft Matter* **2009,** 5, 954.

[8] Valéry, C.; Paternostre, M.; Robert, B. *Proc. Nat. Acad. Sci. U.S.A.* **2003,** 100, 10258.

[9] Mukherjee, S.; Pfeifer, C. M.; Johnson, J. M. *J. Am. Chem. Soc.* **2006,** 128, 2538.

[10] Raviv, U.; Needleman, D. J.; Ewert, K. K. *J. Appl. Crystallogr.* **2007,** 40, 83.

[11] Ballister, E. R.; Lai, A. H.; Zuckermann, R. N. *Proc. Nat. Acad. Sci. U.S.A.* **2008,** 105, 3733

[12] Hou, S.; Harrell, C .C.; Trofin, L.; Kohli, P.; Martin, C. R. *J. Am. Chem. Soc.* **2004,** 126, 5674.

[13] Baker, L. A.; Jin, P.; Martin, C. R. *Crit. Rev. Solid State Matter* **2005,** 30, 183.

[14] Tian, Y.; He, Q.; Cui, Y. *Biomacromolecules* **2006,** 7, 2539.

[15] Qu, X.; Lu, G.; Tsuchida, *E. Chem. Eur. J.* **2008,** 14, 10303.

[16] Decher, G. *Science* **1997,** 277, 1232.

[17] Sukhorukov, G. B. *Colloids Surf., A* **1998,** 137, 253.

[18] Caruso, F., Trau, D.; Mohwald, H.; *Langmuir* **2000,** 16, 1485.

[19] Schlenoff, J. B.; Dubas, S. T. *Macromolecules* **2001,** 34, 592.

[20] Dubas, S. T.; Schlenoff, J. B. *Langmuir* **2001,** 17, 7725.

[21] Shiratori, S. S.; Rubner, M. F. *Macromolecules* **2000,** 33, 4213.

[22] Lu, G.; Ai, S. Li, J. *Langmuir* **2005,** 21, 1679.

[23] Lu, G.; Tsuchida, E.; Komatsu, T. *Chem. Lett.* **2008,** 37, 972.

[24] Peters, T. *All About Albumin: Biochemistry, Genetics, and Medical Applications*; Academic Press, Inc.: USA,1995.

[25] Kratz, F. *J. Controlled Release* **2008,** 132, 171.

[26] Peters, T. *Adv. Protein Chem.* **1985,** 37, 161.

[27] Fogh-Andersen, N.; Bjerrum, P. J.; Siggaard-Andersen, O. *Clin. Chem.* **1993,** 39, 48.

[28] Sadler, P. J.; Tucker, A. *Eur. J. Biochem.* **1993,** 212, 811.

[29] Shang, L.; Wang, Y.; Jiang, J. *Langmuir* **2007,** 23, 2714.

[30] Perkampus, H. H. *UV-VIS Atlas of Organic Compounds*; Wiley VCH: Berlin, 1992.

[31] Yoo, D.; Shiratori, S. S.; Rubner, M. F. *Macromolecules* **1998,** 31, 4309.

[32] Kharlampieva, E.; Sukhishvili, S. A. *Langmuir* **2003,** 19, 1235.

[33] Elzbïeciak, M.; Zapotoczny, S.; Nowak, P., *Langmuir* **2009,** 25, 3255.

[34] Buron, C. C.; Filiâtre, C.; Membrey, F. *Thin Solid Films* **2009,** 517 26,11.

[35] Schlenoff, J. B.; Ly, H.; Li, M. *J. Am. Chem. Soc.* **1998,** 120, 7626.

[36] Picart, C.; Lavalle, P.; Hubert, P. *Langmuir* **2001,** 17, 7414.

[37] Zhang, H.; Ruehe, J. *Macromol. Rapid Commun.* **2003,** 24, 576.

[38] Buron, C. C.; Filiatre, C.; Membrey, F. *Colloids Surf.*, *A* **2007,** 305, 105.

[39] Lee, D.; Nolte, A. J.; Kunz, A. L. *J. Am. Chem. Soc.* **2006,** 128, 8521.

[40] Alem, H.; Blondeau, F.; Glinel, K. *Macromolecules* **2007,** 40, 3366.

[41] Lindquist, G. M. Stratton, R. A. *J. Colloid Interface Sci*. **1976,** 55, 45.

[42] Sui, Z.; Salloum, D.; Schlenoff, J. B. *Langmuir* **2003,** 19, 2491.

[43] Houska, M.; Brynda, E. *J. Colloid Interface Sci.* **2004,** 273, 140.

[44] Lvov, Y. Mohwald, H. *Protein Architechicture: Interfacing Molecular Assemblies and Immobilization Biotechnology*; Marcel Dekker, Inc.: New York, 1999.

[45] Mendelsohn, J. D.; Barrett, C. J.; Chan,V. V. *Langmuir* **2000,** 16, 5017.

[46] Kragh-Hansen, U. *Danish Medical Bulletin* **1990,** 37, 57.

Appendix 3. Towards Biodegradable Segmented Nanorods for Controlled Drug Delivery

Submitted to the MRS Fall 2008 Proceedings

S. Dougherty and J. Liang

ABSTRACT

Heterogeneous, one-dimensional (1D) nanomaterials, such as nanorods and nanowires, have been utilized for a variety of different biomedical applications because they offer a unique combination of properties and provide a material platform for integrating multiple functions. In this paper, we propose a template-assisted wetting approach to fabricate segmented polymer nanorods using biodegradable polymers for controlled drug delivery. Our previous work with polystyrene (PS) and poly(methyl methacrylate) (PMMA) heterogeneous, segmented nanorods is described briefly to introduce our current preliminary work with the fabrication of homogeneous biodegradable nanorods and drug release from polymer thin films. Since the template-assisted fabrication approach provides us unprecedented control over the size, spacing, and length of the heterogeneous polymer nanorods, this technique will provide for the opportunity to evaluate drug release kinetics as a function of the segment spacing, size of the nanorods, and aspect ratio in the future.

INTRODUCTION

Heterogeneous, one-dimensional (1D) nanomaterials, such as nanorods and nanowires, show great potential for a variety of different applications because they offer a unique combination of properties [1] and provide a material platform for integrating multiple functions [1]. Multifunctional 1D polymeric nanomaterials are commonly fabricated using a co-electrospinning process [1-4] to produce core-shell polymer nanorods. Biomedical applications for these structures include biosensing [1,3], drug and gene delivery [1-4], and tissue engineering [1,2,4].

1D polymer nanostructures show the greatest potential for drug delivery applications because of some very recent discoveries regarding particle shape and cellular uptake [5-7]. Studies have shown that wormlike, filamentous nanoparticles are able to avoid the body's natural immune response, allowing them longer circulation than spherical particles [5-7]. It is

hypothesized that macrophages, the cells that are responsible for engulfing foreign particles in a process known as phagocytosis, have difficultly stretching and adjusting their shape to engulf filamentous particles and exhibit significantly reduced phagocytosis than spherical particles [5,8]. Geng et al[7] have demonstrated that paclitaxel loaded filomicelles can circulate up to ten times longer, and provide the same therapeutic effect as spherical micelles with an eightfold smaller paclitaxel dosage per injection. These results show great potential and have created a great need for low cost, simple, and versatile nanofabrication techniques to produce 1D polymer nanostructures for drug and gene delivery applications.

Template wetting is a template-assisted nanofabrication approach that is low cost, simple, and highly versatile [2,9]. Template wetting utilizes the nanochannels of nanoporous materials, such as anodized aluminum oxide (AAO) or polycarbonate, to form 1D nanostructures [2,9]. Template wetting offers unprecedented control over the diameter, length, and morphology of polymer nanostructures and it can accommodate practically all types of polymeric materials. Template wetting utilizes either a polymer solution or a polymer melt to achieve nanotube or nanorod morphologies. By varying the polymer solution concentration nanotube wall thickness can be controlled, and by varying the temperature of the polymer melt, both nanorod and nanotube morphologies can be formed [10]. Overall, template wetting is an approach that allows for a multitude of different nanostructure variations.

Previously we were able to demonstrate the fabrication of 1D heterogeneous, segmented nanorods by template-assisted wetting with an alternating thin film of polystyrene (PS) and poly(methyl methacrylate) (PMMA) [11]. PS and PMMA were used as model polymers to optimize the template wetting conditions for segmented nanorod fabrication. This paper describes our preliminary work with the fabrication and characterization of biodegradable poly(e-caprolactone) (PCL) and poly(L-lactic acid) (PLLA) homogeneous nanorods and drug release profiles for ibuprofen from PLLA thin films. This preliminary work presents the means to which the fabrication of heterogeneous nanostructures and the characterization of drug release from these nanostructures can ultimately be attained.

EXPERIMENTAL

Materials

PLLA (Mw: 100,000 – 150,000 g/mol, T_g: 48.6 ^oC) and PCL (Mw: 70,000 – 90,000 g/mol, T_m: 60 ^oC) were purchased from Sigma Aldrich and used as received. Anodisc 13 commercial AAO templates with average pore diameter of 200 nm were purchased from Whatman and used as received.

Nanostructure fabrication

Thin films of PLLA were cast from chloroform solutions containing ~1 wt% PLLA and 0.05%, 0.1% and 0.2% ibuprofen and allowed to dry in air for several days. These solutions yielded films that should theoretically contain approximately 5%, 10%, and 20% ibuprofen respectively. Films were cut into squares approximately 1 cm^2. A hot plate set to 80 ^oC and 100 ^oC was used for PCL and PLLA wetting respectively. The polymer film was place on top of either a homemade AAO template with 50 nm diameter pores or commercial AAO template with 200 nm diameter pores and placed on the hot plate for approximately 24 hours. The homemade AAO templates were fabricated using a 2 step anodization process which is described in other works [12]. After wetting, the AAO template was dissolved in a 0.01 M NaOH solution for approximately 24 hours, ultrasonicated for 30 minutes, and finally the nanostructures were collected by vacuum filtration using a 50 nm diameter polycarbonate filter. Nanostructure morphology was characterized using TEM.

Drug release from polymer thin films

Thin films of PLLA were cast from solution as described previously. Films were cut into squares approximately 1 cm^2 and the mass of each film was measured using an analytical balance. The total mass of the thin film was used to calculate the total amount of drug in the thin film based on the ratio of drug and polymer in the solution. The thickness of the films was measured at four points using a caliper with precision up to 0.001 mm to insure uniform thickness.

To determine whether the ibuprofen was fully dissolved in the PLLA and to verify the concentration of ibuprofen in the PLLA films, DSC was used to measure the change in the melting temperature as a result of the ibuprofen. This is based upon the principle of freezing point depression; when a solute, in this case the ibuprofen, is dissolved in a pure solvent, in this case PLLA, the freezing/melting point of the solvent decreases as a function of the solute concentration. The depression of the melting point is given by the following equation:

$$\Delta T = Km \tag{1}$$

where ΔT is the change in melting temperature, m is the molality of the solution, and K is the cryoscopic constant which is given by,

$$K = \frac{RT_m^2 M}{\Delta H_f} \tag{2}$$

where R is the gas law constant, T_m is the melting temperature of the pure solvent, M is the molar mass of the pure solvent, and ΔH_f is the enthalpy of fusion of the pure solvent. ΔH_f can be taken from the DSC data as the area under the melting curve for pure PLLA.

PLLA thin films were immersed in 0.01 M phosphate buffer solution (PBS) and incubated at 37°C. After certain time intervals, 1 mL aliquots of the PBS was removed, and the absorbance at 224 nm and 266 nm were measured using UV-vis spectroscopy. A set of standard ibuprofen solutions with concentrations ranging from 0.57 mg/L to 570 mg/L were used to generate standard curves relating ibuprofen concentration to absorbance for both 224 nm and 266 nm. It was determined that the standard curve for 224 nm is most accurate for measuring concentrations less than 22 mg/L and 266 nm is the most accurate for measuring concentrations greater than 22 mg/L. The ibuprofen standard curves are shown in Figure 1.

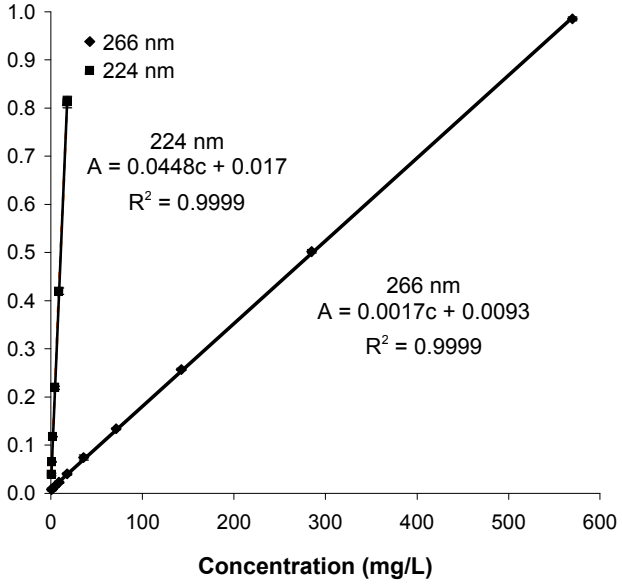

Figure 1. Standard curve for absorbance as a function of ibuprofen concentration in PBS measured by UV-vis spectroscopy at 224 nm and 266 nm

The diffusion coefficients for each drug concentration were calculated based upon two equations that provide an early-time approximation [13], from 0% - 60% drug release, which is given by,

$$\frac{M_t}{M_o} = 4\left(\frac{Dt}{\pi l^2}\right)^{1/2} \tag{3}$$

and a late-time approximation [13], from 40% - 100% drug release, which is given by,

$$\frac{M_t}{M_o} = 1 - \frac{8}{\pi^2}\exp\left(\frac{-\pi^2 Dt}{l^2}\right) \tag{4}$$

where M_t is the mass of drug at time t, M_o is the mass of total drug in the film, D is the diffusion coefficient, and l is the thickness of the thin film.

RESULTS AND DISCUSSION

Biodegradable nanostructure morphology

Biodegradable nanorods were fabricated from PCL and PLLA polymers using a template-assisted wetting approach. One of the major drawbacks of this nanofabrication approach, specifically for biodegradable materials, is that a harsh acidic or basic solution is required to dissolve the AAO template to liberate the nanorods. Treatment of the AAO templates with strong acids and bases as well as the increased surface area of the liberated nanostructures make it essential to verify that the nanostructures do not completely dissolve during the fabrication process. TEM images of PCL and PLLA nanorods, given in Figure 2, show that our nanorods are not completely dissolved during the process.

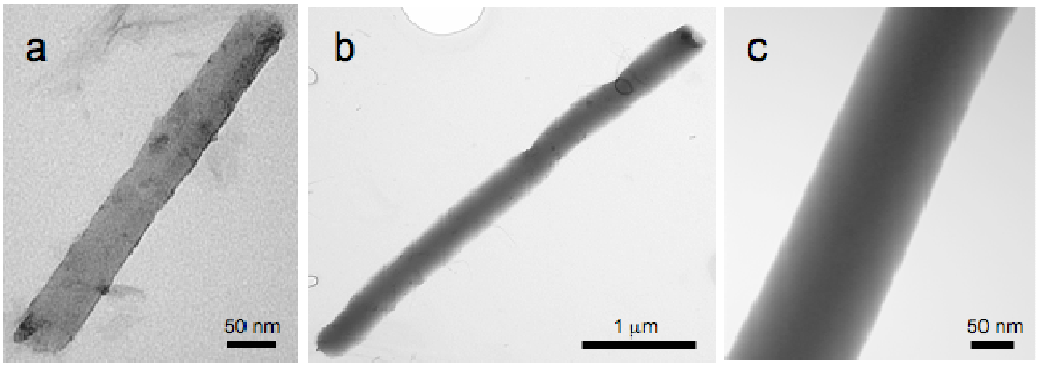

Figure 2. TEM images of a.) PCL nanorod from homemade AAO template with 50 nm diameter pores, b.) PCL nanorod from commercial AAO template with 200 nm diameter pores, and c.) PLLA nanorod from commercial AAO template with 200 nm diameter pores

The TEM images of the PCL nanorods formed both in homemade and commercial AAO templates show that the diameter of the nanorods agrees well with the diameter of the template nanopores, 50 nm and 200 nm respectively. From this we can conclude that the NaOH used to dissolve the AAO templates had little effect on the nanostructure. The TEM image of the PLLA nanorods formed in the commercial AAO template, however, shows that the diameter of the nanorod is only about 125 nm, which is less than the expected 200 nm diameter of the nanopore. This result suggests that the PLLA nanorods did dissolve slightly during the fabrication process. It is likely that the PCL nanorods were less susceptible to hydrolytic degradation than PLLA because PCL is more hydrophobic and slightly more crystalline causing the diffusion of the NaOH solution to be slower. This needs to be further investigated if PLLA nanorods are to be used in the future for drug delivery.

The length of the nanorods varies significantly from a few hundred nanometers up to a few microns. Theoretically the nanorods could be as long as 60 μm, which is the thickness of the template. This wide length distribution is expected. When the template is removed the nanostructures are sonicated to disperse them and this process causes them to fragment into much shorter lengths. In addition, the wide length distribution may also be caused by hydrolytic erosion from the ends of the nanorods.

Polymer dissolution during the nanofabrication process will have a substantial impact on the drug release kinetics. Future work will include efforts towards the fabrication of heterogeneous segmented and/or core-shell biodegradable nanorods for drug release experiments.

Drug release from PLLA thin films

In order to understand and interpret drug release data for nanostructures, preliminary work with polymer thin films has been done. Thin films of PLLA with 5%, 10%, and 20%

ibuprofen were fabricated and the release of ibuprofen from the films was measured with UV-vis spectroscopy as a function of time.

To confirm that ibuprofen was dissolved in the PLLA and not present as crystals, the melting temperature of PLLA was measured for each thin film using DSC. The measured melting temperature for each polymer film is given in Table I.

Table I. Percentage of ibuprofen dissolved in PLLA/Ibuprofen thin films based upon the depression of the melting point measured by DSC

Theoretical % Ibuprofen	Melting Temp (^{o}C)	ΔT	Calculated % Ibuprofen from DSC
0	173.6	-	-
5	169.2	4.3	2.9
10	164.4	9.1	5.7
20	160.4	13.2	7.8

This data show that the melting point of PLLA decreases with increasing amounts of ibuprofen. Using the change in the melting point from the DSC data, the concentration of ibuprofen actually dissolved in the polymer films was calculated from equations (1) and (2) and is also given in Table I.

The concentration of ibuprofen dissolved in the PLLA films calculated from the DSC data is considerably less than the concentration of ibuprofen that should have been in the films based upon the composition of the solutions that the thin films were cast from. No pure ibuprofen peaks were found on the DSC curves for any of the thin films. This result leads to the conclusion that the as cast films were not uniform and homogenous. This conclusion is further supported by the visual appearance of the films. Some regions of the thin films looked as though they were spotted, which is likely caused by drug crystals. The DSC samples and films used for drug release were taken from regions of the polymer films that visually appeared to be homogenous. This could present a problem during nanorod fabrication. Having inhomogeneous regions of drug along the nanorod could cause the rods to loose some mechanical stability. The solubility of ibuprofen in biodegradable polymers is currently being investigated so that an appropriate, homogenous system can be chosen for future drug-loaded nanorod fabrication and drug release studies.

The percent ibuprofen released from the PLLA films as a function of time is given in Figure 3. The polymer film with the highest concentration of ibuprofen had the most rapid drug release and the polymer film with the lowest concentration of ibuprofen had the slowest drug release. This trend was expected because the higher ibuprofen concentration gives the largest concentration gradient, which leads to the fastest diffusion.

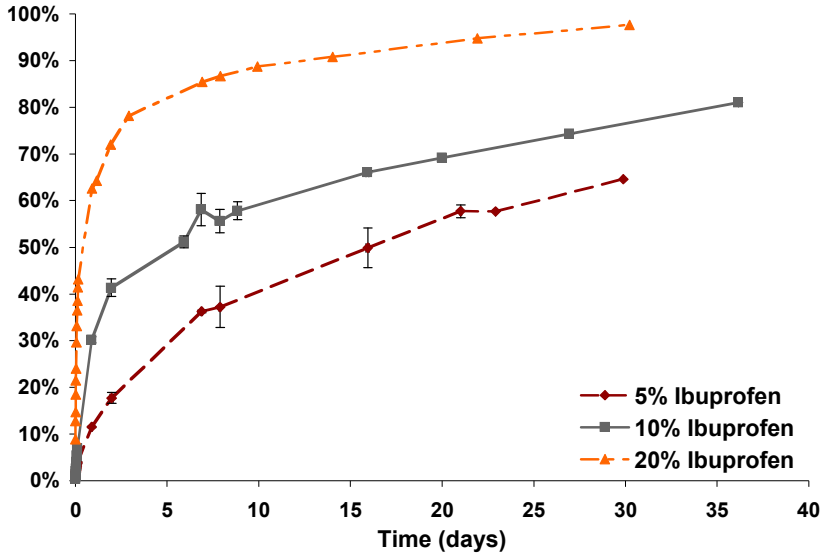

Figure 3. Percent ibuprofen release from PLLA thin films as a function of ibuprofen concentration and time

An early-time approximation and a late-time approximation of the diffusion coefficient for each ibuprofen concentration were calculated using equations (3) and (4). The average thin film thickness was measured to be 0.018±0.009 mm. This value was used for the diffusion coefficient calculations which are given in Table 2.

Table II. Early-time and late-time approximations of the diffusion coefficient D of ibuprofen in PLLA thin films

Ibuprofen	D (m^2/s) Early	D (m^2/s) Late
5%	6.0×10^{-13}	1.0×10^{-17}
10%	22×10^{-13}	1.8×10^{-17}
20%	500×10^{-13}	5.7×10^{-17}

The early-time approximations of the diffusion coefficients are an order of magnitude different in value, showing a large difference in the initial driving force for diffusion. A similar study that measured the release of ibuprofen from poly(ε-caprolactone-c-D,L-lactide) also reported the trend of increasing diffusion coefficient with increasing initial drug concentration [13]. However, the increase in diffusion coefficient was not as significant as our results, and ranged from $2.5x10^{-13}$ m^2/s at 5% ibuprofen to $6.5x10^{-13}$ m^2/s at 20% ibuprofen [13]. This difference in magnitude for the higher ibuprofen concentration may be a result of the inhomogeneous nature of the ibuprofen dissolved and dispersed in the PLLA films that we observed. Once most of the drug has diffused from the polymer film, the diffusion coefficients are much less dependent upon the initial drug loading, which also agrees with previous studies [13]. This preliminary work with thin films will facilitate the interpretation and modeling of future drug release data for biodegradable nanorods.

CONCLUSIONS

This paper demonstrates the fabrication of biodegradable nanorods using a template-assisted wetting approach. The nanorods were fabricated from both PCL and PLLA using both homemade AAO templates with 50 nm pore diameters and commercial AAO templates with 200 nm pore diameters and their structure was characterized with TEM. In addition, this paper describes preliminary drug release data for ibuprofen release from PLLA thin films. Future work will include the incorporation of ibuprofen within biodegradable nanorods and will utilize the preliminary thin film drug release data to interpret and model the drug release behavior of the nanorods.

REFERENCES

[1] M. Wei, J. Lee, B. Kang, and J. Mead, *Macromol. Rap. Comm*. **26** 1127-1132 (2005)

[2] A. Greiner, J. H. Wendorff, A. L Yarin, and E. Zussman, *Appl. Microbiol. Biotechnol*. **71** 387-393 (2006)

[3] D. Li and Y. Xia, *Nano Lett*. **4** 933-938 (2004)

[4] Z. Sun, E. Zussman, A. L. Yarin, J. H. Wendorff, and A. Greiner, *Adv. Mater*. **15** 1929-1932 (2003)

[5] J. Champion and S. Mitragotri, *Pharmaceutical Research* (2008) (in press).

[6] N. Nishiyama, *Nature Nanotechnology* **2** 203-204 (2007).

[7] Y. Geng, P. Dalhaimer, S. Cai, R. Tsai, M. Tewari, T. Minko, and D. Discher, *Nature Nanotechnology* **2** 249-255 (2007).

[8] J. A. Champion and S. Mitragotri, *PNAS.* **103** 4930 – 4934 (2006)

[9] M. Steinhart, R. B. Wehrspohn, U. Gosele, and J. H. Wendorff, *Angew Chem. Int. Ed*. **43** 1334-1344 (2004)

[10] M. Zhang, P. Dobriyal, J. Chen, and T. P. Russell, *Nano. Lett.* **6** 1075-1079 (2006)

[11] S. Dougherty and J. Liang, *J. Nanopart. Res.* 11 743-747 (2009)

[12] S. Dougherty, J. Liang, and T. F Kowalik *J. Nanopart. Res*. 11 385-394 (2009)

[13] N. Ahola, J. Rich, T. Karjalainen, and J. Seppala, *J. Appl. Poly. Sci.* **88** 1279-1288 (2003)

Appendix 4. Preliminary Data for Drug Release from Nanoporous Alumina Membranes

Abstract

The use of nanoporous materials as controlled drug delivery devices is highly desirable. Researchers have demonstrated that solute molecules diffusing from nanochannels which are only slightly larger than the molecular dimensions of the solute yield diffusion profiles which deviate from traditional Fickian diffusion and have the potential to yield zero-order release profiles. The diffusion profiles for nanochannels are typically lower than predicted by Fickian diffusion and have been defined as hindered diffusion, where the solute diffusivity is a function of the ratio between the solute radius and the nanochannel radius. Despite the many empirical and theoretical relationships that have been developed to describe hindered diffusion as a function of the nanochannal radius, few studies have considered other dimensions of the nanochannels such as the length and aspect ratio. In this study we measure the release of ibuprofen diffusing from 200, 50, and 20 nm diameter nanochannels with lengths of 60, 40, and 20 μm respectively. Although conclusions could not be drawn from our limited preliminary data, we are able to offer many considerations that should be taken into account for future drug release experiments.

Introduction

The transport of solute molecules from nanoporous materials is of great interest for applications such as ultrafiltration [1], chromatographic and eletrophoretic separations [1], heterogeneous catalysis [1], and controlled drug delivery [1,2]. For example, the use of nanoporous coatings on implantable devices such as drug-eluting stents has shown promising results and is a highly desirable alternative for controlled release without the use of polymers [3-5].

Obtaining "zero-order" drug delivery, where the same amount of drug is release per unit time for extended periods of time, is a highly sought after goal for controlled drug delivery devices. Ferrari's research group has obtained zero-order release for many molecules from nanochannels and has observed that these release profiles can not be explained by Fick's laws [6]. They reasoned that Fick's laws are based upon the assumption that solute molecules experience Brownian motion in three-dimensions and in nanochannels, where motion is confined to one-dimension, this assumption is not met [6]. Essentially, if the diameter of a nanochannel is

within the same order of magnitude of a drug molecule, the diffusivity of the drug molecules in the nanochannel will be hindered [1,7,8]. The hindered diffusion of the solute is thought to be caused by both a thermodynamic phenomenon and a transport effect [8]. Thermodynamically, the interaction between the solute and the pore wall causes the solute to be excluded from the region near the pore wall causing an intrapore concentration driving force which is less than the bulk solution concentration driving force [1,8]. The transport effect is caused by the hydrodynamic drag that is experienced by the solute molecule, which is higher than the drag experience by the solute in bulk fluids [1,8]. The combination of these two effects has led to the definition of an effective diffusion coefficient to describe hindered diffusion in nanopores. The effective diffusion coefficient is a function of the ratio between the solute particle radius and the nanopore radius which is given by [1,8],

$$\lambda = \frac{r_{solute}}{r_{pore}} \tag{1}$$

Research to understand the of hindered diffusion extends back as early as the 1950's and has generated several phenomen ological models to relate the effective diffusion coefficient to λ. One such empirical relationship was developed by Renkin [1,8] and is given by,

$$D = D_{\infty}\left(1-\lambda\right)^{2}\left(1-2.104\lambda+2.089\lambda^{3}-0.948\lambda^{5}\right) \tag{2}$$

where D is the effective diffusion coefficient and D_∞ is the bulk diffusion coefficient. Renkin's equation is valid for situations where spherical, non-interacting particles are moving along the center of a pore [1]. For spherical solutes the bulk diffusion coefficient is given by the Stokes-Einstein equation,

$$D_{\infty} = \frac{k_{\beta}T}{6\pi\mu r_{solute}} \tag{3}$$

Where k_β is Boltzmann's constant, T is absolute temperature, and μ is the solvent viscosity.

In this study we investigate release of ibuprofen from cylindrical nanochannels with 200, 50, and 20 nm diameters and lengths of 60, 40, and 20 μm respectively. Ibuprofen is a well known anti-inflammatory drug [9] which has a very small size (radius of approximately 5 nm) [9,10], and has very low solubility in water (< 1 mg/mL). Ibuprofen was used as our model drug because it is commonly employed as a model drug for controlled release studies [9] and we used it previously for measuring the release from polymer thin films to characterize the diffusion coefficient [11]. After measuring the release of ibuprofen from the nanochannels of AAO, we

planned to measure the release of ibuprofen from nanochannels of AAO filled with a polymer/ibuprofen mixture. Therefore, it would be used for comparison and enable conclusions to be drawn with regard to thin film geometry versus a cylindrical nanochannel.

Experimental

Materials

Ibuprofen was purchased from Sigma Aldrich and used as received. AAO templates with ~ 200 nm average pore diameter and 60 um thick were purchased from Whatman and used as received. AAO templates with ~ 50 nm average pore diameter and 40 um thick and ~20 nm average pore diameter and 20 um thick were fabricated using a two-step anodization process described elsewhere [12].

Loading AAO templates with drug

Ibuprofen was melted on a hot plate at approximately 40^{o}C. Once the ibuprofen was completely liquid, an AAO template was placed on top of the liquid, and the liquid ibuprofen was allowed to enter the nanochannels via capillary action. The surfaces of the AAO templates were washed with DI water and carefully wiped to remove as much ibuprofen from the surface as possible. The mass of the AAO template was measured with an analytical balance before and after the drug loading to determine the total amount of drug loaded into the nanochannels.

In vitro release tests

The release tests were conducted at room temperature in vitro. Each test sample was placed in capped vials (20 mL) with 5 mL DI water. At predetermined time intervals, the vials were carefully shaken and 1 mL of the solution was removed for analysis. UV-vis spectroscopy was used to determine the amount of ibuprofen in the DI water. The absorbance was measured at 224 nm and 266 nm using a Genesys UV-vis spectrometer. Standard curves were used to correlate the absorbance to the concentration of ibuprofen, to calculate the mass of ibuprofen released from the AAO templates [11]. After measuring the absorbance, the DI water was returned to the sample vial.

Results and Discussion

The release profiles for ibuprofen diffusing from AAO templates with 200, 50, and 20 nm diameters and lengths of 60, 40, and 20 μm respectively were measured using UV-vis spectroscopy. A standard curve of ibuprofen concentration as a function of absorption was used to calculate the mass of ibuprofen released from the templates. The ibuprofen was initially

loaded into the templates by melt wetting and the mass of ibuprofen loaded into each template was calculated by weighing the templates before and after the wetting process. The percentage of the ibuprofen that was released from the template at a given time was calculated by dividing the mass released at that time by the initial mass of ibuprofen loaded into the template. The release profiles of ibuprofen from the three nanochannels are shown in figure 1.

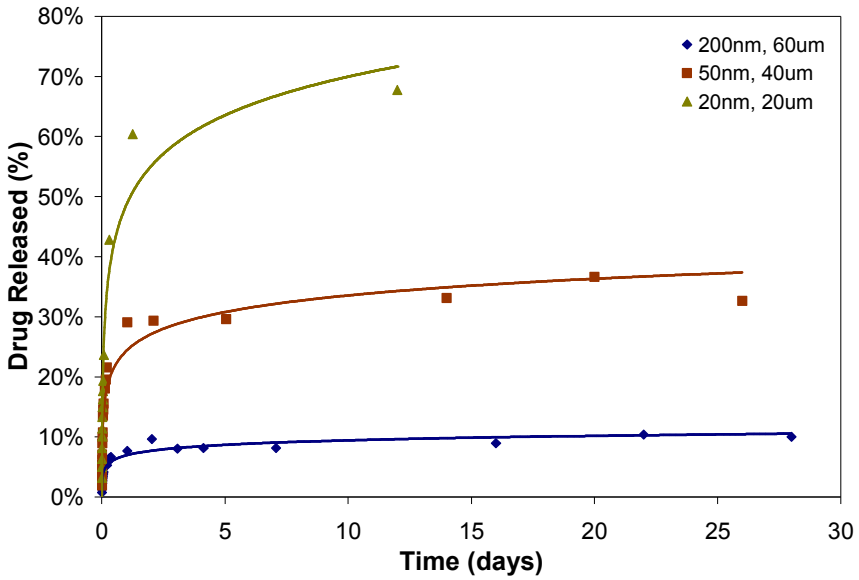

Figure 1: Release profiles for ibuprofen diffusing from nanochannels with 200, 50, and 20 nm diameters and lengths of 60, 40, and 20 μm respectively.

It was observed that the slowest drug release profile was obtained for the 200 nm diameter, 60 μm long nanochannel and the fastest for the 20 nm diameter, 20 μm long nanochannel. This result demonstrates that the drug release profile is strongly dependent upon the length of the nanochannels, which is an obvious result based upon the theory of diffusion. From our results it appears that the diameter of the nanochannels had little to no effect on the drug release profile. This result was further supported by calculating the diffusion coefficient for ibuprofen in water using equation (3) and plotting the effective diffusion coefficient, which was calculated using equation (1) and (2), as a function of the nanochannel diameter. The diffusion coefficient for ibuprofen in water was calculated to be 4.36×10^{-10} m^2/s and figure 2 shows the effective diffusion coefficient as a function of the nanochannel diameter.

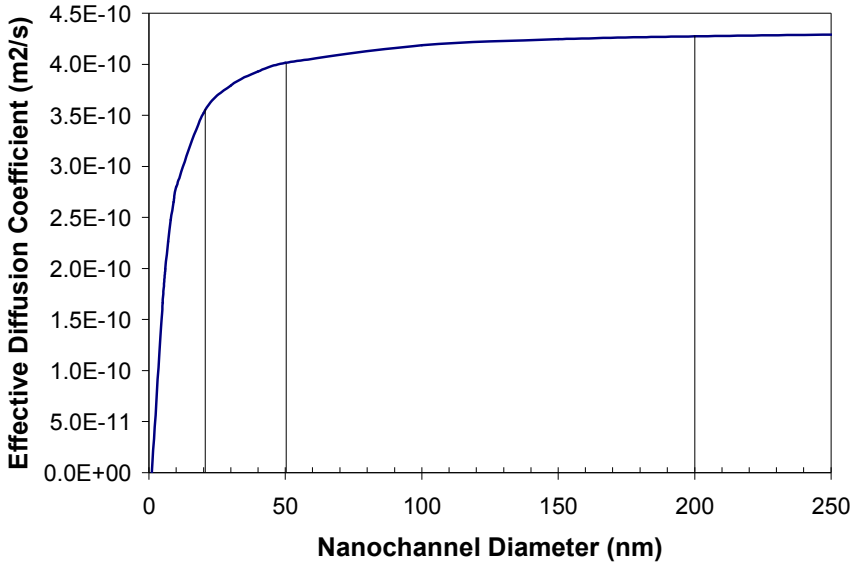

Figure 2: Graph that shows the effective diffusion coefficient as a function of the nanochannel diameter

From figure 2 it can be seen that the effective diffusion coefficients for the nanochannel diameters used in this study are not significantly different. It appears that nanochannels would need to be 10 nm in diameter or less to see the effects of hindered diffusion and the one-dimensional confinement of a drug molecule with a radius of 0.5 nm. Based on this information, we can conclude that we either needed to use nanochannels with smaller diameters or use a larger model drug to draw any conclusions regarding the effects of hindered diffusion and nanoconfinement.

Another observation about the data presented in figure 1 is that 100% drug release was not obtained for any of the nanochannel dimensions within our timeframe and the release profiles began to plateau at values that were inversely proportional to the length of the nanochannels. From our results we have shown that approximately 10%, 35%, and 75% total mass is released from the 60, 40, and 20 μm long nanochannels respectively when the profiles begin to plateau. This result may be the result of two different issues associated with the design of this experiment. First, in our experimental procedure we measured the absorbance of 1 mL of solution then returned the solution to our sample vial. By doing this, the concentration of solute in the sample vial continuously increases with time, which also reduces the driving force for diffusion. Additionally, the driving force would be reduced at a different rate for each of the

samples. This may explain the plateau we observed and also prevents us from drawing any conclusions because the data may not be comparable. The experimental procedure for future drug release experiments should include the replacement of the measured samples with fresh solution so that sink conditions are maintained. Second, we do not know whether the ibuprofen filling was uniform and complete for the three different nanochannel lengths and diameters because the templates were not all the same size. In the future, if templates with the same surface area are used, we can calculate the theoretical upper limit for the total amount of drug in each template based on the porosity, nanochannel diameter, and thickness of the templates if we assume all the nanochannels are uniformly and completely filled. This calculation combined with the weight gain of the template would allow us to estimate how full the nanochannels are, which will be very useful information for interpreting our results. Since we do not know the extent to which our nanochannels are filled with ibuprofen, we also cannot draw any conclusions from these data.

Conclusions

In summary, this study reported the drug release of ibuprofen from three different nanoporous AAO templates, each with a different thickness and nanochannel diameter. We were unable to draw any conclusions with respect to hindered diffusion and nanoconfinement because of several flaws associated with the design of this experiment. These flaws included lack of consideration of the size of ibuprofen with respect to the size of our nanochannels, not maintaining sink conditions in the bulk solution, and inability to estimate the extent to which the nanochannels were initially filled with ibuprofen. In addition, ibuprofen may not have been the most appropriate model drug choice because of its low water solubility and small size. Future drug release studies will take these issues into consideration so that meaningful conclusions can be drawn about the effects of hindered diffusion and nanoconfinement.

References

[1] Ladero M, Santos A and Garcia-Ochoa F 2007 Hindered diffusion of proteins and polymethacrylates in controlled-pore glass: an experimental approach *Chem. Eng. Sci*. **62** 666-78

[2] Yan W, Hsiao V, Zheng Y B, Shariff Y M, Gao T and Huang T J 2009 Towards nanoporous polymer thin film-based drug delivery systems *Thin Solid Films* **517** 1794-8

[3] Kang H J, Kim K J, Park S J, Yoo J B and Ryu Y S 2007 Controlled drug release using nanoporous anodic aluminum oxide on stent *Thin Solid Films* **515** 5184-7

[4] Ayon A A, Cantu M, Chava K, Agrawal C M, Feldman M D, Johnson D, Patel D, Marton D and Shi E 2006 Drug loading of nanoporous TiO_2 films *Biomed. Mater*. **1** L11-5

[5] Desai T A, Sharma S, Walczak R J, Boiarski A, Cohen M, Shapiro J, West T, Melnik K, Cosentino C, Sinha P M, and Ferrari M Nanoporous implants for controlled drug delivery. In: BioMEMs and biomedical nanotechnology. Springer; 2007. p. 263-85

[6] Ferrari M 2008 The mathematical engines of nanomedicine *Small* **4** 20-5

[7] Martin F, Walczak R, Boiarski A, Cohen M, West T, Cosentino C and Ferrari M 2005 Tailoring width of microfabricated nanochannels to solute size can be used to control diffusion kinetics *J. Controlled Rel*. **102** 123-33

[8] Shao J and Baltus R E 2000 Hindered diffusion of dextran and polyethylene glycol in porous membranes *AIChE Journal* **46** 1149-56

[9] Qu F, F Zhu, Lin H, Zhang W, J Sun, S. Li, and S Qui 2006 A controlled release of ibuprofen by systematically tailoring the morphology of mesoporous silica materials. *J Solid State Chem*. **179** 2027-35

[10] Horcajada P, Ramila A, Ferey G and Vallet-Regi M 2006 Influence of superficial organic modification of MCM-41 matrices on drug delivery rate. *Solid State Sciences* **8** 1243-9

[11] Dougherty S and Liang J Towards biodegradable segmented nanorods for controlled drug delivery. Submitted to the Proceedings of the MRS Fall 2008 Conference

[12] Liang J, Chick H, Yin A et al 2002 Two-dimensional lateral superlattices of nanostructures: Nonlithographic formation by anodic membrane template. *J Appl Phys* **91** 2544-6